Titulació:

Grau d'Enginyeria en Tecnologies Aeroespacials

Alumne (nom i cognoms):

Mario Gayete Ibáñez

Enunciat TFG:

Development of CFD codes for the numerical resolution of potential flow and the incompressible form of the Navier-Stokes equations

Contingut:

Memòria

Director TFG:

Carles-David Pérez-Segarra

Codirector del TFG:

Asensio Oliva Llena

Convocatòria del lluirament del TFG:

10/06/2019

Acknowledgements

Primer de tot, m'agradaria agrair al departament del CTTC per haver-me donat l'oportonitat d'endinsar-me en el fascinant món del càlcul computacional. En especial, m'agradiria agrair tot el suport rebut pel professor Carles-David Pérez-Segarra, qui em va donar l'oportunitat de continuar aprenent i m'ha estat guiant i ajudant en aquesta branca de l'enginyeria des de l'estiu passat. També m'agradaria agrair al professor Asensi Oliva pels consells i la motivació que em va donar durant el curs de *Dinàmica de Gasos i transferència de Massa i Calor*. També m'agradaria donar les gràcies al professor Jorge Chiva, qui em va donar consells per optimitzar el codi amb el projecte de l'assignatura de *Dinàmica de Gasos i transferència de Massa i Calor* i per ajudar-me a trobar l'error de codi de les Navier-Stokes.

D'altra banda, m'agradaria expressar la meva immensa gratitud a la meva família ja que sempre ha estat present quan més ho he necessitat i qui ha permés que jo sigui qui sóc i estigui cursant aquesta carrera.

Finalment, vull agrair a totes i a cadascuna d'aquelles persones amb les que he compartit bons moments i que m'han anat donant suport durant tot aquest camí: antics companys i professors de l'escola, companys de la universitat, companys de Cardedeu, companys d'AMES i, en general, a tothom amb qui he tingut un bon contacte.

Abstract

The aim of this project has been to consolidate and amplify the knowledge on fluid dynamics and CFD. It will be developed and verified different numerical codes for each physical case (potential flow, convection-diffusion equation and Navier-Stokes equation).

The first chapter will consist on an introduction, where it will be explained the aim and the requirements of this study, a background of numerical methods, the report organisation and it will be also mentioned the previous knowledge on numerical methods.

On the following three chapters it will be solved and analysed three different cases of numerical approaches to fluid mechanics (non-viscid flows, convection-diffusion equations and, finally, the incompressible flow of Navier-Stokes equations). In each chapter it will be an introduction, a problem definition, a methodology of resolution (where it will be explained the procedure and the algorithm of the code), an analysis of the results (numerical and physical results) and finally a conclusion.

On the fifth chapter it will be presented the budget, the task planning and the environmental impact and on the sixth chapter will consist on a conclusion and recommendations for a future work.

Contents

List of Figures

List of Tables

Nomenclature

β	Piezo-thermal coefficient
$\hat{\phi}$	Normalized variable
ϕ	Velocity potential (only for potential flow)
ψ	Streamline
θ	Non-dimensional temperature
$\vec{v}^P$	Predictor velocity
c_P	Specific heat at constant pressure
CDS	Central-difference scheme
DNS	Direct Numerical Simulation
E	East node
e	East face
LES	Large Eddy Simulation
N	North node
n	North face
P	Treated node
Pr	Prandtl number
$QUICK$	Quadratic upwind interpolation for convective kinematics
R	Gas constant
$RANS$	Reynolds averaged Navier-Stokes
Re	Reynolds number
S	South node
s	South face
$SMART$	Sharp and Monotonic Algorithm for Realistic Transport
$SUDS$	Second-order upwind-difference scheme
UDS	Upwind-difference scheme
W	West node
w	West face

Chapter 1

Introduction

1.1 Aim

The main purpose of this project is to develop different numerical codes programmed in *C++* that will allow the solving of potential flow, the convection-diffusion equation and the incompressible form of the Navier-Stokes equations. The idea is to amplify the knowledge of programming in *C++* and consolidate and amplify the knowledge on fluid mechanics, heat transfer and computational fluid dynamics.

All these programs developed will be verified with analytical solutions (if it is possible) or with solutions proposed by the CTTC (Heat and Mass Transfer Technological Center) department and other research groups.

1.2 Requirements

Since the aim of this project is to develop different numerical simulation programs, the requirements can be specified on the following list:

- The programming language will be *C++* (this is the important part) and the plotting language will be *Matlab*.
- Validation of the codes.
- All the cases treated will be two-dimensional geometries.
- The mathematical approach will be the Finite Volumes Method.

1.3 Background

The equations of fluid dynamics (known for over a century) are analytically solvable for only a limited number of cases. The solutions of these cases are very useful for the understanding of the fluid flow, but in few cases can be used directly in engineering

analysis or design. Thus, it has been forced traditionally to use other approaches.

The most common approach has been the simplifications of the equations. These have been usually based on a combination of simplifications and dimensional analysis, where the empirical results play an important role in this part. A common example can be the drag computation, which can be expressed on the following way:

$$D = \frac{1}{2}\rho v^2 S C_D \tag{1.1}$$

where S is the frontal section perpendicular to the flow, v refers to the flow velocity (relative velocity to the body), ρ is the flow density and the parameter C_D is the drag coefficient (dimensionless parameter that can be obtained empirically for a concrete Reynolds and Mach number).

Another common approach is to leave the Navier-Stokes equations with only the Reynolds number as the only independent variable. If the body shape is fixed, it can be done experiments on a scale model and the results can be extrapolated to the real to the real problem dimensions. However, many flows require more dimensionless parameter and it would be impossible to set an experiment which is correctly scaled. An example can be the flow around an airplane, that in order to achieve the same Reynolds number the fluid velocity on the experiment should be a high Mach number.

Experiments are useful in the way of measuring global parameters, like the lift and drag coefficients, the pressure drop or the heat transfer coefficients. Nevertheless, in many cases details are important, such us knowing if the boundary layer is detached in an airfoil or if the temperature exceeds any limit. For this reason it is essential to find an alternative method to the empirical one.

An alternative, or complementary method, arrived with the computers development. The improvement of the performance-to-cost ratio of computers (a computer on the 1950s only could perform few hundreds operations per second whereas current computers can produce 10^{12} operations per second) and the data storage increment allowed the implementation of key ideas from 20^{th} century for numerical solution methods, that had little use before the computers appearance.

Computational fluid dynamics (CFD) is a field where computers are used to the study of fluid flow in a way easier and more effective than the empirical way. On this field it is obtained an approximated solution discretizing the space in small domains and approximating the partial differential equations on it, where it is obtained a system of algebraic equations. The accuracy of the approximated solution will depend on the quality of discretization.

As it has been mentioned previously, with CFD some of the empirical work problems can be easily dealt, such us knowing the boundary layer detachment. However, these advantages of the CFD are not completely true since it is so difficult to solve high

Reynolds number Navier-Stokes problem with high accuracy. For this reason, it is very important to analyze and judge the obtained results because they are always approximations. Also, it is always important to validate the model with experimental data available.

On a general point of view, a general numerical solution method has the following components:

- Mathematical model: it is the starting point, where it is set the partial differential equations and the boundary conditions.
- Discretization method: is the method chosen of approximating the differential equations into a system of algebraic equations. The different methods will be presented afterwords.
- Coordinate and basis vector system: the coordinate system can be Cartesian (this one will be used on the project), cylindrical, spherical, etc., and the basis determines how vectors and tensors will be defined.
- Numerical grid: is the discrete representation of the domain. It can be structured (or regular) grid, block-structured grid (the are at least two divisions, fine and coarse levels, and it is used for multigrid methods, for example) and unstructured grid (for very complex geometries but it is more complex to program and are widely used on Finite Elements method).
- Finite approximation: it is how it will be approximated the integrals or derivatives (first order, second order, etc.).
- Solution method: it is the way how it is going to be solved the system of algebraic equations, there are direct methods (optimum for low number of equations) or iterative methods (the most used on CFD for computational cost reasons).
- Convergence criteria: it is only needed for iterative methods. When the convergence criteria is accomplished, the iterative process is stopped.

As it has been mentioned on the previous list, there are different types of discretization methods. The oldest method for numerical solutions of partial differential equations (PDE's) is the Finite Difference Method, supposed to been introduced by Euler in the 18^{th} century, and it is the easiest method to use for simple geometries. The starting point of this method is the conservation equation in differential form, where the partial derivatives are approximated in terms of nodal values using Taylor series expansion.

The Finite Volume Method uses the integral form of the conservation equations as the starting point. The domain is divided into a number of control volumes and the conservation equations are approached to each control volume. This method can be

divided into face-centered nodes (the nodes are situated on each domain line division) or cell-centered nodes (the nodes are situated among the domain line divisions).

The Finite Element Method has some common characteristics with the Finite Volume Methods. In this method, the domain is discretized into a number of finite elements that are generally unstructured. The main difference from the Finite Volume Method is that the integrals are calculated with the Gaussian Quadrature, which consists on assigning weights to each node value (according to the geometry of the domain discretization element: triangle, quadrilateral, tetrahedra, etc.) and then summing the products. The main advantage of this method is the ability to easily discretize any complex geometry. However this method present several instabilities when solving a Navier-Stokes problem, since it has been initially thought to solve structures problems. [9]

1.4 Report organisation

This project will been divided into 6 chapters. The first chapter has consisted on an introduction of the project and a background of computational fluid dynamics.

In the second chapter it will be treated the potential flow, where it will be presented the different methodologies of resolution, it will be developed two different methodologies (streamline method and velocity potential method), which will be verified in different ways, and it will be analysed the different obtained solutions (numerical and physical solutions).

In the third chapter it will be studied the convection-diffusion equation, where it will be presented and developed the convective term and it will be analysed the influence of each convective scheme on the solution.

The fourth chapter will consist on the incompressible form of the Navier-Stokes equations. In this chapter it will be introduced the Fractional Step Method and it will be implemented. In the first part of this chapter, it will be developed the mathematical methodology decoupling the energy conservation equation and it will be presented the results of the *Lid-Driven Cavity* problem. In the second part, it will be developed the Fractional Step Method for the case of not decoupling the energy conservation equation from the mass and momentum conservation equations and considering the mass forces (with the Boussinesq approximation) on the momentum equations, and it will be presented the results of the *Differentially Heated Cavity*.

In the fifth chapter it will be presented the summary of the budget, the project planning with the justification of its deviations and the environmental impact and in the last chapter it will be the project conclusion and it will be mentioned the different ways to continue with this project.

1.5 Previous knowledge

This study it is not started from zero in the sense that there has been some previous knowledge on the numerical computation field. Concretely, there has been some previous subjects during the career where it has been learned about numerical simulations.

The first subject where it has been taught numerical computation has been the subject *Dinàmica de gasos, transferència de massa i calor*, where apart from learning the basis of this field, it has consisted on a introduction to the *Finite Volume Methods*. Also, it has been developed an optional project to solve the conduction case (on figure 1.1 it is represented the solution for a plate with 4 different materials).

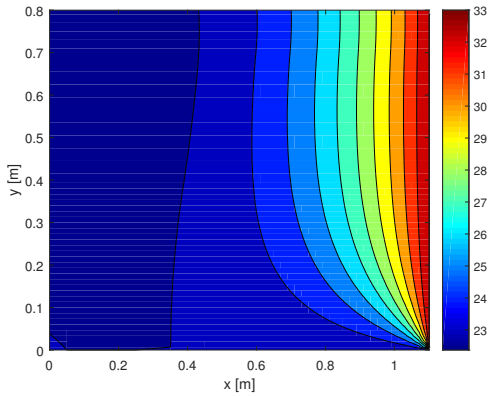

FIGURE 1.1: Temperatures distribution (in degrees Celsius) for a plate with 4 materials

A part, the subject *Enginyeria aeroespacial computacional* has to an introduction to *Finite Elements Method*, where it has been solved heat conduction cases, elasticity and elastodynamic cases.

It has been cursed other subjects, like *Disseny d'aeronaus* or *Aerodinàmica* where it has been shown numerical computation, but these subjects has not centered the attention on this field.

Chapter 2

Potential flow

2.1 Introduction

The flow around aerodynamic objects can be divided in two regions, there is a little region in contact to the object's wall (the boundary layer) where there is a high gradient of velocities and temperatures and there is friction and heat transfer, and the other region is the rest of the domain, where effects of the viscosity and heat transfer can be neglected. Knowing this, it can be assumed that the disturbance of the non-viscous flow, caused by the body and the boundary layer, is very similar to the one caused by the body alone, so the boundary layer can be neglected and the entire flow can be assumed inviscid. This flow is called ideal (or potential) flow and its solution is relatively simple (there is only a single equation to solve) and it is quite accurate for the majority of aerodynamic problems (without shockwaves nor detachment of boundary layer (low attack angles)).

On the aerodynamics field it has been developed a concrete method called *Vortex Panel Method*. In this method, apart of considering an non-viscous flow, it is also assumed incompressible. The procedure of this method is to divide the airfoils surface in a discrete number of lines (panels) where on its center point (the control point) it is induced a velocity from to the other panels (at each panel there is a source strength that generates this induced velocity). The equation to solve in this method is that there should not be an inner or outer velocity at each panel (the normal velocity to the panel evaluated at the control point should be zero), considering the free stream flow velocity and the induced velocities. Finally, it is obtained an algebraic equations systems that can be easily solved with the source strengths as unknowns (once it has been solved this equations system it can be obtained the pressure at each control point, and with it the lift, drag and all the others aerodynamic characteristics). [1]

The *Vortex Panel Method* can be simplified using the Thin-Airfoil theory (the airfoil thickness is neglected, so it only remains the camber's line). This method, called

Discrete Vortex Method [13], has a similar basis to the *Vortex Panel Method*, but in this case it is only discretized the camber line and it is considered that there is a lumped vortex on the control point.

On the other hand, there are two methods based on the finite volumes method: the Streamline method and the Velocity potential method. In these methods it will be appreciated the diffusion phenomenon, which it also appears on the conduction heat transfer. In this chapter it is going to be developed these methods, due to the fact that on the subject *Gas dynamics, heat and mass transfer* it has been developed the code for the case of conduction heat mass transfer and a wide part of the code has been easily adapted to the two methods previously mentioned. With this code developed it has been able to solve the conduction heat transfer for a case of 4 different materials in contact and it has been also developed and verified the *blocking-off* method (it has been tested the case of a cylinder with different heat transfer coefficients).

2.2 Problem definition

The analysis of the potential flow will be focused on a 2-dimension and irrotational flow problem, where there is prism with an infinite depth, a height H and a width L. On the left surface it will be located the inlet flow and on the right surface, the outlet flow. The bottom and top surfaces will be walls, so there will not be inner neither outer flow. At the center (or close to the center in the case of the NACA airfoil) of this rectangle, it will be located a solid object (cylinder or NACA airfoil) with infinite depth.

It is going to be used a structured cartesian mesh (the mesh will consist on a group of rectangles) and the method used will be the finite volume method with the nodes centered at each control volume. In order to make easier the implementation of the boundary conditions, it has been added nodes without volume on the problem boundaries (at each edge of the rectangle).

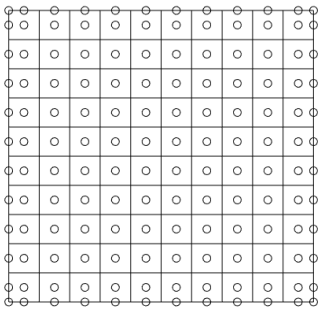

FIGURE 2.1: Representation of the mesh (the nodes are represented with circles)

Since it will be treated no-rectangular objects, the mesh will not be adapted to the

contour of the object. For this reason, it has been used the *blocking-off* method, where the control volume material depends on if its node belongs to the solid or the fluid.

2.3 Methodology of resolution

There are two different ways to treat the potential flow, with streamline or with velocity potential. The advantages of working with streamline method is that there are Dirichlet boundary conditions (the convergence is faster) and the flux can be rotational but the disadvantage is that the flux must be steady 2D. On the other hand, the advantages of working with velocity potential are that the flux can be 3D and transient and the disadvantages are that there are Neumann boundary conditions (it is harder to converge at higher precision) and the flux must be irrotational.

In this project, it has been worked with both methodologies, as a way of verification of results, and they are going to be presented on the following to sections.

2.3.1 Streamline method

Before starting with the procedure, it must be said that it will be analyzed internal nodes and nodes located on the boundary of the geometry separately.

Internal nodes (i=1 to N, j=1 to M) [1]

As it has been mentioned in section 2.2, the flux will be irrotational, so it can be obtained the discretization equations from the following statement:

$$\int_{S_p} (\nabla \wedge \vec{V}) dS = 0 \tag{2.1}$$

Taking into account the Stokes theorem it can be obtained the following expression

$$\oint_{l_p} \vec{V} \cdot \vec{dl} = 0 \tag{2.2}$$

On figure 2.2, it can be observed a generic control volume. From equation 2.2 and according to this figure, it can be obtained the following discretized equation

$$v_{ye} \cdot \Delta y_p - v_{xn} \cdot \Delta x_p - v_{yw} \cdot \Delta y_p + v_{xs} \cdot \Delta x_p = 0 \tag{2.3}$$

On the streamline method the velocities can be calculated as

$$v_x = \frac{\rho_0}{\rho} \frac{\partial \psi}{\partial y} \tag{2.4}$$

[1] This numbering is according to the *C++* matrix numbering, which starts at 0 instead of 1.

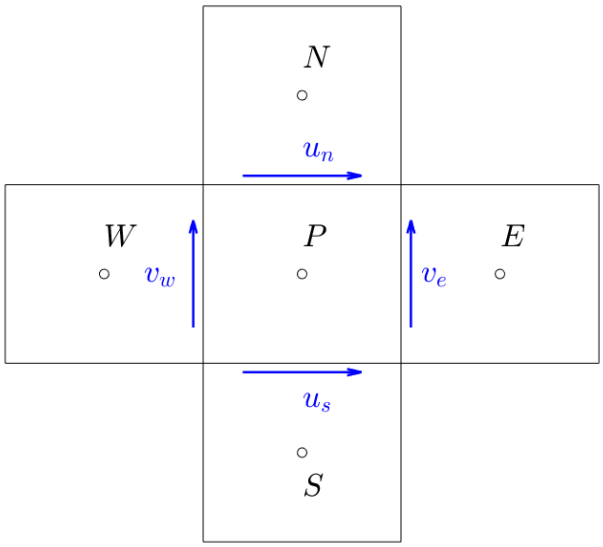

FIGURE 2.2: Internal control volume (the circulation is positive in the counterclockwise direction)

$$v_y = -\frac{\rho_0}{\rho}\frac{\partial \psi}{\partial x} \tag{2.5}$$

where ρ_0 is a reference value (in this case will be the inlet density).

Applying a second order approximation on the derivative the following expressions are obtained

$$v_{ye} = -\frac{\rho_0}{\rho_e}\frac{\psi_E - \psi_P}{d_{PE}} \tag{2.6}$$

$$v_{yw} = -\frac{\rho_0}{\rho_w}\frac{\psi_W - \psi_P}{d_{PW}} \tag{2.7}$$

$$v_{xn} = -\frac{\rho_0}{\rho_n}\frac{\psi_N - \psi_P}{d_{PN}} \tag{2.8}$$

$$v_{xs} = -\frac{\rho_0}{\rho_s}\frac{\psi_S - \psi_P}{d_{PS}} \tag{2.9}$$

In addition, it is defined the following parameter

$$\tau = \frac{\rho_0}{\rho} \tag{2.10}$$

For solids, the value of this τ is 10^{30}.

Introducing the expressions 2.6, 2.7, 2.8, 2.9 and 2.10 on the equation 2.3 and reorganizing terms, finally, it is obtained the discretization equation

$$a_P \cdot \psi_P = a_E \cdot \psi_E + a_W \cdot \psi_W + a_S \cdot \psi_S + a_N \cdot \psi_N \tag{2.11}$$

where

$$a_E = \frac{\tau_e}{d_{PE}} \Delta y_P \tag{2.12}$$

$$a_W = \frac{\tau_w}{d_{PW}} \Delta y_P \tag{2.13}$$

$$a_S = \frac{\tau_s}{d_{PS}} \Delta x_P \tag{2.14}$$

$$a_N = \frac{\tau_n}{d_{PN}} \Delta x_P \tag{2.15}$$

$$a_P = a_E + a_W + a_N + a_S \tag{2.16}$$

It should be noticed that the parameter τ is referred on the boundary of the control volume, and it is calculated with the harmonic mean between the closest two nodes. For example, on the control volume's top surface:

$$\tau_n = \frac{d_{PN}}{\frac{d_{Pn}}{\tau_P} + \frac{d_{Nn}}{\tau_N}} \tag{2.17}$$

Left nodes (i=0)

Through these nodes it is represented the inlet flow condition. Concretely, the inlet condition is that there is an horizontal inlet velocity constant along the y axis. Taking this into account, it can be obtained the streamline for each node:

$$v_x = \frac{\rho_0}{\rho} \frac{\partial \psi}{\partial y} = v_{in} \tag{2.18}$$

In order to find the streamlines, it is only needed to impose the streamline on a single node. Then the other streamlines can be obtained with the discretized equation from 2.18. In this case, it has been decided to impose streamline equal to zero on the lower node (node [0,0]).

The discretized equation is

$$v_{in} = \frac{\rho_{in}}{\rho_{in}} \frac{\psi_j + \psi_{j-1}}{\Delta y} \tag{2.19}$$

From this equation it can be isolated ψ_j, since all the other variables are known. For example, this is the expression to find the [0,1] node's streamline

$$\psi_1 = \psi_0 + v_{in} \cdot \Delta y \tag{2.20}$$

This process will be done until the last node, which its value will be $v_{in} \cdot H$. On figure 2.3 it is represented the inlet streamline distribution

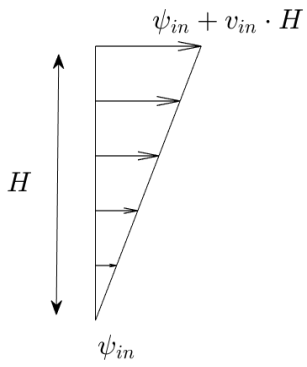

FIGURE 2.3: Inlet streamline distribution

Right nodes (i=N+1)

Through these nodes it is represented the outlet flow condition. Similarly to the left nodes, it is supposed that the outlet flow velocity is horizontal, but in this case the velocity is unknown. So, the condition can be represented as

$$v_y \approx 0 \tag{2.21}$$

$$-\frac{\rho_{in}}{\rho}\frac{\partial \psi}{\partial x} \approx 0 \tag{2.22}$$

With this, the discretized equation is obtained

$$\psi_P = \psi_W \tag{2.23}$$

Top and bottom nodes (j=0 & M+1)

The boundary condition for this nodes is that there is no flow through these nodes, in other words, the normal velocity to these walls is zero

$$v_n = v_y = 0 \tag{2.24}$$

So, the discretized equation is the same as equation 2.23. Although, in this case these nodes will not be included in the iterative solver because its streamlines are already known (the streamline remains constant along the wall).

Velocity computation

In this section it will be discussed how to calculate the velocity at each node.

At each face of the control volume it can be obtained the velocity with the equations 2.6, 2.7, 2.8 and 2.9. In order to find the velocity vector at the node, it will be carried the arithmetic mean between the two velocities of each component:

$$v_{xP} = \frac{v_{xs} + v_{xn}}{2} \tag{2.25}$$

$$v_{yP} = \frac{v_{ye} + v_{yw}}{2} \tag{2.26}$$

Then, the velocity modulus is obtained with the following expression

$$v_P = \sqrt{v_{xP}^2 + v_{yP}^2} \tag{2.27}$$

Thermodynamic properties computation

In order to calculate the thermodynamic properties (such as temperature or pressure), it will be taken into account that the potential flow is isentropic (entropy remains constant).

To calculate the node's temperature it will be used the stagnation temperature conservation:

$$h_{in} + \frac{v_{in}^2}{2} = h_P + \frac{v_P^2}{2} \tag{2.28}$$

Operating with the enthalpy and reorganizing terms it can be obtained the node's temperature

$$T_P = T_{in} + \frac{v_{in}^2 - v_P^2}{2\overline{c_{p_P}}} \tag{2.29}$$

where

$$\overline{c_{p_P}} = \frac{1}{T_P^* - T_{in}} \cdot \int_{Tin}^{T_P^*} c_p dT \tag{2.30}$$

To find the node's pressure, it will be used the isentropic relationship between pressure and temperature

$$P_P = P_{in} \cdot \left(\frac{T_P}{T_{in}}\right)^{\frac{\widehat{\gamma_P}}{\widehat{\gamma_P}-1}} \tag{2.31}$$

where

$$\widehat{c_p} = \frac{1}{ln\left(\frac{T_P^*}{T_{in}}\right)} \int_{T_{in}}^{T_P^*} c_p dT \tag{2.32}$$

$$\widehat{\gamma_P} = \frac{\widehat{c_p}}{\widehat{c_p} \cdot R} \tag{2.33}$$

In this case, R refers to the ideal gas constant ($8.31 \frac{J}{kgK}$).

Finally, the density can be found considering the ideal gas state equation

$$\rho_P = \frac{P_P}{R \cdot T_P} \tag{2.34}$$

Object's streamline

Through out all this section it has been analyzed the streamlines on the fluid in order to calculate all the other properties (velocity, temperature, pressure, density). Nevertheless, it has not been analyzed the interference of the object inside the fluid. This object will be a streamline, but this streamline will not be trivial to find.

The procedure to follow up will be an iterative process with the body's streamline (ψ_{body}) until a condition is accomplished. For example, in the case of the cylinder a condition can be that the circulation around the body is known (or the angular velocity) or a velocity the velocity is known in a point of the cylinder. In the case of an airfoil (such as a NACA airfoil), the condition can be the Kutta condition (the velocity must be zero on the trailing edge).

Algorithm of resolution

To end up with the streamline method, it will be presented the algorithm of resolution for this method.

1. Input data
   - 1.1. Physical data: inlet flow conditions, problem's height and width and fluid properties
   - 1.2. Numerical data: number of horizontal control volumes (N), number of vertical control volumes (M), relaxation factor (f_r), maximum error allowed (δ).
2. Previous calculations: mesh generation, identification of solid and fluid control volumes.
3. Inlet flow conditions: $\psi[0][j] = \psi[0][j-1] + v_{in} \cdot \Delta y$
4. If ϕ_{body} is unknown, estimate ϕ_{body}
5. Estimated values for fluid nodes
   - 5.1. $\psi^*[i][j] = \psi[0][j]$
   - 5.2. $\rho^*[i][j] = \rho_{in}$
   - 5.3. $T^*[i][j] = T_{in}$
   - 5.4. $P^*[i][j] = P_{in}$

6. Discretization coefficients computation
7. Computation of $\psi[i][j]$
   7.1. $\psi[i][j] = (a_E[i][j] \cdot \psi[i+1][j] + a_W[i][j] \cdot \psi[i-1][j] + a_N[i][j] \cdot \psi[i][j+1] + a_S[i][j] \cdot \psi[i][j-1])/a_P[i][j]$
   7.2. $\psi[i][j] = \psi^*[i][j] + f_r \cdot (\psi[i][j] - \psi^*[i][j]$
8. Velocity computation
9. Thermodynamic properties computation (T, P, ρ)
10. Is $max|\phi_P - \phi_P^*| < \delta$? $(\phi = T, P, \rho)$
    a. Yes $\rightarrow$ go to 11
    b. No $\rightarrow \phi_P^* = \phi_P$ $(\phi = T, P, \rho) \rightarrow$ go to 6
11. Is the object's condition accomplished?
    a. Yes $\rightarrow$ go to 12
    b. No $\rightarrow \phi_P^* = \phi_P$ $(\phi = T, P, \rho) \rightarrow$ It is the first ψ_{body} iteration?
       b.a Yes $\rightarrow$ Estimate new $\psi_{body} \rightarrow$ go to 6
       b.b No $\rightarrow$ With Newton-Raphson methodology find the new $\psi_{body} \rightarrow$ go to 6
12. Final calculations and print results
13. End

2.3.2 Velocity potential

The velocity potential can be defined as

$$\vec{v} = -\nabla\phi \tag{2.35}$$

where

$$v_x = -\frac{\partial\phi}{\partial x} \tag{2.36}$$

$$v_y = -\frac{\partial\phi}{\partial y} \tag{2.37}$$

As it has been mentioned before, the velocity potential treats irrotational potential flows. This can be verified by the definition of rotational vector:

$$\vec{\omega} = \int_{S_p} (\nabla \wedge \vec{V}) dS = -\int_{S_p} (\nabla \wedge (\nabla\phi)) dS = 0 \tag{2.38}$$

The equation 2.35 is obtained from the mass conservation equation. This equation will be the procedure's start point.

Internal nodes (i=1 to N, j=1 to M)

In a steady 2D flow, the mass conservation equation can be written as

$$\int_{S_p} (\rho \cdot \vec{v} \cdot \vec{n}) dS = 0 \tag{2.39}$$

This equation can be discretized as

$$\rho_e v_{xe} S_e - \rho_w v_{xw} S_w + \rho_n v_{yn} S_n - \rho_s v_{ys} S_s = 0 \tag{2.40}$$

Following the second order approximation on the derivative, the velocities on the control volume faces can be defined as

$$v_{xe} = -\frac{\phi_E - \phi_P}{d_{PE}} \tag{2.41}$$

$$v_{xw} = -\frac{\phi_W - \phi_P}{d_{PW}} \tag{2.42}$$

$$v_{ys} = -\frac{\phi_S - \phi_P}{d_{PS}} \tag{2.43}$$

$$v_{yn} = -\frac{\phi_N - \phi_P}{d_{PN}} \tag{2.44}$$

The surfaces can be expressed on the folling way

$$S_e = S_w = \Delta y \cdot W \tag{2.45}$$

$$S_n = S_s = \Delta x \cdot W \tag{2.46}$$

where W corresponds to the prism depth.

Operating and reorganizing terms it can be obtained the following equation.

$$a_P \cdot \psi_P = a_E \cdot \psi_E + a_W \cdot \psi_W + a_S \cdot \psi_S + a_N \cdot \psi_N + b_P \tag{2.47}$$

In this case the coefficients will have the following values:

$$a_E = \frac{\rho_e}{d_{PE}} \Delta y_P \tag{2.48}$$

$$a_W = \frac{\rho_w}{d_{PW}} \Delta y_P \tag{2.49}$$

$$a_S = \frac{\rho_s}{d_{PS}} \Delta x_P \tag{2.50}$$

$$a_N = \frac{\rho_n}{d_{PN}} \Delta x_P \tag{2.51}$$

$$a_P = a_E + a_W + a_N + a_S \tag{2.52}$$

$$b_P = 0 \tag{2.53}$$

As it has been done with the streamline method, the densities on the control volume faces will be calculated with the harmonic mean.

Left nodes (i=0)

The condition that this nodes must accomplish is that the its velocity should be the inlet velocity, so the equation that must be satisfied is:

$$v_{in} = -\frac{\partial \phi}{\partial x} \approx -\frac{\phi_E - \phi_P}{d_{PE}} \tag{2.54}$$

Reorganizing terms in this equation it can be achieved the equation 2.47, where the coefficients will have the following values

$$a_N = 0 \tag{2.55}$$

$$a_S = 0 \tag{2.56}$$

$$a_W = 0 \tag{2.57}$$

$$a_E = 1 \tag{2.58}$$

$$a_P = 1 \tag{2.59}$$

$$b_P = -v_{in} \cdot d_{PE} \tag{2.60}$$

Right nodes (i=N+1)

In a same way as in the streamline method, the outlet flow velocity is supposed to be horizontal (and it is not known). So the condition can be represented as

$$v_y = -\frac{\partial \phi}{\partial y} \approx 0 \rightarrow \phi = constant \tag{2.61}$$

In order to determinate an unique solution, the velocity potential value at one node of these will be imposed to be 0 (it has been done the same on the streamline method but imposing the value on one of the left nodes).

Top and bottom nodes (j=0 & M+1)

For these nodes, as it happened with the right nodes, the condition is the same as in the streamline method, there is no vertical velocity on this nodes.

$$v_y = -\frac{\partial \phi}{\partial y} = 0 \tag{2.62}$$

For the top nodes the discretized equation is

$$\phi_P = \phi_S \tag{2.63}$$

and for the bottom nodes

$$\phi_P = \phi_N \tag{2.64}$$

Further calculus

The velocity computation and the thermodynamic properties as temperature, pressure and density can be computed in the same way as it has been explained on the streamline method, because it has been taken into account the same hypothesis to develop this resolution. The only difference is the computation of the control volume faces velocities, that in this case can be obtained with the equations 2.41, 2.42, 2.43 and 2.44. Also, when it is being computed the velocity, it must be evaluated the mass flow through this face, due to the fact that in this method it does not appear the density on the face to compute the velocity, so without the mass flow it would not be possible to distinguish fluid from solid faces. Analyzing the mass flow, if it is zero (or close to zero), the velocity will be imposed to be zero (there is no mass flow through the solid object).

Object's velocity potential

In the velocity potential method, the object's density will be 0 (through the object there will no be inner neither outer flux) and its velocity potential value will be arbitrary imposed to 0. The main reason for this is that this value will not affect on the solution.

The main difference from the streamline method is that in this method it is not need an iterative process to find the object's velocity potential.

Algorithm of resolution

As it has been done on section 2.3.1, it will be presented the algorithm of resolution for the velocity potential method.

1. Input data
   - 1.1. Physical data: inlet flow conditions, problem's height and width and fluid properties
   - 1.2. Numerical data: number of horizontal control volumes (N), number of vertical control volumes (M), relaxation factor (f_r), maximum error allowed (δ).
2. Previous calculations: mesh generation, identification of solid and fluid control volumes.
3. Right nodes potential velocity value $\phi[N+1][j] = 0$
4. Estimated values for fluid nodes
   - 5.1. Estimate the velocity value as it were the case of undisturbed flow.
   - 5.2. $\rho^*[i][j] = \rho_{in}$
   - 5.3. $T^*[i][j] = T_{in}$

5.4. $P^*[i][j] = P_{in}$

5. Distretization coefficients computation

6. Computation of $\phi[i][j]$

6.1. $\phi[i][j] = (a_E[i][j] \cdot \phi[i+1][j] + a_W[i][j] \cdot \phi[i-1][j] + a_N[i][j] \cdot \phi[i][j+1] + a_S[i][j] \cdot \phi[i][j-1] + b_P[i][j])/a_P[i][j]$

6.2. $\phi[i][j] = \phi^*[i][j] + f_r \cdot (\phi[i][j] - \phi^*[i][j]$

7. Velocity computation

8. Thermodynamic properties computation (T, P, ρ)

9. Is $max|\Phi_P - \Phi_P^*| < \delta$? $(\Phi = T, P, \rho)$

a. Yes $\rightarrow$ go to 10

b. No $\rightarrow \Phi_P^* = \Phi_P$ $(\Phi = T, P, \rho) \rightarrow$ go to 5

10. Final calculations and print results

11. End

2.3.3 Lift and Drag computation

Once it has been computed the properties at each node (it has been converged to a solution), some extra calculus will be taken so as to get further information from the solution. In this section it is going to be explained how is it going to be computed the lift (L), the drag (D) and its non-dimensional coefficient (c_l and c_d) [2].

Before computing these forces, it should be computed the normal vector to the object at each boundary node and the differential of the object's boundary surface (dS) that is on each node.

In the case of the cylinder, the dS will be the same on each node and will be approximated to:

$$dS = \frac{2\pi R^2}{N_{bound.nodes}} \tag{2.65}$$

The normal vector will be computed as it is represented on the following equation

$$\vec{n} = \frac{\vec{r} - \vec{C}}{R} \tag{2.66}$$

[2]Note that this coefficients are represented with lowercase letter because it is treated a 2-dimensional problem

where $\vec{r}$ represents the node's position and $\vec{C}$ represent the cylinder's center. With this, it can be computed the lift and drag forces

$$L = -\sum_{k=1}^{N_{bound.nodes}} P_k n_{y_k} dS \tag{2.67}$$

$$D = -\sum_{k=1}^{N_{bound.nodes}} P_k n_{x_k} dS \tag{2.68}$$

And the coefficients can be adimensionalized as:

$$c_l = \frac{L}{\frac{1}{2}\rho v^2 R} \tag{2.69}$$

The same expression can be used for the drag coefficient.

2.4 Verification

Before presenting the numerical and physical results, it has been carried out some verifications to ensure that the code and the results that will be obtained are correct.

2.4.1 Numerical verification

A numerical verification that it has been done is, for the streamline method, the accomplishment of the rotational on each control volume. Due to the fact it is treated an irrotational flow, the equation to verify is the equation 2.3. For the velocity potential, it has been verified the accomplishment of the mass conservation equation at each control volume (concretely, equation 2.40).
For both cases, the maximum error of these equations has the same order of the maximum convergence error allowed (δ).

2.4.2 Uniform flow

An other code verification has been to simulate an uniform flow. In terms of code, it has not been changed anything except for the cylinder's radius, which has been turned to 0. As it can be on figures 2.4 and 2.5, the streamlines (in case of figure 2.4) or the lines of constant velocity potentials (in case of figure 2.5) are parallel and equidistant one to each other, which means that the velocity remains constant (undisturbed).

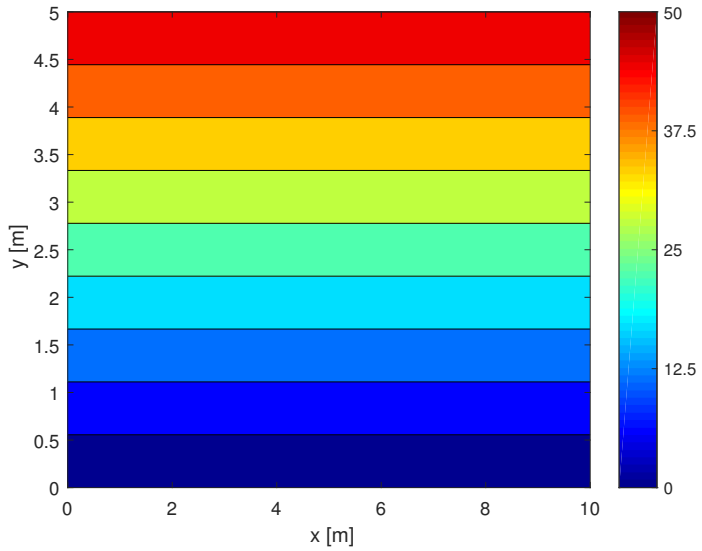

FIGURE 2.4: Streamlines on an uniform horizontal flow

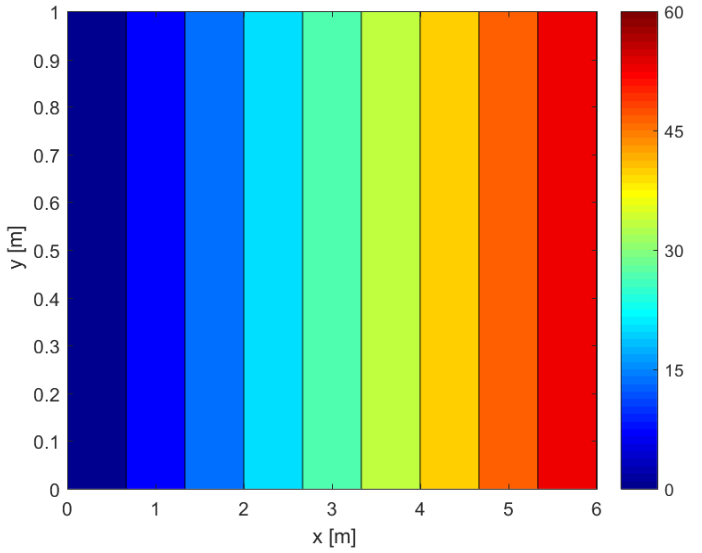

FIGURE 2.5: Lines of constant potential velocity on an uniform horizontal flow

Also, it must be noticed that streamlines are perpendicular to lines of constant potential velocity, which it can be proved developing the following statement:

$$\Delta\psi \cdot \Delta\phi = 0 \tag{2.70}$$

A part from the horizontal flow, it has been also analysed the vertical flow, where it is only changed the boundary conditions.

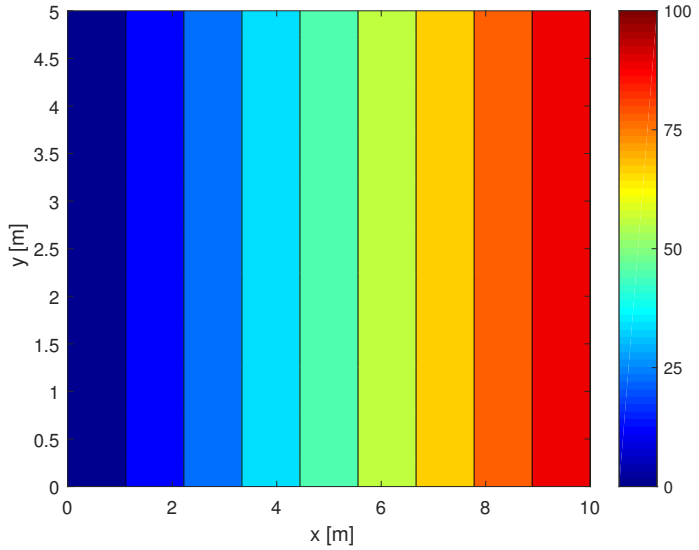

FIGURE 2.6: Streamlines on an uniform vertical flow

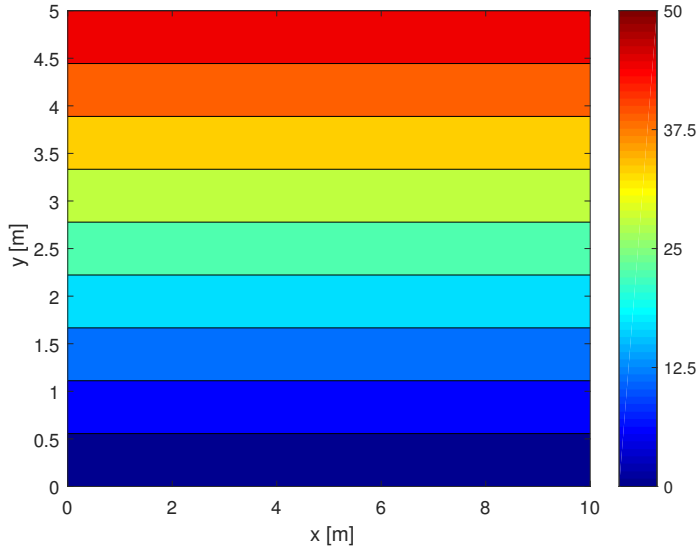

FIGURE 2.7: Lines of constant potential velocity on an uniform horizontal flow

As it can be seen, the solutions obtained are analogous to the ones obtained on the horizontal flow, the streamlines (and the lines of constant velocity potential) are parallel

and equidistant between them and the streamlines are perpendicular to the lines of constant potential velocity.

2.4.3 Incompressible potential flow

An other type of verification done has been to compare the results obtained with the analytical result. In this case, it has been added an extra restriction, which has been incompressible flow.
It has been the code based on the streamline method only in two points: the density and the pressure computation. First of all, the density will remain constant along all the flow, so the parameter τ will be 1 on each fluid control volume (it can not be deleted this parameter because the faces where there is a solid-fluid contact, this parameter will be different to 1). Regarding to the pressure, instead of using the isentropic relation (the flow is not isentropic), it will be used the Bernoulli's equation for incompressible flows (considering that the potential energy remains constant):

$$\frac{1}{2}\rho_{in}v_{in}^2 + P_{in} = \frac{1}{2}\rho_{in}v_P^2 + P_P \tag{2.71}$$

Also, it has been modified the boundary condition, which in this case it will correspond to the analytical solution:

$$\psi(r,\theta) = v_{in}rsin(\theta)\left(1-\frac{R^2}{r^2}\right) + \frac{\Gamma}{2\pi}ln\left(\frac{r}{R}\right) \tag{2.72}$$

where Γ is the circulation around the cylinder

$$\Gamma = 2\pi\Omega R^2 \tag{2.73}$$

Finally, on the following figures it is represented the comparison of the numerical result and the analytical result expressed on the treated mesh:

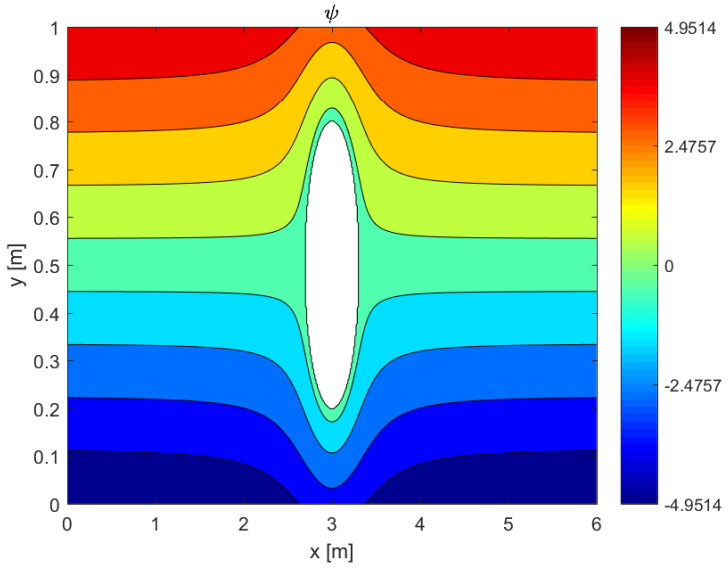

FIGURE 2.8: Analytical solution for incompressible flow ($\Omega = 0 rad/s$)

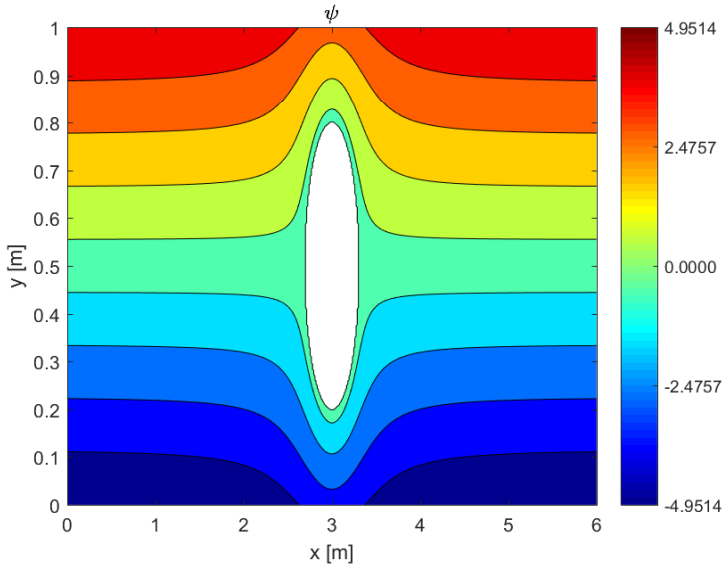

FIGURE 2.9: Numerical solution for incompressible flow ($\Omega = 0 rad/s$)

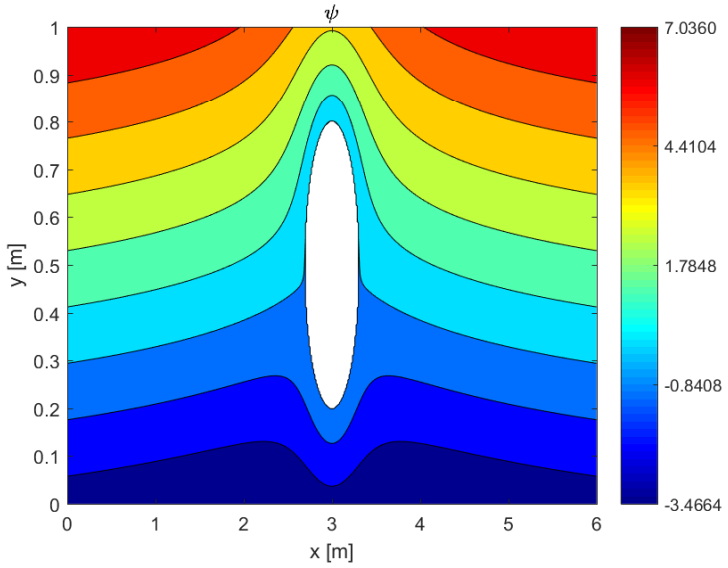

FIGURE 2.10: Analytical solution for incompressible flow ($\Omega = 10 rad/s$)

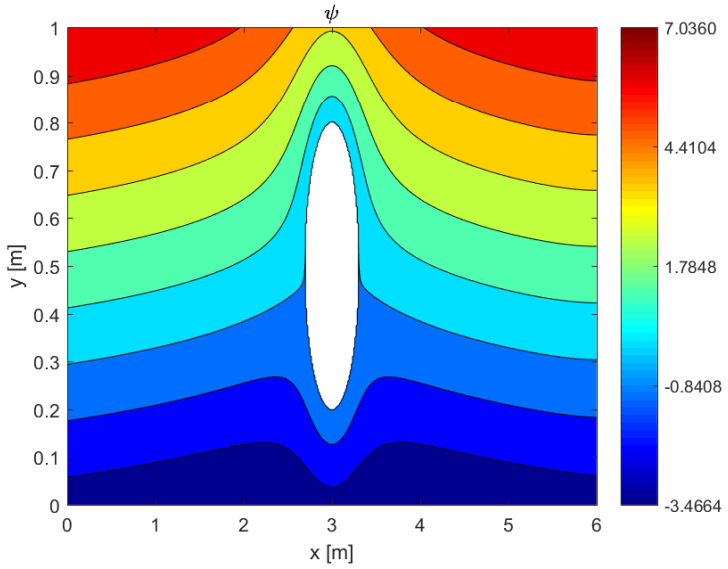

FIGURE 2.11: Numerical solution for incompressible flow ($\Omega = 10 rad/s$)

As it can be appreciated, there is no noticeable difference between the analytical solution and the numerical solutions for both the static cylinder and the cylinder rotating at 10 rad/s, which means that the code developed must be correct.

2.5 Results analysis

2.5.1 Numerical results

In this section it is going to be presented the analysis of the numerical results from the code developed.

First of all, it has been done a convergence analysis on the velocity of a point close to the cylinder, where there is a high velocity gradient and the velocity obtained is very sensitive to the mesh. In the following figure it is represented the convergence analysis for the case of a cylinder of 0.3 meters of diameter, located at the center of a rectangle with 10 meters base and 5 meters height. The point selected for the analysis has been the point located at the x-coordinate 5 and y-coordinate 2.9 meters.

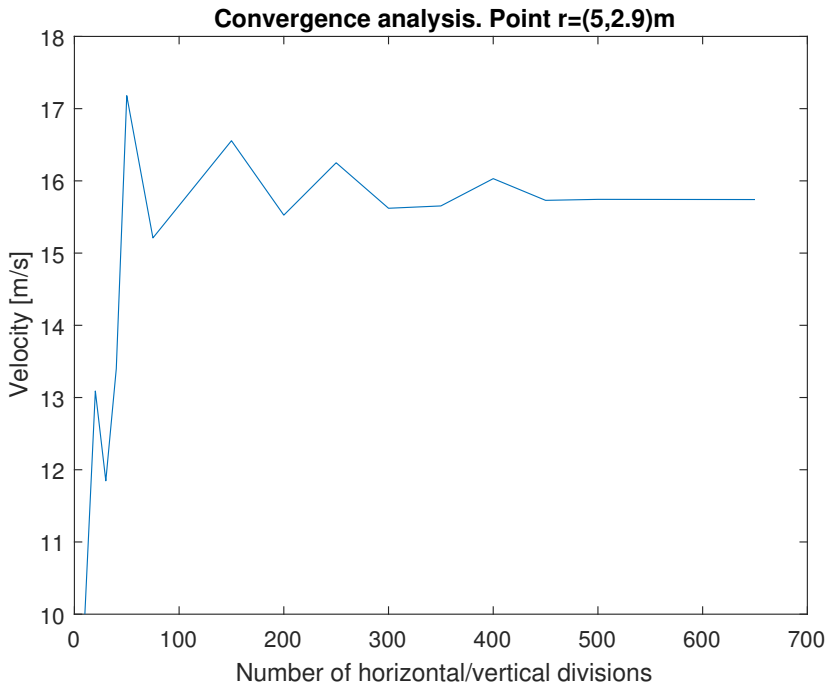

FIGURE 2.12: Convergence analysis

For the rest of analysis, it will be used a 450x450 control volumes mesh because in this mesh it has been achieved the convergence.

A part from the convergence analysis, it has been carried out a study about the influence of the relaxation factor on the computational cost.

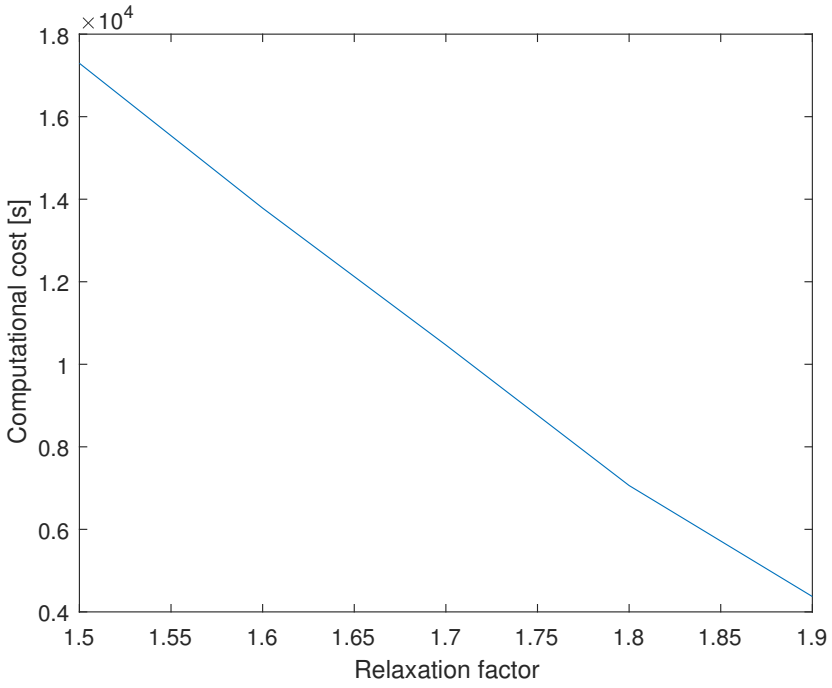

FIGURE 2.13: Influence of the relaxation factor

It must be remarked that initially it has been tested the influence of the relaxation factor for low dense mesh to realise more or less where it should be the optimum factor, which would be around 1.8. As it can be seen, for this code the relaxation factor is indispensable due to the high gain of computation time (there is a difference of more than three hours and a half of computation between using a relaxation factor of 1.9 instead of 1.5). However, the relaxation factor could not be higher than 1.9 because it appeared convergence instabilities. So, according to the previous figure, it has been chosen the factor of 1.9 in order to get the results spending the minimum time possible.

2.5.2 Physical results

In order to analyze the physical results, it has been fixed a reference case and it has been modifying only one parameter (height, type of fluid or rotating velocity) for each case so as to be easier to get conclusions while comparing the different results.

Reference case

The reference case will have the following properties:

TABLE 2.1: Reference case parameters

Height	5 m
Length	10 m
Cylinder radius	0.3 m
Cylinder's center position	(2.5,5) m
Inlet flow velocity	10 m/s
Inlet flow temperature	288 K
Inlet flow pressure	$1.013 \cdot 10^5 Pa$
Inlet flow density	1.2256 kg/m^3
Specific heat at constant pressure (air)	$c_P(T) = 1034.09 - 2.849 \cdot 10^{-1} \cdot T + 7.817 \cdot 10^{-4} \cdot T^2 - 4.971 \cdot 10^{-7} \cdot T^3 + 1.077 \cdot 10^{-10} \cdot T^4$ $[\frac{J}{kgK}]$
Air constant (R)	287 $\frac{J}{kgK}$

With all these parameters, the results are plotted on the following figures.

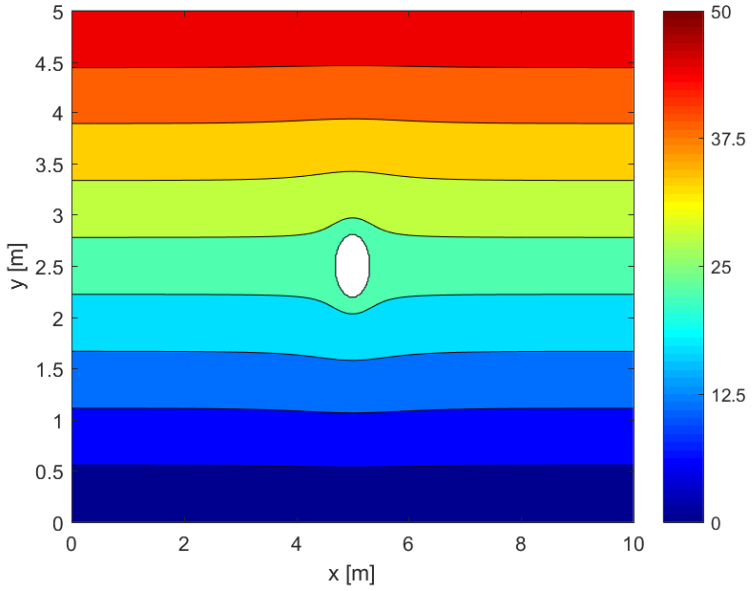

FIGURE 2.14: Streamline distribution for the reference case

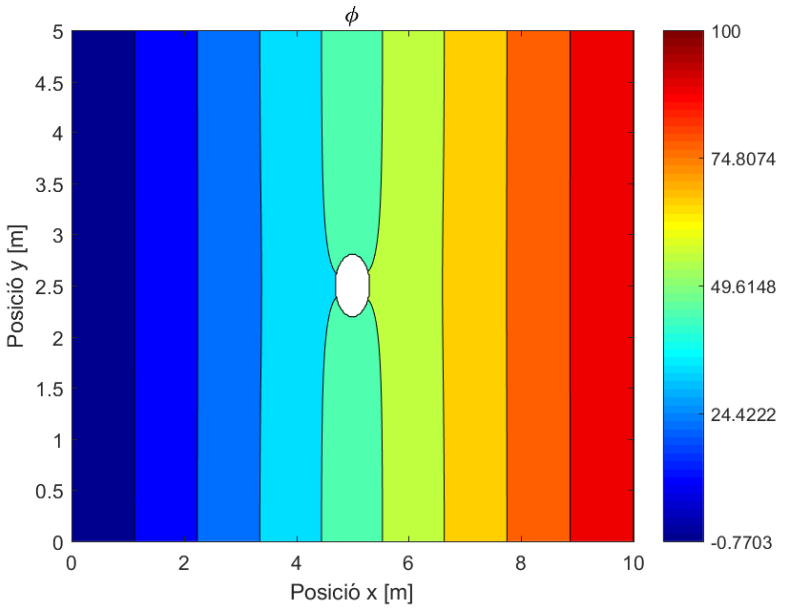

FIGURE 2.15: Velocity potential distribution for the reference case

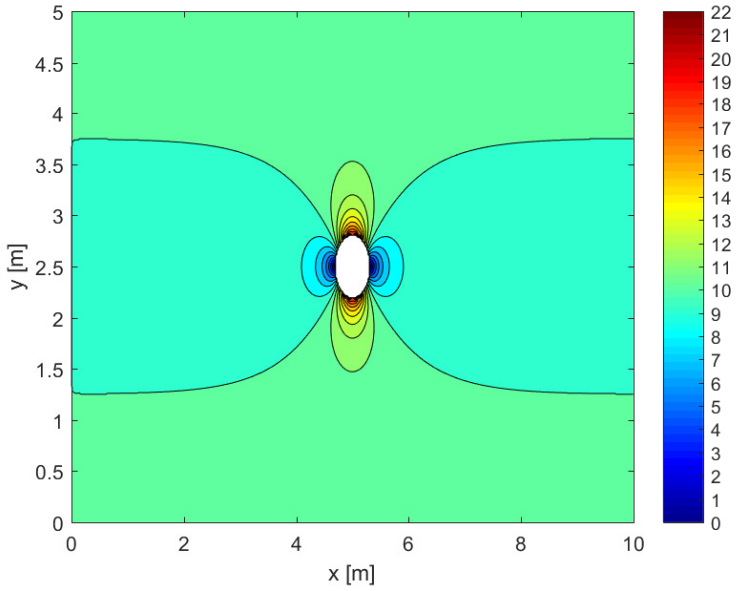

FIGURE 2.16: Velocity distribution for the reference case (in m/s)

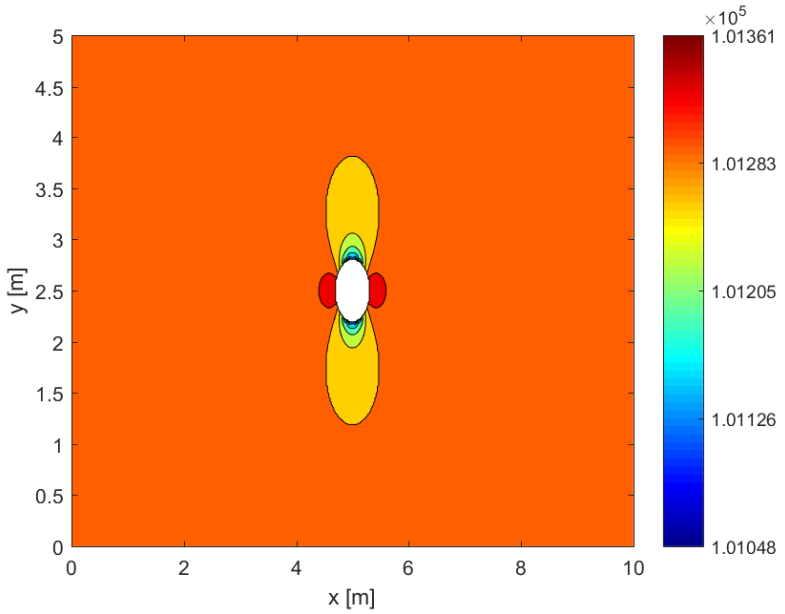

FIGURE 2.17: Pressure distribution for the reference case (in Pa)

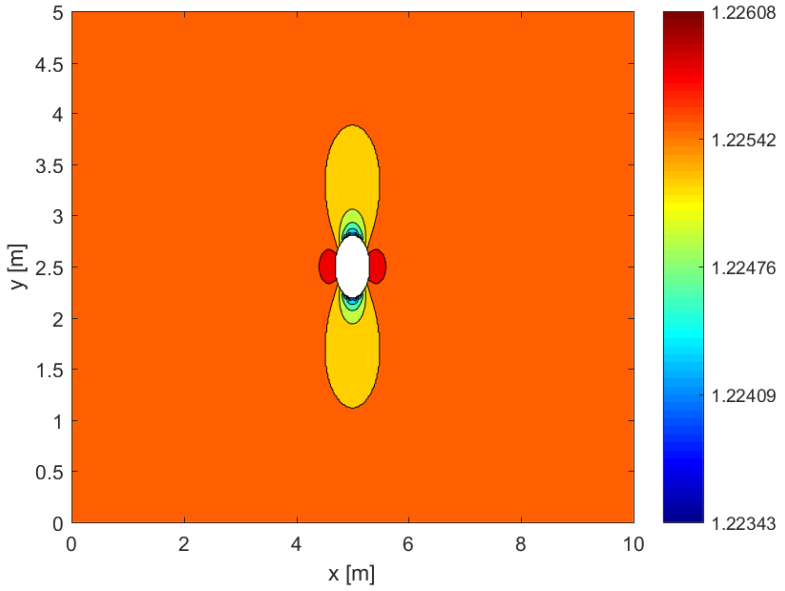

FIGURE 2.18: Density distribution for the reference case (in kg/m^3)

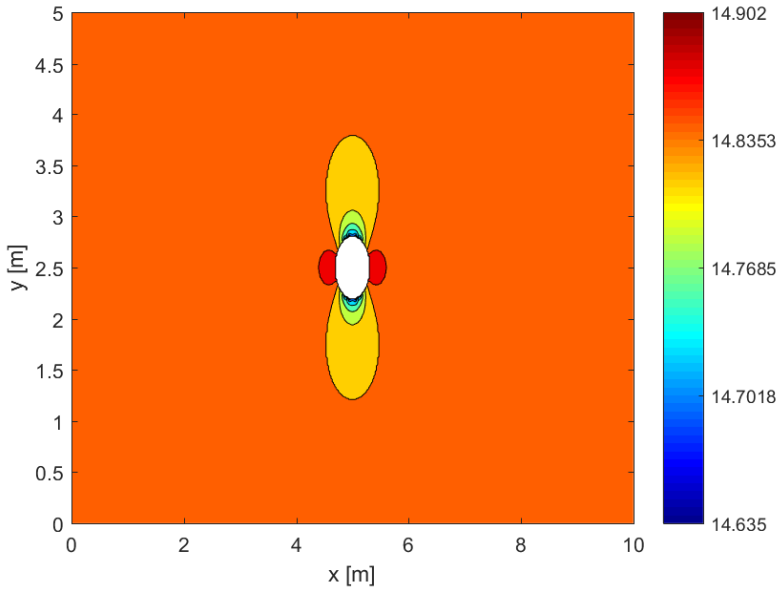

FIGURE 2.19: Temperature distribution for the reference case (in ^{o}C)

From all the previous figures it can be appreciated the symmetry of the problem, where the symmetry center corresponds to the cylinder's center. A part from this, which could be used as a way to verify the solution, it can be seen that in the cylinder's furthest points on the x-direction there is the maximum pressure, temperature and density and the minimum velocity, which corresponds to the stagnation point. However, in the cylinder's furthest points on y-direction it occurs the opposite, there is the minim pressure, temperature and density and the maximum velocity. As it has been expected, in this case the lift coefficient is close to zero, $2.81914 \cdot 10^{-5}$ (it is not exactly zero due to numerical errors) and the drag coefficient, since there is no viscosity nor boundary layer detachment, it is also close to zero, $-4.19242 \cdot 10^{-6}$.

On the other hand, another verification that could have been done for both codes is that the obtained solutions for the velocity, pressure, temperature and density are the same. However, on the following cases the potential velocity method will not be used because, although the solution is the same, its computational cost is too high compared to the streamline due to the Neumann boundary conditions presented on the inlet flow. So, at the end, it could be said the the velocity potential method has only served to verify the streamline method code.

Increasing height

In this case, the only parameter that will be changed it is the rectangle's height, which will be of 10 meters instead of 5 meters.

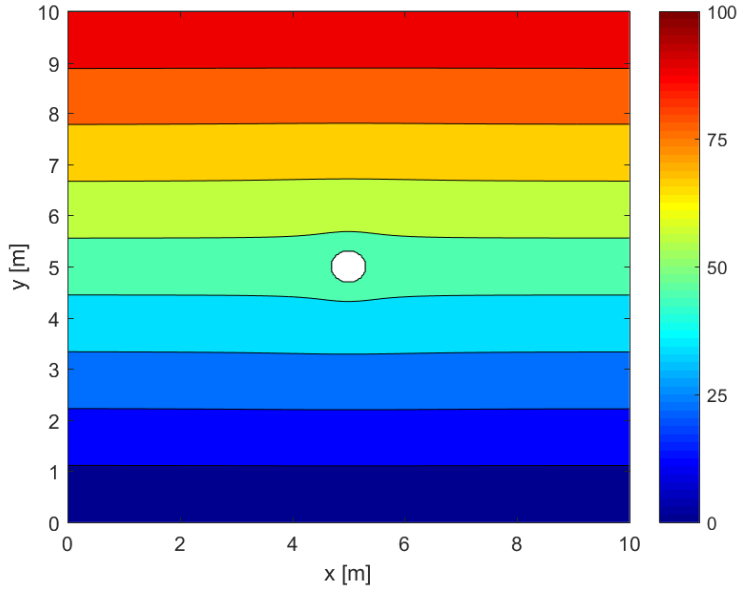

FIGURE 2.20: Streamline distribution for the increasing height case

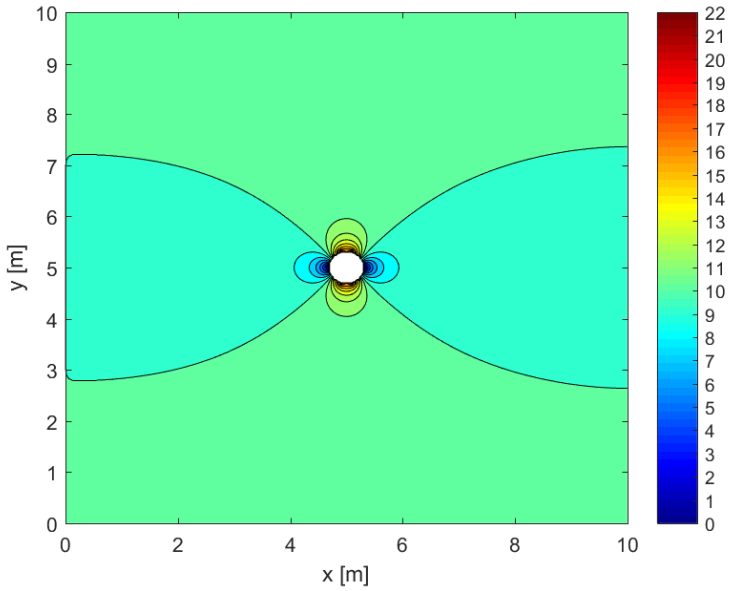

FIGURE 2.21: Velocity distribution for the increasing height case (in m/s)

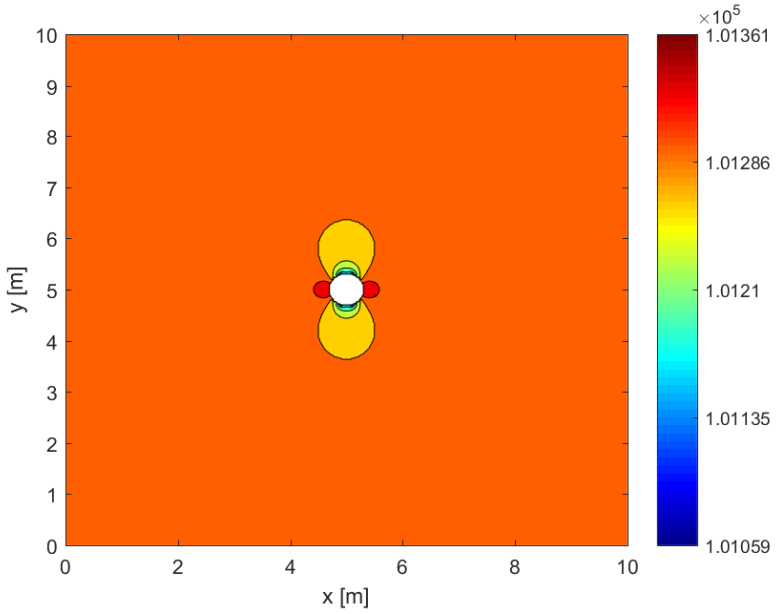

FIGURE 2.22: Pressure distribution for the increasing height case (in Pa)

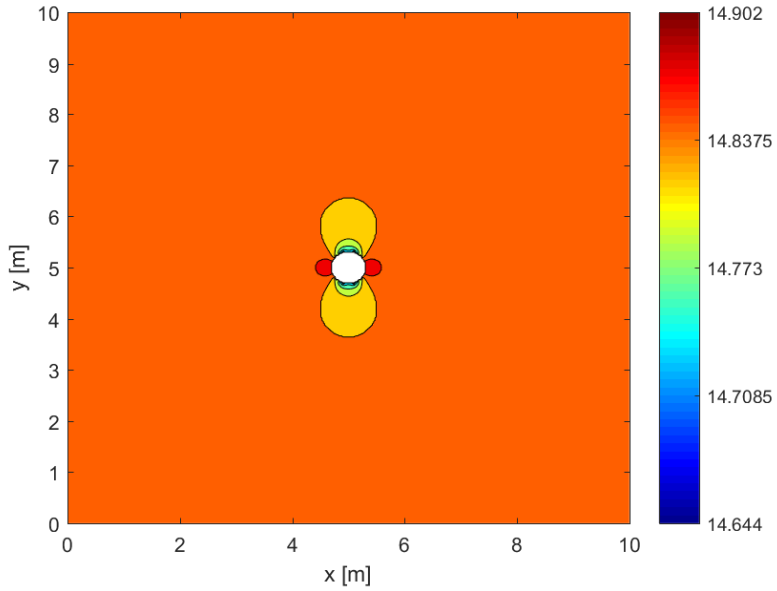

FIGURE 2.23: Temperature distribution for the increasing height case (in ^{o}C)

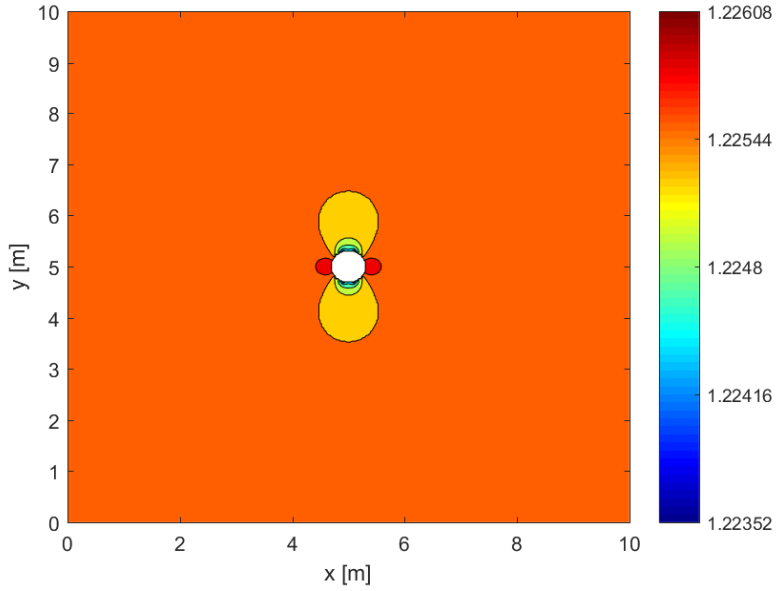

FIGURE 2.24: Density distribution for the increasing height case (in kg/m^3)

Comparing to the reference case, it can be seen that there is no difference with the thermodynamic properties, since in the reference case the top and bottom walls do not

influence the solution, which means that if the height it is increased the solution will not be changed. The only difference is that the streamlines have an other values due to the fact that it has been taken the zero on the lefter bottom corner, thus, due to the fact that there is more distance between the bottom wall and the cylinder, the cylinder's streamline will be higher.

Decreasing height

As it occurred whit the previous case, in this case it will be modified the height too, but in this case instead of increasing the height, the height will be decreased to 3 meters.

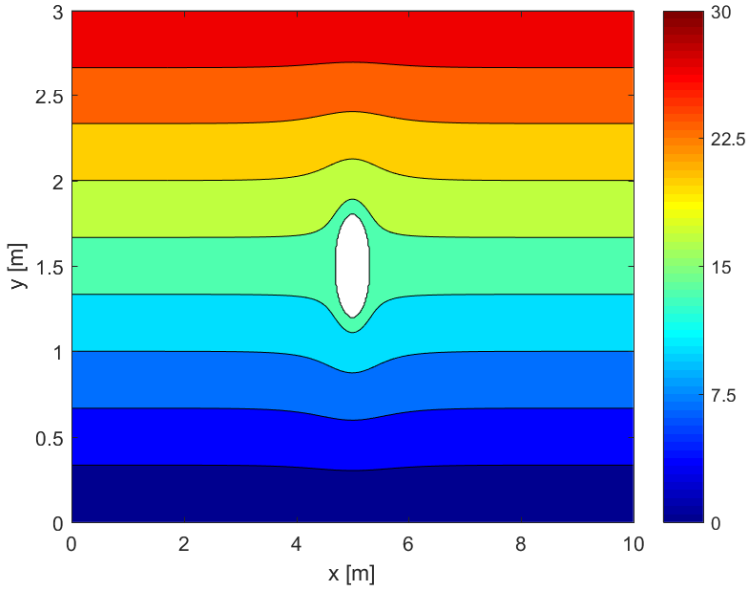

FIGURE 2.25: Streamline distribution for the decreasing height case

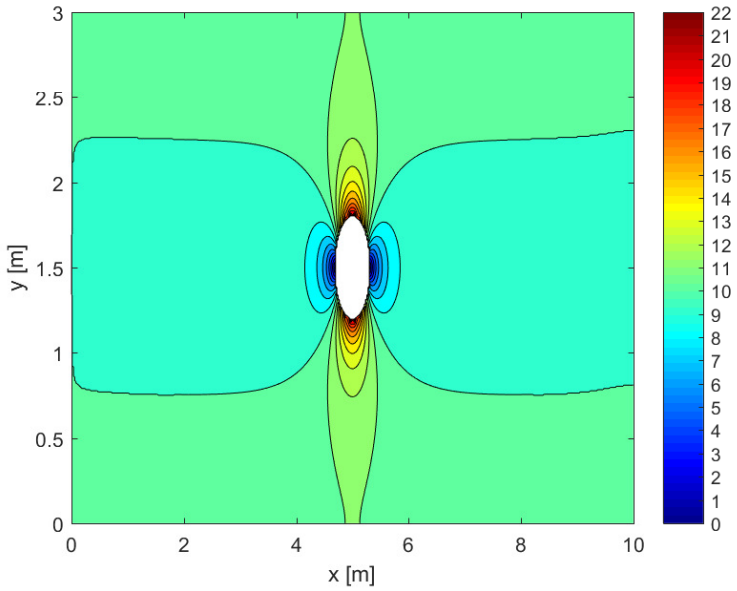

FIGURE 2.26: Velocity distribution for the decreasing height case (in m/s)

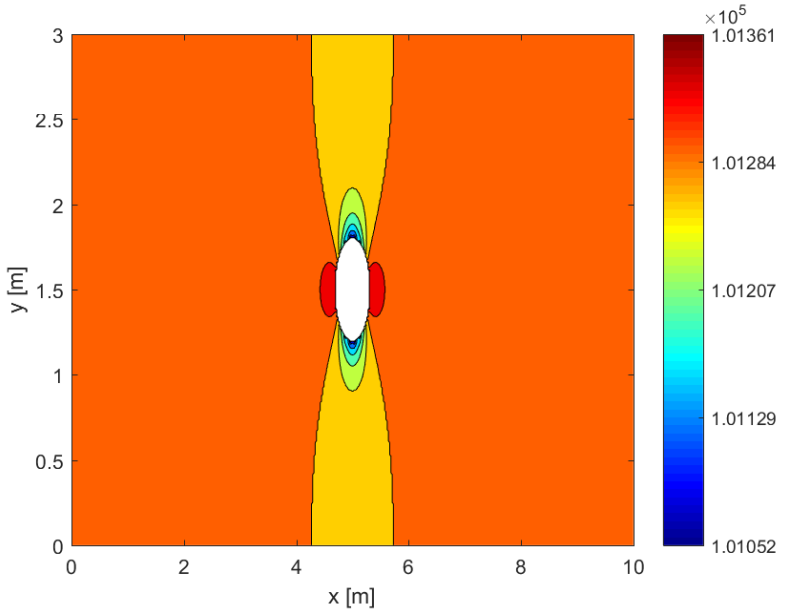

FIGURE 2.27: Pressure distribution for the decreasing height case (in Pa)

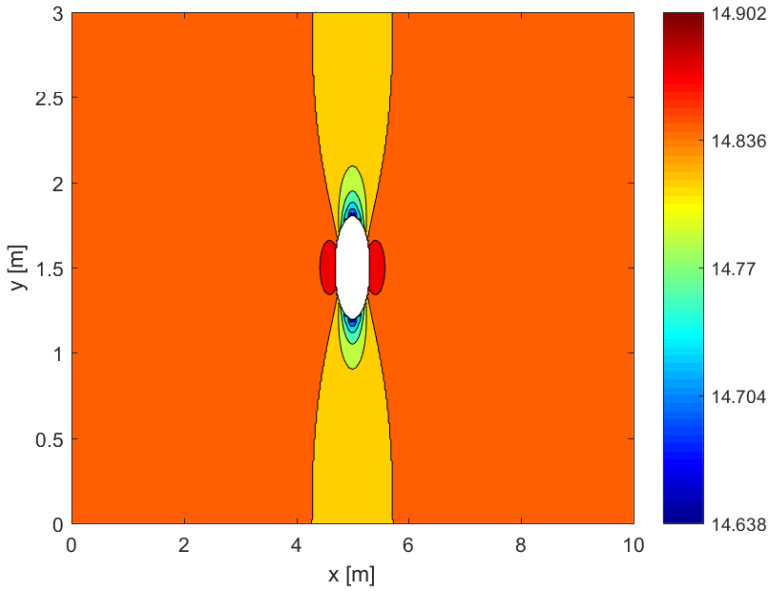

FIGURE 2.28: Temperature distribution for the decreasing height case (in ^{o}C)

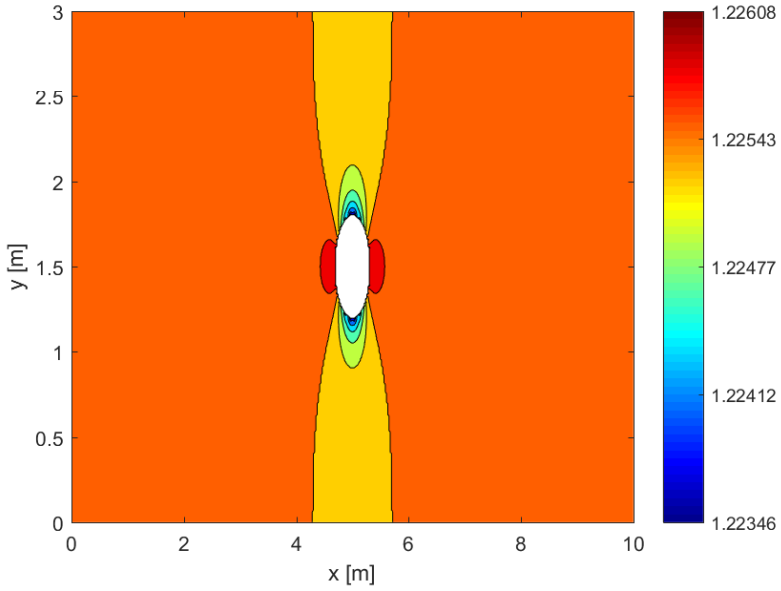

FIGURE 2.29: Density distribution for the decreasing height case (in kg/m^3)

The results obtained in this case are slightly different from the previous two cases. First of all, the streamlines distribution is a bit different, since in this case the walls have

an influence over the flow around the cylinder. This can be better appreciated on the following figures, where the velocity [3] on the top and bottom walls is not uniform, there is an acceleration on the closest points of the cylinder. Because of this, the density, pressure and temperature along the two walls are not constant. Moreover, it can also be appreciated the influence of the walls on the solution due to the fact that around the cylinder there is an increment of the maximum velocity, which in this case is of 22.48 m/s, whereas in the reference case the maximum velocity is of 22.21 m/s. With it, the minimum pressure, temperature and densities are lower than in the reference case. On the other hand, there are some similarities with the reference case, which are that the drag and lift are still zero (due to the symmetry of the problem) and the stagnation points are in the same place (on the furthest cylinder's x-coordinate points form the center), and the maximum pressure, temperature and density are the same since the lowest velocity is the same does not change (on the stagnation point the velocity is 0).

Testing another fluid

Another case that it has been studied is the change of the fluid, which instead of air it has been analyzed a gas only composed of helium. The parameters that will be modified are [15]:

- Gas constant (R): 2063 $\frac{J}{kgK}$
- Specific heat at constant pressure (c_P): 5188 $\frac{J}{kgK}$
- Taking into account the ideal gas state equation, if the inlet temperature and pressure are the same than in the reference case, the inlet density will be 0.1705 kg/m^3.

With this, the results obtained are represented on the following figures.

[3] There is a program issue with the entering and exiting velocity that it represents that this velocity is not the same along the edge and surroundings. However, it has been verified that the two exiting velocity colours represent the same velocity, $10m/s$.

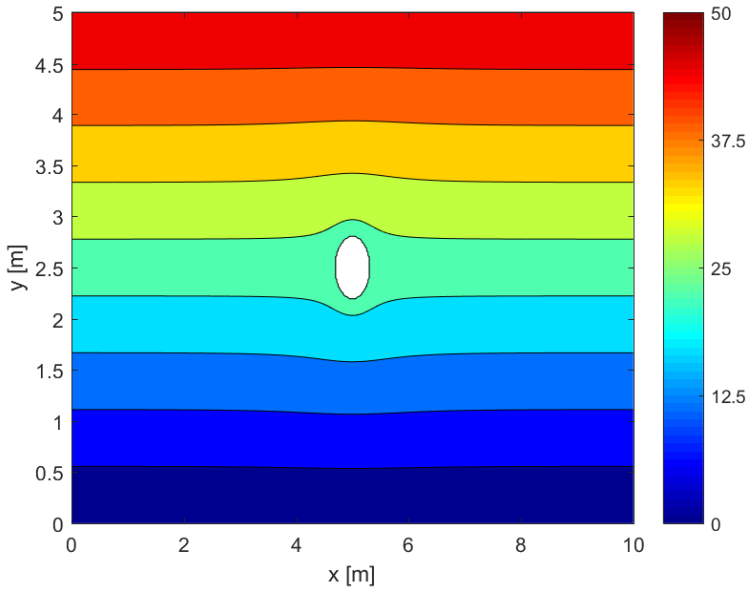

FIGURE 2.30: Streamline distribution for the Helium case

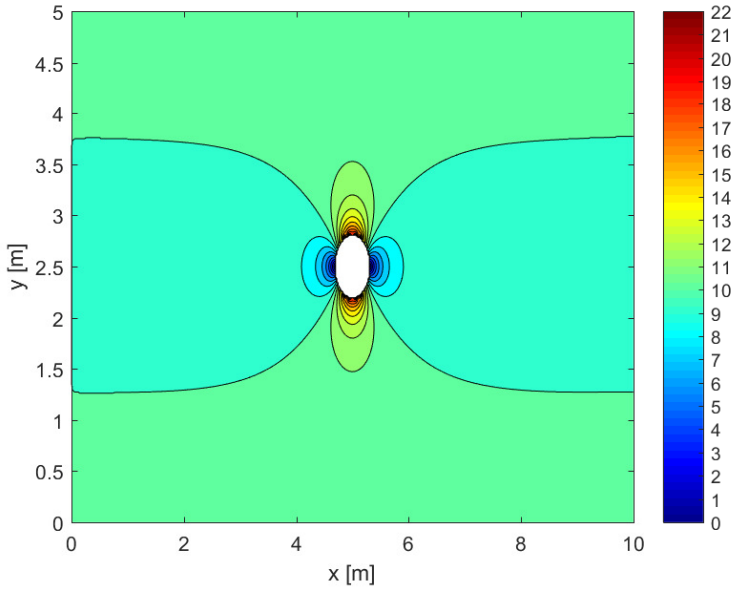

FIGURE 2.31: Velocity distribution for the Helium case (in m/s)

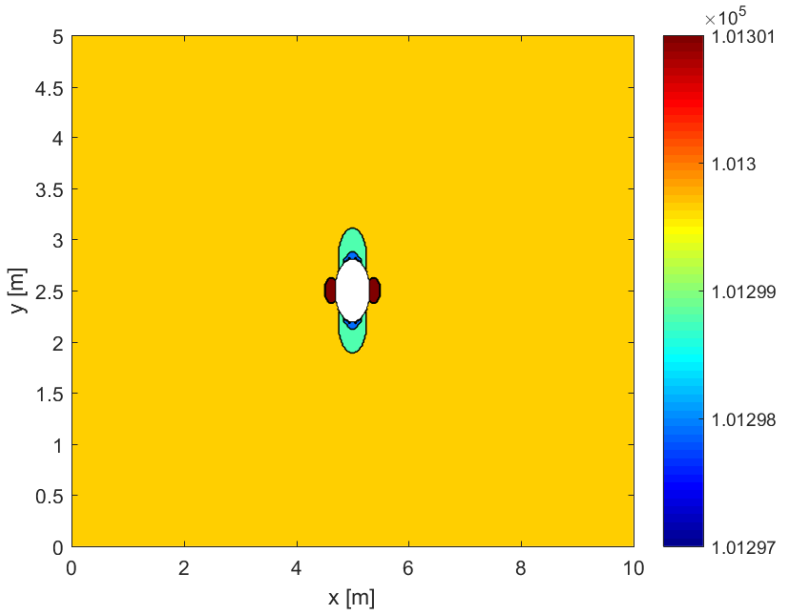

FIGURE 2.32: Pressure distribution for the Helium case (in *Pa*)

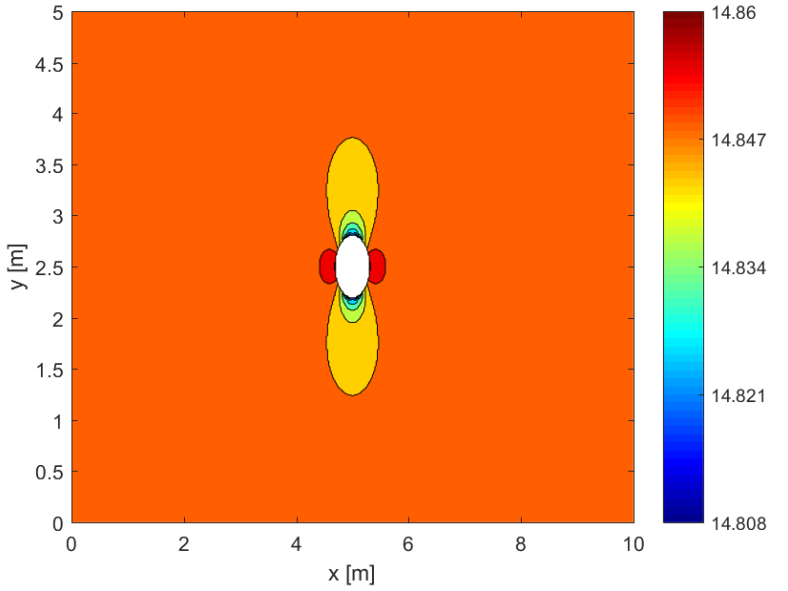

FIGURE 2.33: Temperature distribution for the Helium case (in ^{o}C)

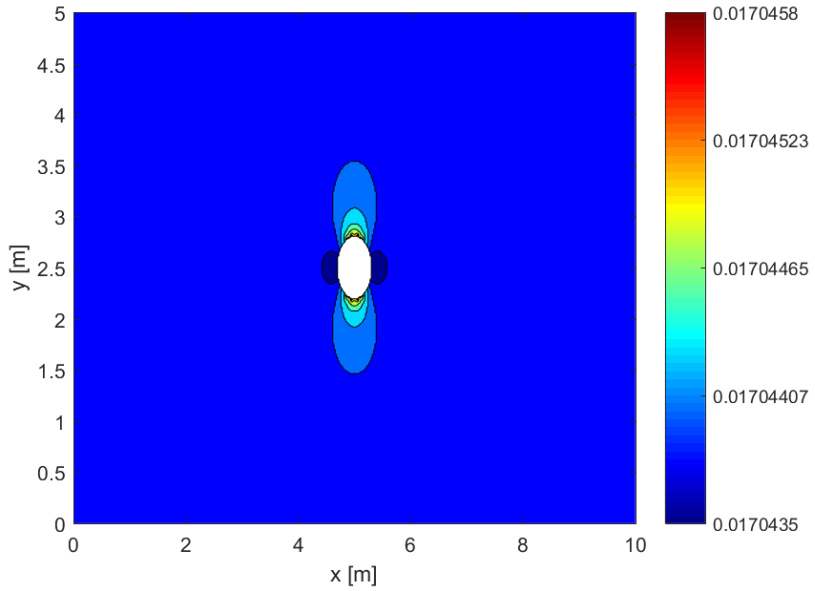

FIGURE 2.34: Density distribution for the Helium case (in kg/m^3)

As it can be seen, in this case the density, the pressure and the temperatures distribution do not have a similar shape as it occurred with the reference case. In this case, the maximum velocity (in this case is 22.59 m/s), the minimum pressure and temperature have been increased. Furthermore, it should be remarked that the maximum pressure and temperature have been decreased due to the fact that in this case the material has been changed, so on the stagnation point (where the velocity is zero) the pressure and the temperature don't have to be the same than in the case of the air. According to the density, it can be seen that in this case the variation of the density is on the sixth decimal, so the helium could be analyzed as an incompressible fluid, which would allow a lower computation cost (in incompressible flow, the thermodynamic properties are calculated after the iterations, whereas in compressible flow at each iteration all the thermodynamic properties are calculated).

Rotating velocity of 10 rad/s

In this case, it has been analyzed the results of a rotating cylinder with $\Omega = 10 rad/s$. Concretely, it has been analyzed the influence of the walls' distance and the difference between Helium and air.

The results from the reference case just varying the angular velocity are the following ones:

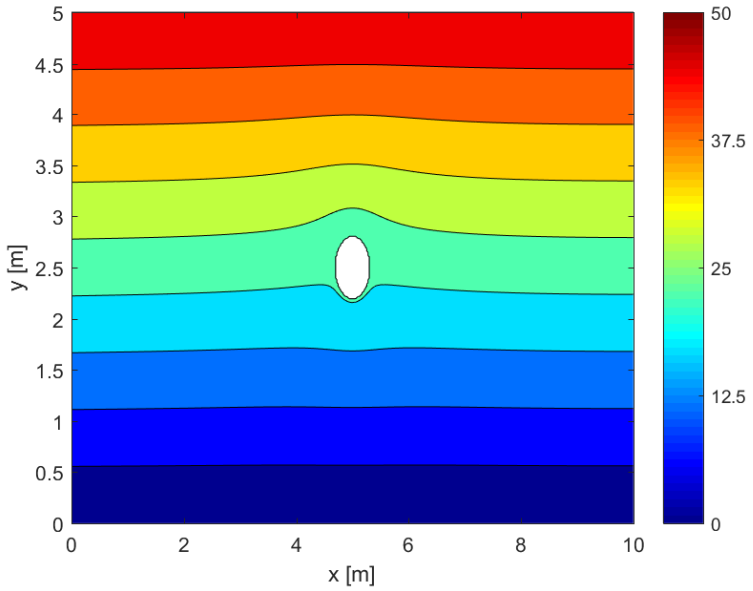

FIGURE 2.35: Streamline distribution for the reference case for $\Omega = 10 rad/s$

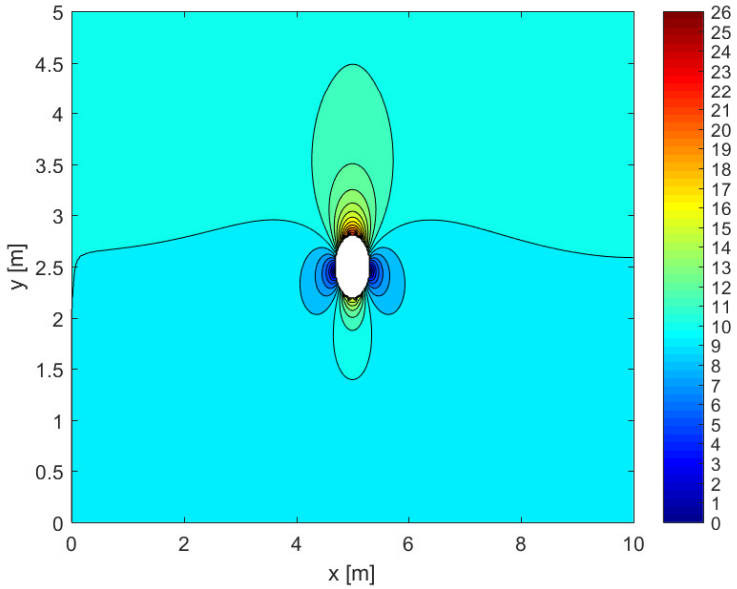

FIGURE 2.36: Velocity distribution for the reference case for $\Omega = 10 rad/s$ (in m/s)

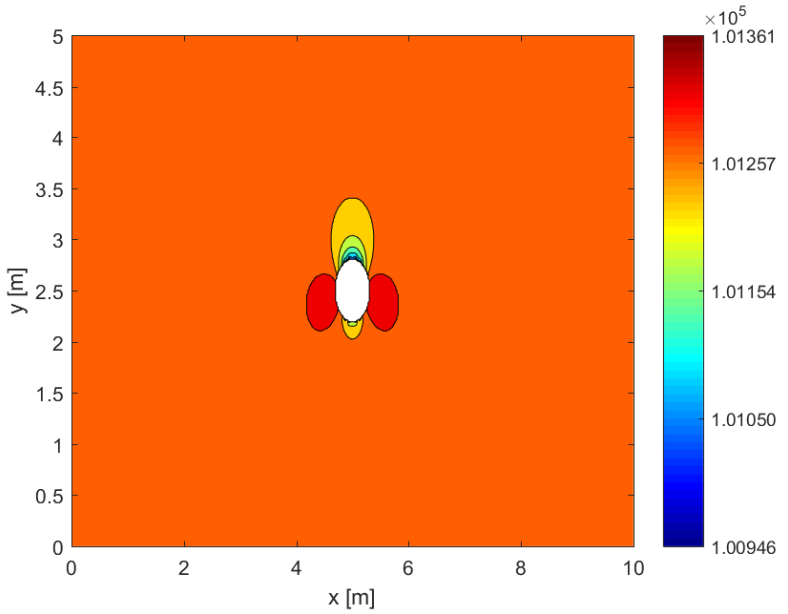

FIGURE 2.37: Pressure distribution for the reference case for $\Omega = 10 rad/s$ (in Pa)

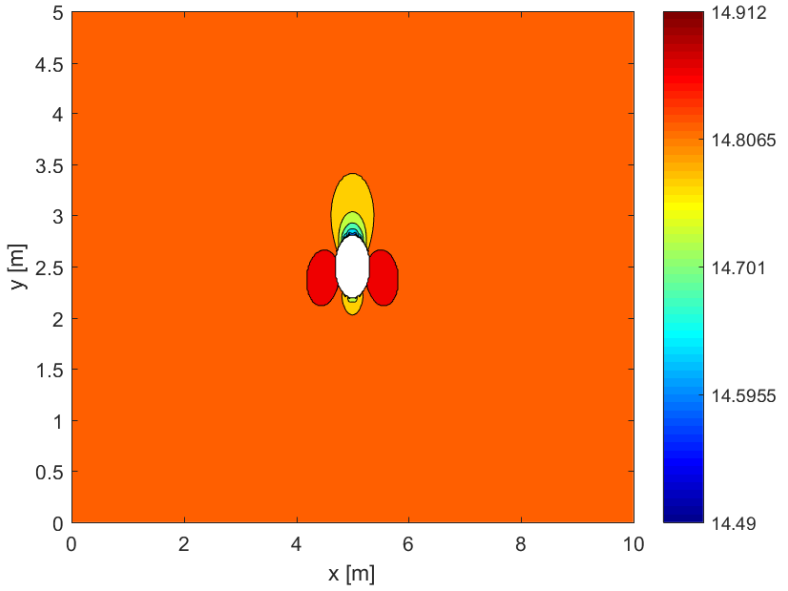

FIGURE 2.38: Temperature distribution for the reference case for $\Omega = 10 rad/s$ (in ^{o}C)

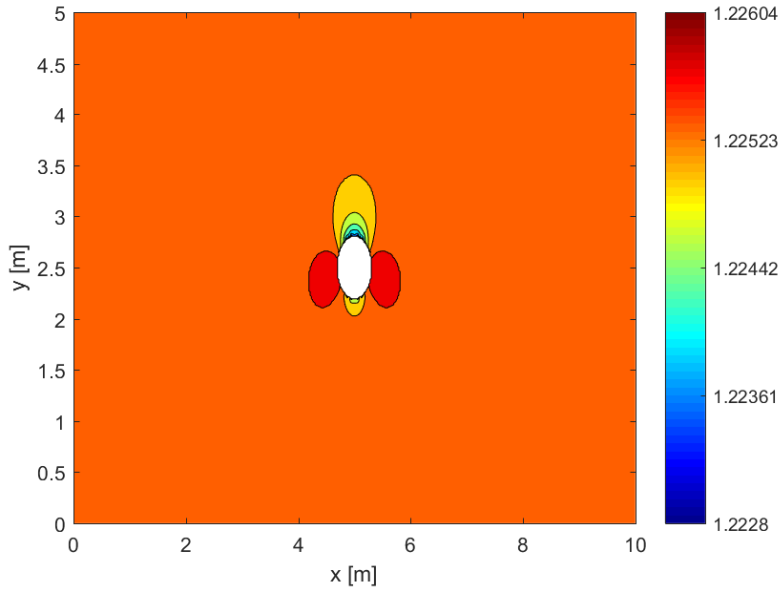

FIGURE 2.39: Density distribution for the reference case for $\Omega = 10 rad/s$ (in kg/m^3)

Also it has been tested the case with a height of 3 meters with the same angular velocity

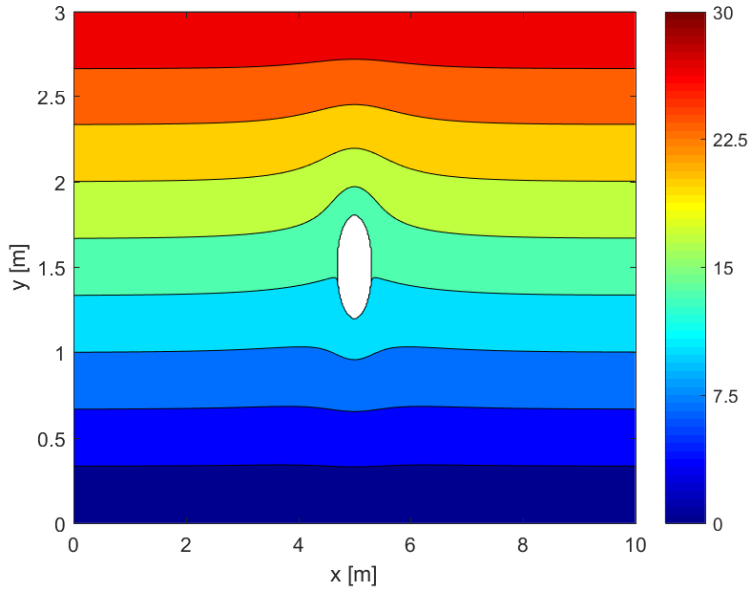

FIGURE 2.40: Streamline distribution for the decreasing height case for $\Omega = 10 rad/s$

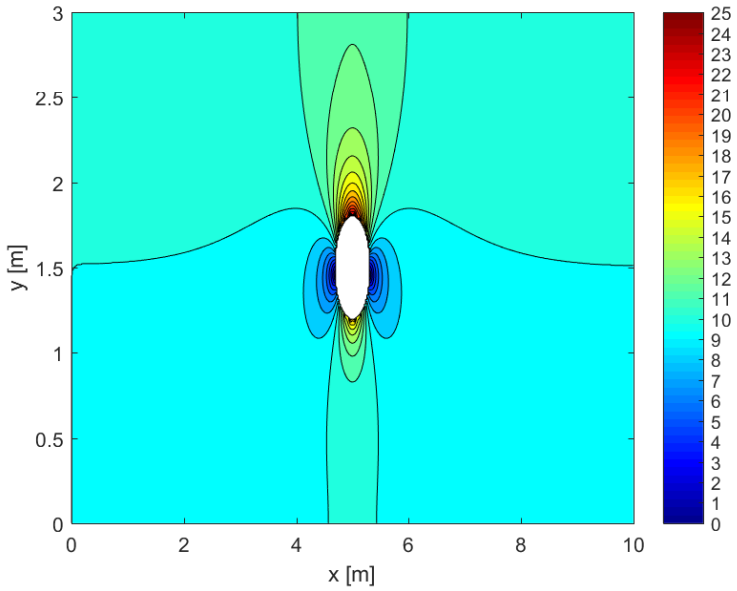

FIGURE 2.41: Velocity distribution for the decreasing height case for $\Omega = 10 rad/s$ (in m/s)

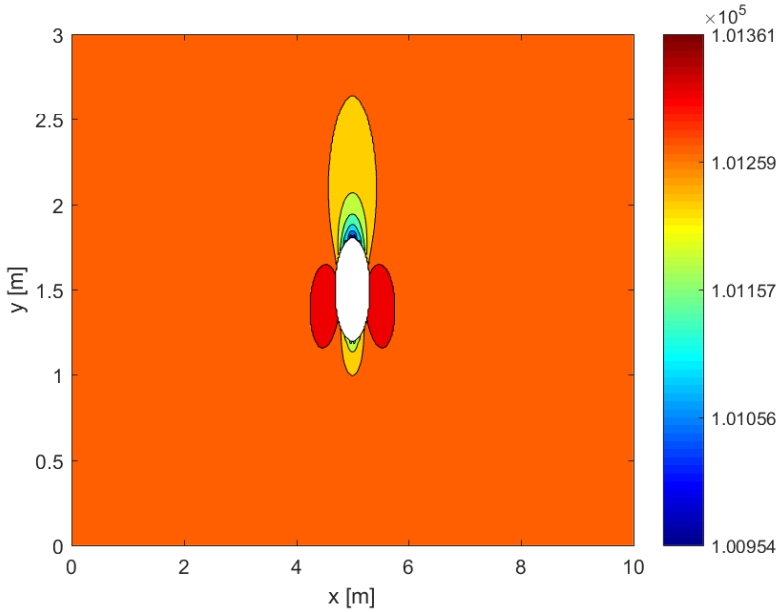

FIGURE 2.42: Pressure distribution for the decreasing height case for $\Omega = 10 rad/s$ (in Pa)

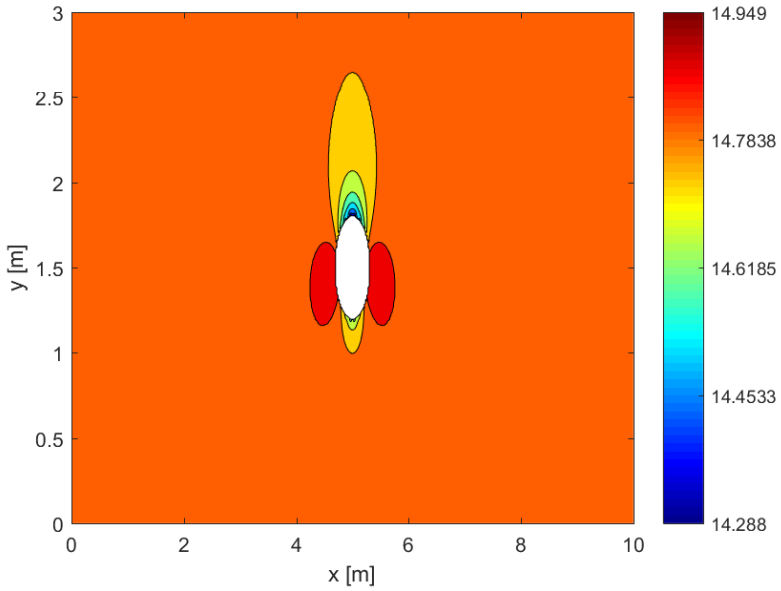

FIGURE 2.43: Temperature distribution for the decreasing height case for $\Omega = 10 rad/s$ (in ^{o}C)

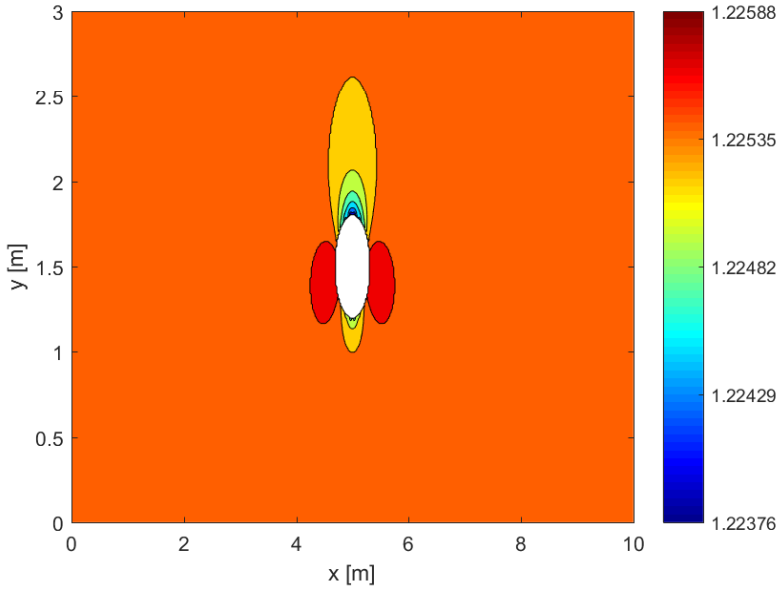

FIGURE 2.44: Density distribution for the decreasing height case for $\Omega = 10 rad/s$ (in kg/m^3)

And finally, it has been also solved the case of Helium maintaining the height of 5 meters:

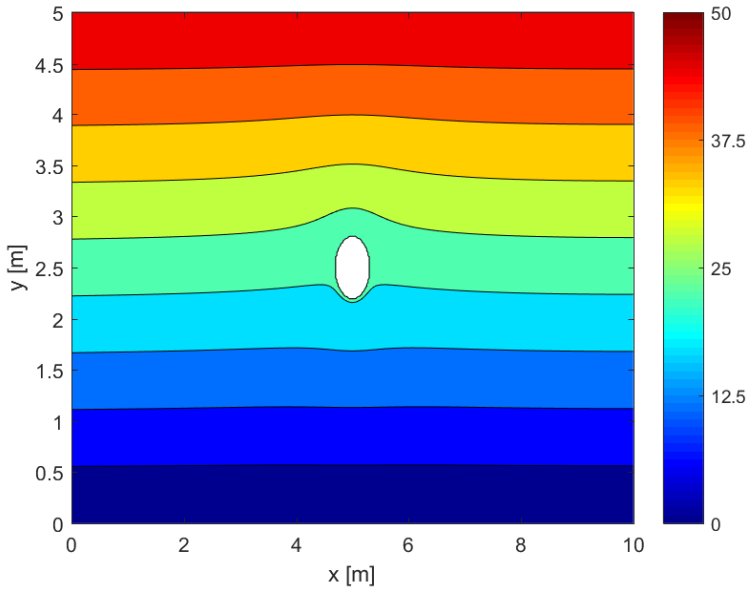

FIGURE 2.45: Streamline distribution for the Helium case for $\Omega = 10 rad/s$

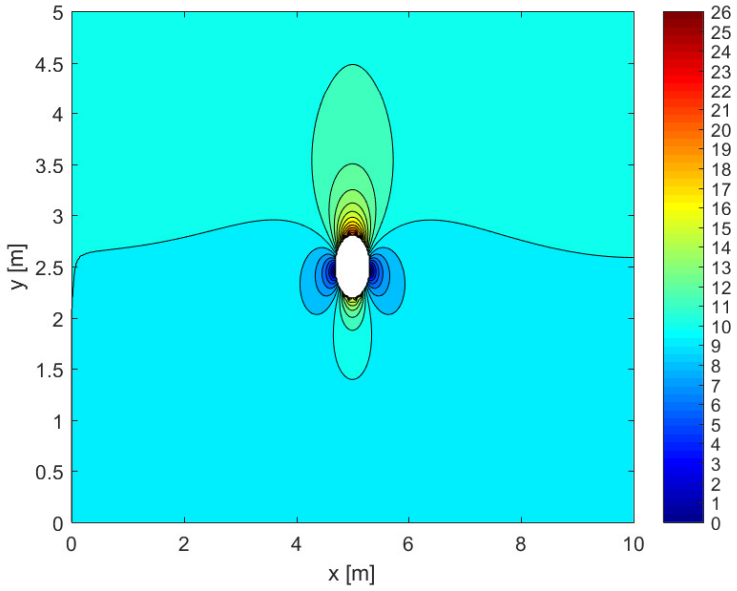

FIGURE 2.46: Velocity distribution for the Helium case for $\Omega = 10 rad/s$ (in m/s)

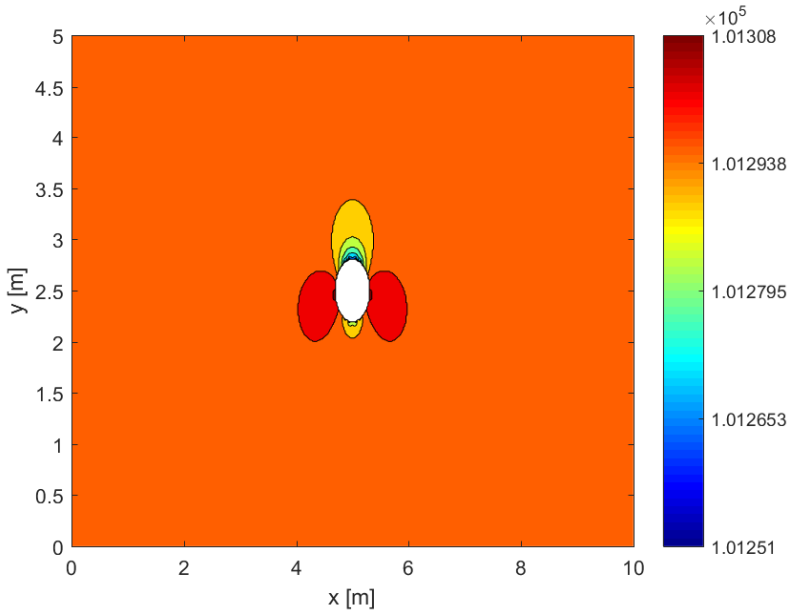

FIGURE 2.47: Pressure distribution for the Helium case for $\Omega = 10 rad/s$ (in Pa)

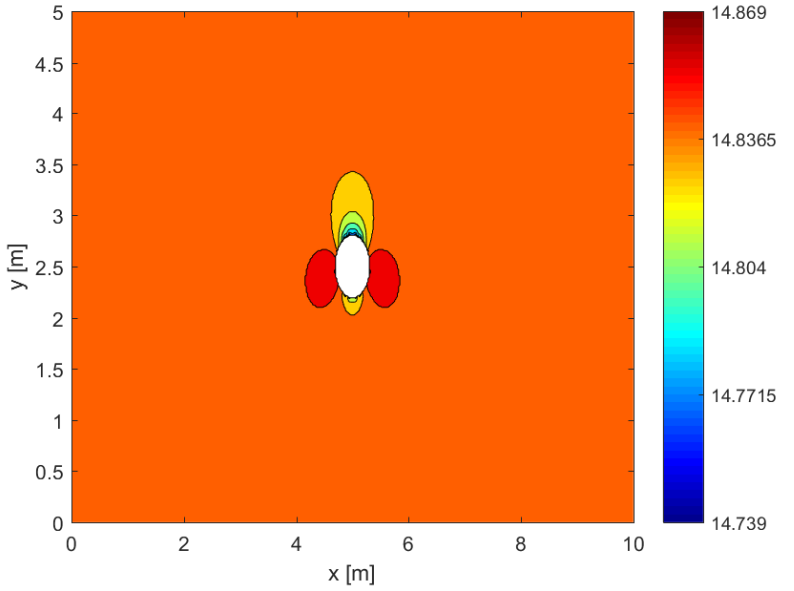

FIGURE 2.48: Temperature distribution for the Helium case for $\Omega = 10 rad/s$ (in ^{o}C)

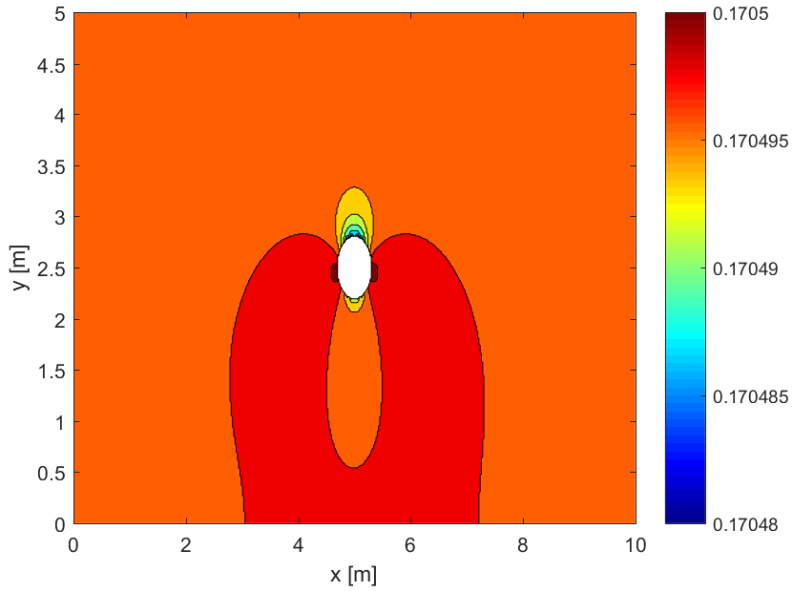

FIGURE 2.49: Density distribution for the Helium case for $\Omega = 10 rad/s$ (in kg/m^3)

At first view, it can be seen some differences between the three treated cases, such as the velocity, pressure, temperature and density gradients. Also, the streamline, unlike the static case, is not the same for each problem, for example, on the Helium case, the cylinder's streamline is 22.8735, whereas in the rotating reference case the cylinder's streamline is 22.8907, which is slightly different. Moreover, since the pressure gradient is not the same, the lift [4] [5] or the lift coefficient are not the same. For the reference rotating case, the lift coefficient is 2.803, whereas in the Helium case it is 2.804 (the small difference is due to the compressibility of the gas, since in incompressible flow the only difference between the air and the Helium cases would be the temperatures distribution) and in the decreasing height case it is 2.48. So, it can be seem that decreasing the height implies a reduction of the lift coefficient and lift. However, it should be remarked that although the lift coefficient on the Helium case is higher than the other two cases, the lift is far smaller (on the reference case there is a lift of 51.53 N/m and on the Helium case there is a lift of 7.17 N/m). The main reason of this change is the upwind dynamic pressure, which is a function of the upwind density, and in the Helium case the density is about 10 times smaller than in the rotating reference case.

Although there are several differences in all these cases, it can be found a similarity, which is the drag (or also the drag coefficient). In all these cases the drag is zero. This phenomenon has the name of the *D'Alembert's paradox*, which says that for potential

[4] The lift in this case will have units of N/m since it is treated a 2-D problem.

[5] The appearance of lifting force due to the cylinder's rotation is called the Magnus effect. [8]

flow the drag must be zero since there is not viscous force or a resistance force due to the detaching of the boundary layer, since both of them have been neglected.

A part from this, it must be remarked that the cylinder's streamline has been found with the circulation method (it has been trying different cylinder's streamlines until the circulation has been the same as the one obtained from the expression 2.73 [6]). However, after knowing the velocities distribution it has been used the velocity method (the method is the same as the circulation one, but instead of fixing circulation, it has been fixed a velocity at on point) in order to verify the previous solution, and, as it has been expected, the solution is completely the same. However, if a NACA airfoil had been analyzed, the method that would have been used should be the velocity method since it is known that on the trailing edge there is a stagnation point whereas the circulation is a priori unknown.

2.6 Conclusions

In this chapter it has been seen two types of numerical methods for the potential flow, the streamline method and the potential velocity method. It has been discussed the differences between both methods and it has been arrived to the conclusion that the streamline method is computationally cheaper than the velocity potential method because this last method includes Neumann boundary conditions on the inlet flow, which means that it is harder to converge with an iterative solver.

On the other hand, it has been analyzed the influence of the mesh on the solution obtained from the streamline method (convergence analysis) and it has been also analysed the influence of the relaxation factor on the computational cost, and it has been appreciated that in this case, this factor could make a significant reduction of the computational cost.

Finally, it has been analysed different cases focused on a static or rotating cylinder, where it has been seen the influence of approaching or putting away the top and bottom walls or changing the gas. Also, it has been checked the d'Alembert's paradox and Magnus effect.

Regarding the code, it can be easily modified in order to solve the flow around a NACA or around and ellipse (it is only needed to change the geometry parameters condition), which could be the following interesting analysis.

[6] The cylinder's streamlines tested have not been arbitrary, it has been used the Newton-Raphson method in order to find the desired cylinder's streamline.

Chapter 3

Convection-diffusion transport equation

3.1 Introduction

In the previous chapter it has been analyzed the solutions for a non-viscous flow, but it is known that actually the boundary layer can play an important role on aerodynamics because in the boundary layer there a high gradient of velocities and temperatures, that in many cases this layer can become turbulent or indeed detach the object's wall, which means that the drag will increase significantly. So, the follow up to the potential flow should be to solve the flow taking into account its viscosity, which means solving the Navier-Stokes equations (with or without simplifications).

Only taking into account the simplification of constant specific heat transfer at constant volume ($c_v = constant$), the Navier-Stokes can be written as

$$\frac{\partial \rho}{\partial t} + \nabla \cdot (\rho \vec{v}) = 0 \tag{3.1}$$

$$\frac{\partial (\rho \vec{v})}{\partial t} + \nabla \cdot (\rho \vec{v}\vec{v}) = \nabla \cdot (\mu \nabla \vec{v}) + [\nabla \cdot (\vec{\tau} - \mu \nabla \vec{v}) - \nabla p + \rho \vec{g}] \tag{3.2}$$

$$\frac{\partial (\rho T)}{\partial t} + \nabla \cdot (\rho \vec{v} T) = \nabla \cdot \left(\frac{\lambda}{c_v} \nabla T \right) + \left(\frac{-\nabla \cdot \vec{q}^R - p \nabla \cdot \vec{v} + \vec{\tau} : \nabla \vec{v}}{c_v} \right) \tag{3.3}$$

It can be appreciated that these three equation presented have a common structure which consist on an unsteady term, a convective term, a diffusion term (in the case of the continuity equation this term does not appear) and other terms (source or sink terms). For a generic variable (ϕ, which will be further discussed on section 3.3) it can be written the generic convection-diffusion equation (equation 3.4).

In this chapter it is not going to be solved the Navier-Stokes equation, this chapter will

be the previous step for it. In it, it will be developed and verified the convective term evaluation, which will be an important part on the Navier-Stokes resolution.

3.2 Problem definition

On this chapter it will be solved three different problems (they will be widely explained on section 3.4) in order to verify the code developed for solving the convection diffusion equation. What these problems have in common is that the domain is rectangular, so a structured uniform Cartesian mesh, like in the previous chapter, will be appropriated.

Also, it will be used the finite volume method with the nodes centered at each control volume, and it will be added nodes with no volume on the rectangle's edges in order to make easier the implementation of the boundary conditions. So, at the end, the mesh used will be the same than the mesh used on chapter 2 (figure 2.1).

3.3 Methodology of resolution

Being ϕ a generic variable (velocity, temperature, entropy, etc.), the generic convection-diffusion transport equation can be written as

$$\frac{\partial(\rho\phi)}{\partial t} + \nabla\cdot(\rho\vec{v}\phi) = \nabla\cdot(\Gamma_\phi\nabla\phi) + s_\phi \tag{3.4}$$

where Γ_ϕ corresponds to the diffusion coefficient and s_ϕ corresponds to the source terms.

Considering the Navier-Stokes equations presented previously and considering perfect gases, it can be defined each parameter according to the equation treated:

TABLE 3.1: Correlation between the general convection-diffusion equation's parameters and the Navier-Stokes equation's variables

Equation	ϕ	Γ_ϕ	s_ϕ
Continuity	1	0	0
Momentum [1]	$\vec{v}$	μ	$\nabla\cdot(\vec{\tau}-\mu\nabla\vec{v})-\nabla p+\rho\vec{g}$
Energy	T	$\frac{\lambda}{c_v}$	$\frac{1}{c_v}(-\nabla\cdot\vec{q}^R - p\nabla\cdot\vec{v}+\vec{\tau}:\nabla\vec{v})$

As it has being mentioned on section 3.2, it is going to be a finite volume method, concretely, cell-centered nodes.

The numerical approach will be presented treating the different terms separately. Before starting with the procedure, it must be explained the notation that will be used. For the previous time step, instead of being the notation of the superindex n, it will be the

[1] The momentum conservation is defined by 3 equations according to the axis x,y and z

superindex o and for the current time step, the superindex $n+1$ will be eliminated. Regarding to the diffusion coefficient Γ_ϕ, due to the fact that this coefficient will take the value on the control volume's faces, the subindex ϕ will be dropped and will only appear the subindex according to the face.

The unsteady term can be integrated on the following way

$$\int_{t^n}^{t^{n+1}} \int_{V_P} \frac{\partial(\rho\phi)}{\partial t} dV dt \approx V_P \int_{t^n}^{t^{n+1}} \frac{\partial(\rho_p \phi_p)}{\partial t} dt = V_P(\rho_P \phi_P - \rho_P^o \phi_P^o) \tag{3.5}$$

It should be remarked that the density ρ_P has been assumed to be the average of the density inside the control volume

$$\rho_P \approx \bar{\rho_P} = \frac{1}{V_P} \int_{V_P} \rho dV \tag{3.6}$$

As regards the convective term, it is going to be applied the Gauss divergence theorem to convert the volume integral to a surface integral:

$$\int_{t^n}^{t^{n+1}} \int_{V_P} \nabla \cdot (\rho \vec{v} \phi) dV dt = \int_{t^n}^{t^{n+1}} \oint_{S_p} \rho \vec{v} \phi \vec{dS} dt \tag{3.7}$$

The time integral in this case it will be be treated in a different way from the unsteady term because in this case the variables are line function.

$$\begin{aligned} \int_{t^n}^{t^{n+1}} \oint_{S_p} \rho \vec{v} \phi \vec{dS} dt \approx [\beta(\dot{m}_e \phi_e - \dot{m}_w \phi_w + \dot{m}_n \phi_n - \dot{m}_s \phi_s) + \\ (1-\beta)(\dot{m}_e^o \phi_e^o - \dot{m}_w^o \phi_w^o + \dot{m}_n^o \phi_n^o - \dot{m}_s^o \phi_s^o)]\Delta t \end{aligned} \tag{3.8}$$

The mass flows can be computed as:

$$\dot{m}_e = \int_{S_e} \rho \vec{v} \vec{dS} \tag{3.9}$$

$$\dot{m}_w = -\int_{S_w} \rho \vec{v} \vec{dS} \tag{3.10}$$

and $\dot{m}_n$ and $\dot{m}_s$ can be computed as $\dot{m}_e$ and $\dot{m}_w$, respectively. With this, it can be seen that the mass flow in any face ($\dot{m}_f$) will be positive in the positive coordinate direction).

The value of the parameter β will depend on the type of time integration. If it is Crank-Nicolson, its value will be 0.5, if it is the explicit integration, it's value will be 0 and if it is the implicit integration the value will be 1. The explicit integration will not be taken into account due to the fact that the time step needed should be very little in order to do not have convergence issues, although this time integration is faster since it is only

needed the previous step values which are known. On the other hand, the integration by Crank-Nicolson will not be carried out since the expression obtained in the equation 3.8 will be further developed and it is preferred to work with simpler expressions. So, at the end, the type of integration that will be used is the implicit one, since it does not present convergence issues related to the time steps and is an easier expression to work with.

The procedure for the diffusive term will be analogous to the one presented for the convective term.

$$\int_{t^n}^{t^{n+1}} \int_{V_P} \nabla \cdot (\Gamma_\phi \nabla \phi) dV dt = \int_{t^n}^{t^{n+1}} \oint_{S_p} \Gamma_\phi \nabla \phi \vec{d} S dt \tag{3.11}$$

As it has been mentioned before, the time integration scheme will be the implicit. Also, the derivative of phi will be done as it has been done on the potential flow, with a second order accuracy approximation.

$$\int_{t^n}^{t^{n+1}} \oint_{S_p} \Gamma_\phi \nabla \phi \vec{d} S dt = \left(\Gamma_e \frac{\phi_E - \phi_P}{d_{PE}} S_e - \Gamma_w \frac{\phi_P - \phi_W}{d_{PW}} S_w + \Gamma_n \frac{\phi_N - \phi_P}{d_{PN}} S_n - \Gamma_s \frac{\phi_P - \phi_S}{d_{PS}} S_s \right) \Delta t \tag{3.12}$$

The source term will be treated as in the following way:

$$\int_{t^n}^{t^{n+1}} \int_{V_P} S_\phi dV dt = \bar{S}_\phi V_P \Delta t \approx (S_c^\phi + S_p^\phi \phi_P) V_P \Delta t \tag{3.13}$$

For numerical reasons, the source term has been linearized [2] [5]. In this linearization, the coefficient S_p^ϕ never should be positive to ensure that the coefficient a_P (it will be presented later) is always positive provided that the neighbours coefficients a_{nb} are always positive. [14]

Once it has been integrated all the different parts, it is obtained the following equation:

$$\begin{aligned} &\frac{V_P(\rho_P \phi_P - \rho_P^o \phi_P^o)}{\Delta t} + \dot{m}_e \phi_e - \dot{m}_w \phi_w + \dot{m}_n \phi_n - \dot{m}_s \phi_s \\ &= D_e(\phi_E - \phi_P) - D_w(\phi_P - \phi_W) + D_n(\phi_N - \phi_P) - D_s(\phi_P - \phi_S) + (S_c^\phi + S_p^\phi \phi_P) V_P \end{aligned} \tag{3.14}$$

where

$$D_e = \frac{\Gamma_e S_e}{d_{PE}} \tag{3.15}$$

and so for the west, north and south face.

Introducing the continuity equation it can be obtained the following equation

$$\begin{aligned} &\rho_P^o \frac{\phi_P - \phi_P^o}{\Delta t} V_P + \dot{m}_e(\phi_e - \phi_P) - \dot{m}_w(\phi_w - \phi_P) + \dot{m}_n(\phi_n - \phi_P) - \dot{m}_s(\phi_s - \phi_P) \\ &= D_e(\phi_E - \phi_P) - D_w(\phi_P - \phi_W) + D_n(\phi_N - \phi_P) - D_s(\phi_P - \phi_S) + (S_c^\phi + S_p^\phi \phi_P) V_P \end{aligned} \tag{3.16}$$

[2] The linearization of the source term will be analysed after presenting the discretization coefficients

Rearranging terms, it can be obtained the discretization coefficients for a general control volume (the inner control volumes):

$$a_E = D_e \tag{3.17}$$

$$a_W = D_w \tag{3.18}$$

$$a_N = D_n \tag{3.19}$$

$$a_S = D_s \tag{3.20}$$

$$a_P = a_E + a_W + a_N + a_S + \frac{\rho_P^o V_P}{\Delta t} - \dot{m}_e + \dot{m}_w - \dot{m}_n + \dot{m}_s - S_p^\phi V_P \tag{3.21}$$

$$b_P = \frac{\rho_P^o \phi_P^o V_P}{\Delta t} - \dot{m}_e \phi_e + \dot{m}_w \phi_w - \dot{m}_n \phi_n + \dot{m}_s \phi_s + S_c^\phi \tag{3.22}$$

However, before making a step forward to the boundary conditions, it must be presented the way to compute the ϕ_f value.

3.3.1 Convective term analysis

The simplest method of computation is the central-difference schemes (CDS), which assume a linear distribution of ϕ. This is a second-order accurate scheme but presents convergence problems.

For incompressible flows (or gases at low Mach) the convective term is more influenced by upstream conditions than the downstream ones. The upwind-difference schemes (UDS) is a first-order accurate scheme (it is too diffusive) based on this phenomenology. In this scheme, the value on the face is the same as the closest upstream node.

There are more accurate schemes, such us second-order upwind scheme (SUDS), or the second/third order QUICK scheme (quadratic upwind interpolation for convective kinematics).

Before presenting a table where it is represented the algorithms of computation for each scheme, it is necessary to show previously the normalization of variables. First of all, it should be identified the downstream node (D), the upstream node (U), and the central node (C) according to the mass flow direction. After that, the position and the variable ϕ can be normalized as

$$\hat{x} = \frac{x - x_U}{x_D - x_U} \tag{3.23}$$

$$\hat{\phi} = \frac{\phi - \phi_U}{\phi_D - \phi_U} \tag{3.24}$$

The following table shows the presented schemes written in terms of the normalized variables.

TABLE 3.2: Different schemes for the convective term computation

Scheme	Normalized face value
CDS	$\hat{\phi}_f = \frac{\hat{x}_f - \hat{x}_c}{1-\hat{x}_c} + \frac{\hat{x}_f - 1}{1-\hat{x}_c}\hat{\phi}_c$
UDS (or FUDS)	$\hat{\phi}_f = \hat{\phi}_c$
SUDS	$\hat{\phi}_f = \frac{\hat{x}_f}{\hat{x}_c}\hat{\phi}_c$
QUICK	$\hat{\phi}_f = \hat{x}_f + \frac{\hat{x}_f(\hat{x}_f-1)}{\hat{x}_c(\hat{x}_c-1)}(\hat{\phi}_c - \hat{x}_c)$

The second or higher-order schemes presented before (CDS, SUDS and QUICK) can present convergence instabilities. Due to this issues, it has been proposed bounded convective schemes in the literature [3]. One of this schemes is the SMART scheme (Sharp and Monotonic Algorithm for Realistic Transport) [2]:

$$If \;\; 0 < \hat{\phi}_c < \frac{\hat{x}_c}{3} \rightarrow \hat{\phi}_f = -\frac{\hat{x}_f(1-3\hat{x}_c+2\hat{x}_f)}{\hat{x}_c(\hat{x}_c-1)}\hat{\phi}_c$$

$$If \;\; \frac{\hat{x}_c}{6} < \hat{\phi}_c < \frac{\hat{x}_c}{\hat{x}_f}(1+\hat{x}_f-\hat{x}_c) \rightarrow \hat{\phi}_f = \frac{\hat{x}_f(\hat{x}_f-\hat{x}_c)}{1-\hat{x}_c} + \frac{\hat{x}_f(\hat{x}_f-1)}{\hat{x}_c(\hat{x}_c-1)}\hat{\phi}_c$$

$$If \;\; \frac{\hat{x}_c}{\hat{x}_f}(1+\hat{x}_f-\hat{x}_c) < \hat{\phi}_c < 1 \rightarrow \hat{\phi}_f = 1$$

$$otherwise \rightarrow \hat{\phi}_f = \hat{\phi}_c$$

3.3.2 Boundary conditions

As it has been seen on chapter 2, there are two types of boundary conditions: Dirichlet and Neumann boundary conditions.

In the case of Dirichlet boundary conditions, the value of ϕ is know (it is imposed). So, in this case the discretization coefficients are

$$a_P = 1 \tag{3.25}$$

$$b_P = \phi_{BC} \tag{3.26}$$

and the rest of coefficients are 0.

In the case of Neumann boundary conditions, the value of the flux is known. For example, if the flux on the right wall is known

$$j_E = -\Gamma_W \frac{\phi_P - \phi_W}{d_{PW}} \rightarrow \phi_P = \phi_W - \frac{j_E d_{PW}}{\Gamma_W} \tag{3.27}$$

[3] The bounded convective schemes are schemes that satisfy conditions for stability and accuracy, such as that $\hat{\phi}_f$ must be continuous, if $\hat{\phi}_c = 0$ or 1, $\hat{\phi}_f$ must be 0 or 1 and that $\hat{\phi}_f$ must lie between $\hat{\phi}_c$ and 1

With this, the discretization coefficients for the nodes on this wall will be

$$a_P = 1 \tag{3.28}$$

$$a_W = 1 \tag{3.29}$$

$$b_P = -\frac{j_E d_{PW}}{\Gamma_W} \tag{3.30}$$

The rest of coefficients will be zero.

And for the procedure will be analogous on the rest of the wall.

3.3.3 Source term analysis

In this section it will only be shown the linearization of the source term for the energy equation, which is the one that is going to be treated.

The source term is composed by three different terms, one related to the heat flow, another related to the pressure and the other related to the viscosity. In order to simplify the development, each term is going to be treated separately.

Regarding to the flux term, the equation is the following one

$$-\frac{1}{c_v}\nabla\cdot\vec{q}^R = -\frac{1}{c_v}\nabla^2 T = -\frac{1}{c_v}\nabla^2\phi \tag{3.31}$$

As it can be seen, this term is a second order derivative and will be neglected. For the term related to the pressure, it will be used the ideal (and perfect) gas state equation

$$p = \rho R T = \rho R \phi \tag{3.32}$$

If the flow is incompressible, the term related to the pressure will be zero because the divergence of the velocity will be zero.

As regards the last term, the temperature (and, in this case, ϕ) does not depend on this term, so the term related to the viscosity will be part of S_c^ϕ. It should be remarked that for uniform flows, this term will be 0.

Finally, the source term can be written as

$$S_\phi = \frac{\vec{\tau} : \nabla\vec{v}}{c_v} - \frac{\rho R \nabla\cdot\vec{v}}{c_v}\phi_P \tag{3.33}$$

3.3.4 Simplification to the steady case

In order to make the code verification, it has been simplified the equation 3.16 to an steady form to be able to compare the obtained solution with the analytical solution. Also, there is a case (Smith-Hutton case) where the result is known and it can be easily

compared.

The simplification will consist on turning to zero the transient term (or turning to infinite the step time), so the only coefficients that will be modified will be a_P and b_P

$$a_P = a_E + a_W + a_N + a_S - \dot{m}_e + \dot{m}_w - \dot{m}_n + \dot{m}_s - S_p^{\phi} V_P \tag{3.34}$$

$$b_P = -\dot{m}_e \phi_e + \dot{m}_w \phi_w - \dot{m}_n \phi_n + \dot{m}_s \phi_s + S_c^{\phi} \tag{3.35}$$

3.3.5 Algorithm of resolution

First of all, it is going to be presented the general algorithm of resolution To end up with the streamline method, it will be presented the algorithm of resolution for this method.

1. Input data
   - 1.1. Physical data: inlet flow conditions, problem's height and width, fluid properties, boundary conditions, initial values of ϕ.
   - 1.2. Numerical data: number of horizontal control volumes (N), number of vertical control volumes (M), relaxation factor (f_r), maximum error allowed (δ).
2. Previous calculations: mesh generation
3. Initial map: $\phi^o[i][j] = \phi(t=0)[i][j]$ and $t = 0$
4. Time step: $t = t + \Delta t$
5. Estimated values: $\phi^*[i][j] = \phi^o[i][j]$
6. Discretization coefficients computation
   - 6.1. a_P,a_E,a_W,a_N,a_S
   - 6.2. b_P: convective term computation (its algorithm will be presented after this algorithm)
7. Computation of $\phi[i][j]$ with Gauss-Seidel or line-by-line
8. Is $max|\phi_P - \phi_P^*| < \delta$?
   - a. Yes $\rightarrow$ go to 9
   - b. No $\rightarrow \phi_P^* = \phi_P \rightarrow$ In case of constant λ and c_v go to 6.2; otherwise, go to 6.1.
9. New time step?
   - (a) Yes $\rightarrow \phi_P^o = \phi_P \rightarrow$ go to 4 (and skip 6.1 in the case of constant λ and c_v)
   - (b) No $\rightarrow$ go to 10

10. Final calculations and print results
11. End

As it has been told on the global algorithm, the following two algorithms will show the subroutines of the computation of the dependent variables at the east (or north) face and at the west (or south face).

For the east face all the algorithm is presented:

1. Input data: $\dot{m}_e$, x_e,x_P,ϕ_P, x_E, ϕ_E, x_W, ϕ_W, x_{EE}, ϕ_{EE} and the convective scheme.
2. According to the mass flow, locate the upstream, downstream and central nodes:
   a. If $\dot{m}_e > 0$: $x_D = x_E, \phi_D = \phi_E, x_C = x_P, \phi_C = \phi_P, x_U = x_W, \phi_U = \phi_W$
   b. If $\dot{m}_e < 0$: $x_D = x_P, \phi_D = \phi_P, x_C = x_E, \phi_C = \phi_E, x_U = x_{EE}, \phi_U = \phi_{EE}$
3. Normalization of $\hat{\phi}_c$, $\hat{x}_c$ and $\hat{x}_e$
4. Evaluate $\hat{\phi}_e$
5. Dimensional value: $\phi_e = \phi_U + (\phi_D - \phi_U)\hat{\phi}_e$
6. Return ϕ_e

For the west and south faces the only steps that change are 1 and 2:

1. Input data: $\dot{m}_w$, x_w,x_P,ϕ_P, x_W, ϕ_W, x_E, ϕ_E, x_{WW}, ϕ_{WW} and the convective scheme.
2. According to the mass flow, locate the upstream, downstream and central nodes:
   a. If $\dot{m}_w > 0$: $x_D = x_P, \phi_D = \phi_P, x_C = x_W, \phi_C = \phi_W, x_U = x_{WW}, \phi_U = \phi_{WW}$
   b. If $\dot{m}_w < 0$: $x_D = x_W, \phi_D = \phi_W, x_C = x_P, \phi_C = \phi_P, x_U = x_E, \phi_U = \phi_E$

3.4 Verification

For the code verification it has been solved three different cases where the solution can be known. These three cases have in common that the flow is incompressible and the velocity is known, so it is going to be solved the energy conservation equation.

The first case has been uniform flow, horizontal and vertical flow, with the inlet and outlet values as knonw. It has been tested different Péclet number on different meshes so as to see the differences between schemes. On the following tables it will be represented the numerical error of each convective scheme according to the mesh and the Péclet number. The normalized numerical error can be expressed on the following way

$$error = \frac{max(abs(\phi_{numeric} - \phi_{analytic}))}{\phi_{out} - \phi_{in}} \tag{3.36}$$

Since it is an one-dimensional problem, the analytical solution can be obtained.

$$\frac{\phi - \phi_{in}}{\phi_{out} - \phi_{in}} = \frac{e^{\frac{xPe}{L}} - 1}{e^{Pe} - 1} \tag{3.37}$$

TABLE 3.3: Normalized numerical error for Pe=0.001

N \ Scheme	UDS	CDS	SUDS	QUICK	SMART
12	$3.50 \cdot 10^{-6}$	$1.25 \cdot 10^{-6}$	$1.25 \cdot 10^{-6}$	$1.25 \cdot 10^{-6}$	$1.25 \cdot 10^{-6}$
52	$1.49 \cdot 10^{-7}$	$7.21 \cdot 10^{-8}$	$7.21 \cdot 10^{-8}$	$7.21 \cdot 10^{-8}$	$7.21 \cdot 10^{-8}$
202	$4.01 \cdot 10^{-8}$	$4.05 \cdot 10^{-8}$	$4.05 \cdot 10^{-8}$	$4.05 \cdot 10^{-8}$	$4.05 \cdot 10^{-8}$

TABLE 3.4: Normalized numerical error for Pe=1

N \ Scheme	UDS	CDS	SUDS	QUICK	SMART
12	$3.97 \cdot 10^{-3}$	$1.91 \cdot 10^{-3}$	$2.10 \cdot 10^{-3}$	$1.20 \cdot 10^{-3}$	$1.20 \cdot 10^{-3}$
52	$1.11 \cdot 10^{-3}$	$7.85 \cdot 10^{-5}$	$8.03 \cdot 10^{-5}$	$7.90 \cdot 10^{-5}$	$7.90 \cdot 10^{-5}$
202	$2.95 \cdot 10^{-4}$	$4.94 \cdot 10^{-6}$	$4.96 \cdot 10^{-6}$	$4.94 \cdot 10^{-6}$	$4.94 \cdot 10^{-6}$

TABLE 3.5: Normalized numerical error for Pe=100

N \ Scheme	UDS	CDS	SUDS	QUICK	SMART
52	0.37	0.37	0,37	0,37	0,37
202	$4.84 \cdot 10^{-2}$	$2,88 \cdot 10^{-2}$	$2,88 \cdot 10^{-2}$	$2,88 \cdot 10^{-2}$	$2,88 \cdot 10^{-2}$
1002	$1.63 \cdot 10^{-2}$	$1.23 \cdot 10^{-3}$	$1.23 \cdot 10^{-3}$	$1.23 \cdot 10^{-3}$	$1.23 \cdot 10^{-3}$

As it can be appreciated from the previous tables, for low Péclet number (where the diffusion is stronger than the convection phenomenon), there is a low error for all the convective schemes. The main reason is that for the case of low Péclet number there is a heat conduction phenomenon (similar to a solid conduction case) and the convection practically has no importance. It should be remarked that the first order UDS error is always higher than the higher order schemes, which is something that it was expected to happen. A part from this, it can be seen that the error increases with the Péclet number. The main reason might be that for higher Pe it is needed a more concentrated mesh due to the fact that on the last nodes there is a high gradient of temperatures (it is higher with

a higher Pe), and it is needed more nodes on this section to get correctly this gradient.

On the following figures (figs. 3.1, 3.2 and 3.3) it is represented the differences between the solution obtained with UDS and QUICK schemes and the analytical solution for the case of a Pe of 50. As it can be seen, for a low nodes mesh the numerical result is quite different from the analytical solution. It must be said that in this case it has been needed a relaxation factor of 0.3 due to convergence reasons (with 12 nodes the solution becomes unstable). However, for 52 nodes, the QUICK solution is practically identical to the analytical one whereas the UDS solution is a bit different, which was expected since the QUICK scheme is a higher order shceme and the UDS is a first order scheme. Even in the 202 nodes mesh the UDS solution has not achieved the analytical solution. So, as it has been mentioned on section 3.3.1, the UDS scheme is quite diffusive.

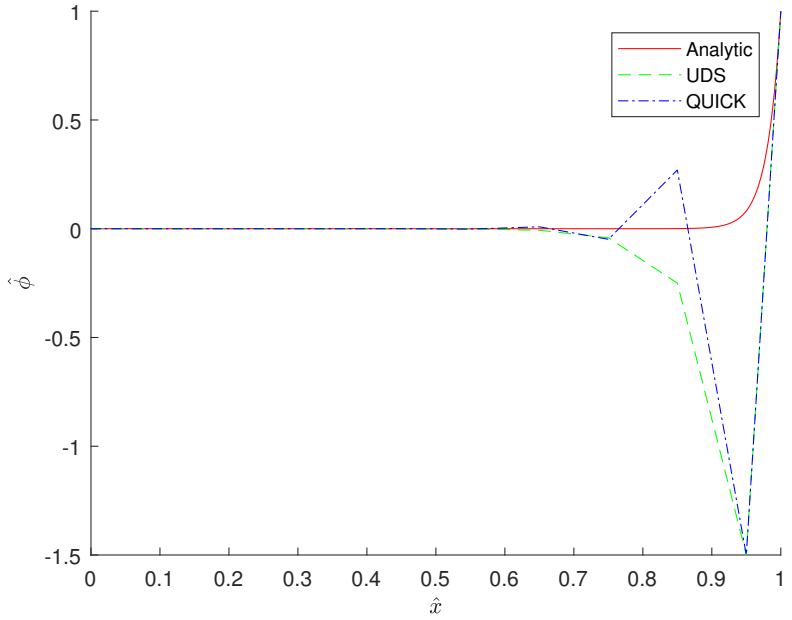

FIGURE 3.1: Comparison between UDS and QUICK for Pe=50 and N=12

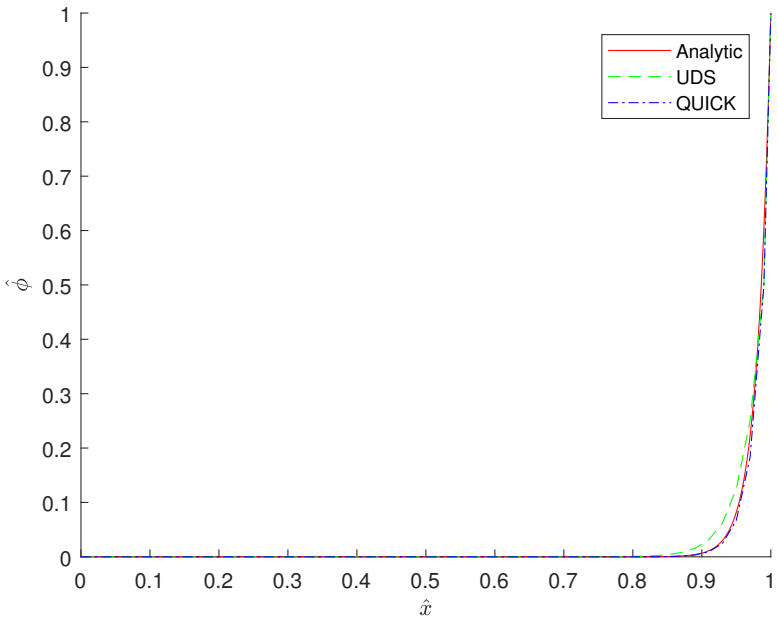

FIGURE 3.2: Comparison between UDS and QUICK for Pe=50 and N=52

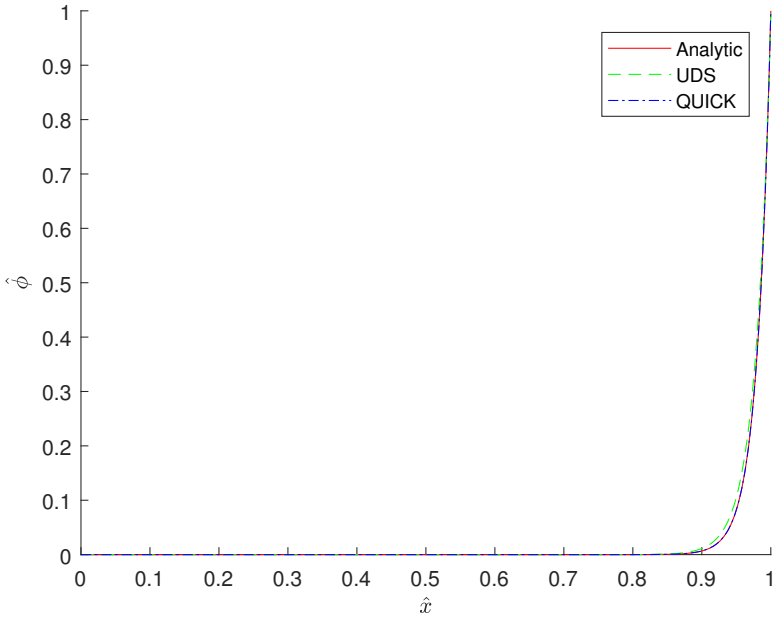

FIGURE 3.3: Comparison between UDS and QUICK for Pe=50 and N=202

A second verification case has been the diagonal flow: a square domain of 2x2 meters, with a constant diagonal velocity field (the inclination is 45 degrees) and the boundary conditions are that the left and top walls have a prescribed temperature (400K) and the right and bottom walls an other (288K). On the following figure it is represented the solution obtained for different Péclet numbers (there is an image processor issue on the last two figure because the Garnet and red colors represent the same temperature). As it can be seen, as the Pe increases, there is a higher gradient on the diagonal and in the rest of the domain the temperature is constant and equal to the respective boundary conditions (288 and 400K). Also, as it has been expected, for a low Pe number there is a classical conduction problem.

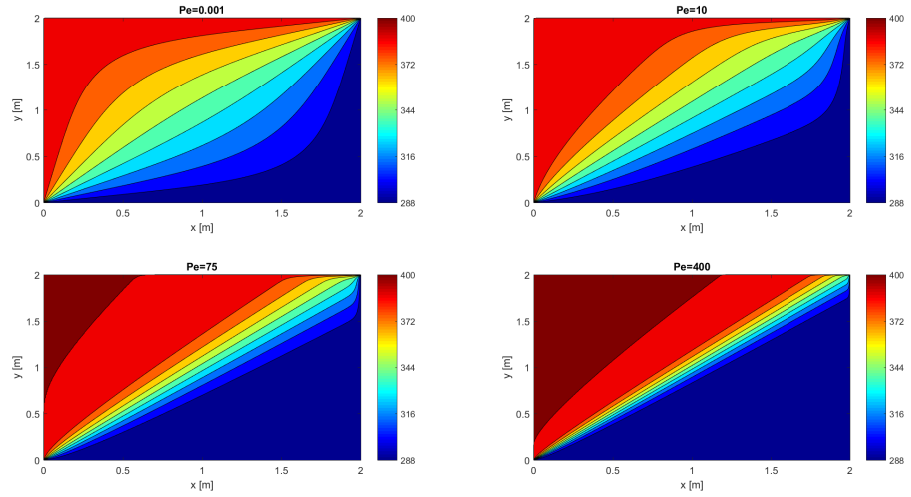

FIGURE 3.4: Representation of different Pe solutions

The last verification that it has been carried out is the Smith-Hutton case. This case consists on a rectangular domain of 2x1 meters. The velocity field can be expressed as

$$u = 2y(1-x^2) \tag{3.38}$$

$$y = -2x(1-y^2) \tag{3.39}$$

It could be demonstrated that this field verifies the incompressibility condition.

The boundary conditions are defined on the following way [4]:

- Inlet flow (x<0, y=0): $\phi = 1 + tanh[10(2x+1)]$
- Outle flow (x>0, y=0): $\frac{\partial \phi}{\partial y} = 0$

[4] In this case, the left nodes x-coordinate will be -1 instead of 0

- Rest of boundary conditions: $\phi = 1 - tanh(10)$

On the following two figures (figures 3.5 and 3.6), it is represented the solution for different Péclet numbers, a low Pe to see the diffusion dominant phenomenon and a high Pe to see the convection phenomenon. It can be appreciated that in the high Pe case the lines of constant temperatures are close to be circular, which means that the particle that enter with a temperature practically leaves with the same temperature (the convective term is dominant).

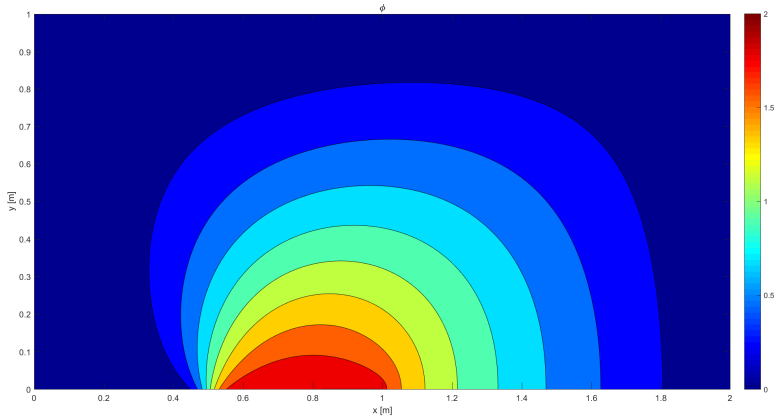

FIGURE 3.5: Smith-Hutton case solution for Pe=20

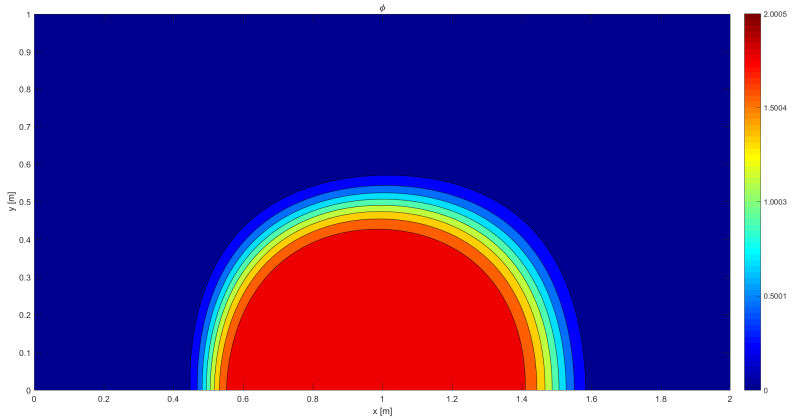

FIGURE 3.6: Smith-Hutton case solution for Pe=2000

To end up with the verification, it has been compared the outlet values for each different scheme (figure 3.7). On figure 3.7a it can be appreciated what happened on the first case,

the is no difference between schemes because the diffusive term is dominant. However, on figure 3.7b it can be appreciated a slightly difference between UDS and the other schemes due to the fact that a the first order upwind scheme is too diffusive. On the other hand, in must be remarked that for the selected mesh there is no significant difference between all the high order schemes, to appreciate some differences the number of nodes should be reduced, where the the QUICK and SMART schemes will differ from the second order schemes CDS and SUDS.

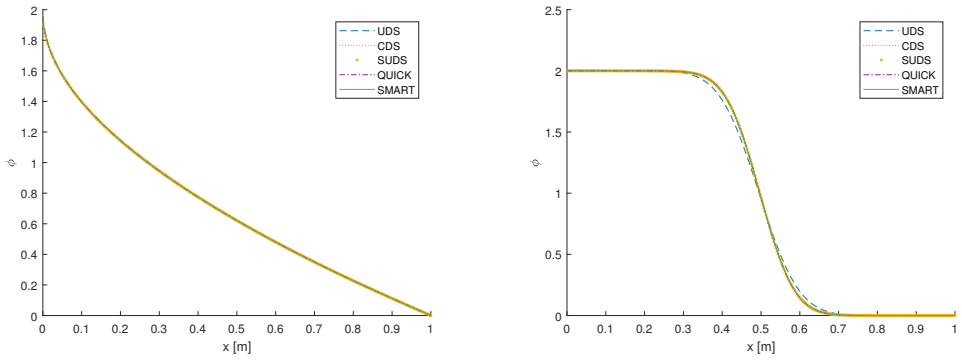

(A) Pe=20 (B) Pe=2000

FIGURE 3.7: Comparison of the different schemes on the outlet section for two different Péclet numbers

3.5 Conclusions

This chapter has served as a preamble of the following chapter in which it has been developed and verified different convective schemes in order to be able to calculate the physical values on the control volume faces. It has been tested three different problems so as to verify the code where this convective schemes are implemented.

A part from the verification, it has analyzed the differences between schemes and it has been seen that the UDS is quite diffusive, as it has been expected due to the fact that it is a first order scheme. Also, as the Péclet number increases, the numerical error using the same mesh increases since the convective scheme are not exact and become more inaccurate when the convective term gains importance.

As regards the code, it has been developed a general code to solve any convection-diffusion problem (with some limitations, such as not having solids inside the problem's geometry or having only one type of fluid, etc.), where only it should be added the boundary conditions and the velocity field.

Chapter 4

Incompressible Navier-Stokes

4.1 Introduction

The Navier-Stokes equations compose a differential equations systems in coupled partial derivatives (presented on section 3.1). Due to its complexity, there is no analytical solution for a general case (it can be found analytical solution for very simple cases), so, in order to find a solution it is needed to solve the system numerically.

These equations can be solved directly with a Direct Numerical Simulation (DNS), but it presents the problem that for complex geometries or on a 3-D case (such as solving the flow around an operating helicopter) the time of computation would be terribly high, although it is still high for simpler cases because it is needed a fine grid to solve the smallest length scales (Kolmogorov scales) and a enough small time scale to be able to get the fastest fluctuations [11]. However, turbulence has an interesting characteristic, which is that small turbulent scales are always the same so smaller scales could be modeled (these scales can be seen as a diffusive action), but a wrong modeling of this scales could carry big scales inaccurate solutions.

There are two important turbulent models, RANS and LES. RANS (Reynolds averaged Navier-Stokes) equations are time-averaged equations, where the velocity can be decomposed into a steady velocity and a velocity perturbation or fluctuation that depends on the time.

$$\vec{v}(\vec{x},t) = \bar{\vec{v}}(\vec{x}) + \vec{v}'(\vec{x},t) \tag{4.1}$$

LES (Large Eddy Simulation) focuses on larger turbulent scales, ignoring the smallest turbulent scales (which are the most computationally expensive to solve). This filtering can be viewed as a spatial-averaging.

$$\vec{v}(\vec{x},t) = \tilde{\vec{v}}(\vec{x},t) + \vec{v}'(\vec{x},t) \tag{4.2}$$

The advantage of the RANS method is that it has a lower computational cost and it is good for high Reynolds but it is less accurate than the LES method, specially in

turbulence transitions or in completely turbulent flows. On the other hand, RANS should not be used on transient flows (it has been developed a similar model to RANS in order to work with transient flows, called URANS (Unsteady RANS)) and LES should not be used on two dimensional meshes.

4.2 Problem definition

In this chapter it is going to be treated the Naiver-Stokes solution for incompressible flows (liquid or gases at low Mach number) in a 2D problem. As it has been done on the previous chapters, it will be used a Cartesian mesh, but in this case it may not be uniformly distributed (it some cases it will be interesting to concentrate nodes on a concrete zone to have more accuracy on the results).

The main difference with respect to the potential flow treatment is that the velocities and the pressure will not be on the same mesh, the pressure mesh will be a cell-centered nodes mesh, and for the horizontal and vertical velocity its mesh will be face-centered nodes (one mesh for each component of the velocity). This type of mesh it is known as staggered mesh (figure 4.1), and it has been introduced by Harlow and Welsh on 1965 and offers several advantages respecting to the collocated mesh (the mesh used on chapter 2). One advantage is that with this mesh it will not be needed to interpolate in order to get face values, which means that is more accurate that the collocated mesh. On the other hand, the biggest advantage of the staggered mesh is that there is a strong coupling between the velocities and the pressure, which it helps to avoid some convergence issues and oscillations in pressure and velocity (the checkerboard problem).

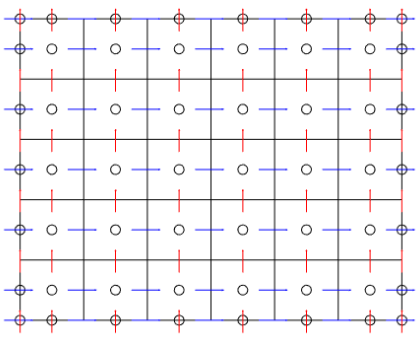

FIGURE 4.1: Representation of the staggered mesh: blue arrows represent the horizontal component of the velocity, red arrows represent the vertical component and circles represent the pressure nodes

The main disadvantage of this type of mesh is that the code is more complicated and if it is used and unstructured mesh or a 3D problem it is better to use a collocated mesh, since it has been developed algorithms to achieve a better coupling between the velocities and the pressure.

The methodology of resolution, presented on the following section, will be based on the fractional step method (introduced by Kim and Moin (1985)) [9]. This method consists on a semi-explicit time integration where the pressure will be calculated from the velocity field on a previous time instant. Since it is part of an explicit time integration, the solution will be obtained faster that in a implicit or a high order time integration but the disadvantage is that the time step will have some restrictions in order to avoid instabilities.

4.3 Methodology of resolution

As it has been mentioned on the previous section, in this chapter it is going to be solved the Navier-Stokes equations for an incompressible flow (or gases at low Mach). With this, it will be started with the following non-dimensional Navier-Stokes equations.

$$\nabla \cdot \vec{v} = 0 \tag{4.3}$$

$$\frac{\partial \vec{v}}{\partial t} + (\vec{v} \cdot \nabla)\vec{v} = -\nabla p + \frac{1}{Re}\nabla^2 \vec{v} \tag{4.4}$$

where all these variables are non-dimensional, which can be expressed on the following way:

$$u^* = \frac{u}{u_0} \tag{4.5}$$

$$v^* = \frac{v}{u_0} \tag{4.6}$$

$$x^* = \frac{x}{L} \tag{4.7}$$

$$y^* = \frac{y}{L} \tag{4.8}$$

$$p^* = \frac{p - p_0}{\rho u_0^2} \tag{4.9}$$

$$t^* = \frac{t}{\frac{L}{u_0}} \tag{4.10}$$

$$Re = \frac{\rho u_0 L}{\mu} \tag{4.11}$$

In order to simplify the notation, the superindex * (which represents the non-dimensional variable) has been eliminated since all the variables treated are

non-dimensional.

The second expression involves 3 different equations (or 2 equations in the case of a 2-dimensional problem), one for each coordinate.

The integration of each equation will be treated separately. The continuity equation (mass conservation equation) will be implicitly integrated, whereas the momentum equation will be semi-explicit integrated (it will be described afterwords widely).

So, the integration of the continuity equation can be expressed as

$$\nabla \cdot \vec{v}^{n+1} = 0 \tag{4.12}$$

and for the integration of the momentum equation

$$\frac{\vec{v}^{n+1} - \vec{v}^{n}}{\Delta t} = \frac{3}{2}\vec{R}(\vec{v}^{n}) - \frac{1}{2}\vec{R}(\vec{v}^{n-1}) - \nabla p^{n+1} \tag{4.13}$$

where

$$\vec{R}(\vec{v}) = -(\vec{v}\cdot\nabla)\vec{v} + \frac{1}{Re}\nabla^2\vec{v} \tag{4.14}$$

In this case, it should be remarked that the semi-explicit integration consists on considering that the value of $\vec{R}(\vec{v})$ at the time instant $n+\frac{1}{2}$ can be linearly extrapolated from the values at the time instants n and $n-1$. A part from this, it should be noticed that the pressure term has been implicitly integrated.

Considering the Helmholtz-Hodge theorem [1] and taking into account the equation 4.12, the velocity can be decomposed as

$$\vec{v}^{p} = \vec{v}^{n+1} + \Delta t \nabla p^{n+1} \tag{4.15}$$

With this decomposition, the momentum equation can be transformed into a velocity projection equation

$$\frac{\vec{v}^{p} - \vec{v}^{n}}{\Delta t} = \frac{3}{2}\vec{R}(\vec{v}^{n}) - \frac{1}{2}\vec{R}(\vec{v}^{n-1}) \tag{4.16}$$

where it can be isolated $\vec{v}^{p}$ as

$$\vec{v}^{p} = \vec{v}^{n} + \Delta t \left[\tfrac{3}{2}\vec{R}(\vec{v}^{n}) - \tfrac{1}{2}\vec{R}(\vec{v}^{n-1})\right] \tag{4.17}$$

And the pressure equation can be obtained applying the divergence operator on the velocity decomposition

$$\nabla \cdot \vec{v}^{p} = \nabla \cdot \vec{v}^{n+1} + \nabla \cdot \Delta t \nabla p^{n+1} \tag{4.18}$$

[1] This theorem states that "a given vector field $\vec{\omega}$ in a bounded domain Ω with smooth boundary $\delta\Omega$, is uniquely decomposed in a pure gradient field and a divergence free vector parallel to $\delta\Omega$, $\vec{\omega} = \vec{a} + \nabla\psi$, where $\nabla \cdot \vec{a} = 0$ $(a \in \Omega)$".

Due to the fact that $\nabla \cdot \vec{v}^{n+1} = 0$ (it is the continuity equation), it can be obtained a final Poisson equation for the pressure

$$\nabla^2 p^{n+1} = \Delta t \nabla \cdot \vec{v} \tag{4.19}$$

Once it has been to the two equations to discretize, it is going to be developed the numerical approximation on the following subsections.

4.3.1 Staggered-x mesh

In this mesh it is going to be calculated the horizontal component of the velocity (u), concretely u^p at each node.

From the equation 4.17, it is known the velocity u^n and the time step Δt. the only thing that should be calculated in order to know u^p is the term $R(u)$. This term is defined as

$$R(u) = -(\vec{v} \cdot \nabla)u + \frac{1}{Re}\nabla^2 u \tag{4.20}$$

Integrating over the control volume it can be obtained the following

$$R(u) = \frac{1}{\Omega_{x_P}} \left(- \int_{\Omega_{x_P}} (\vec{v} \cdot \nabla) u dV + \int_{\Omega_{x_P}} \frac{1}{Re} \nabla^2 u dV \right) \tag{4.21}$$

Applying the Gauss theorem the following expression it is obtained

$$\begin{aligned} R(u) &= \frac{1}{\Omega_{x_P}} \left(- \int_{\partial\Omega_{x_P}} (\vec{v}) u \vec{dS} + \int_{\partial\Omega_{x_P}} \frac{1}{Re} \nabla u \vec{dS} \right) \\ &= \frac{1}{\Omega_{x_P}} \Bigg(- \left[F_e u_e - F_w u_w + F_n u_n - F_s u_s \right] + \\ &\frac{1}{Re} \left[\frac{u_E - u_P}{d_{PE}} A_e - \frac{u_P - u_W}{d_{PW}} A_w + \frac{u_N - u_P}{d_{PN}} A_n - \frac{u_P - u_S}{d_{PS}} A_s \right] \Bigg) \end{aligned} \tag{4.22}$$

where F_f is the non-dimensional mass flow. As it occurred on chapter 3, the mass flow (in this case, the non-dimensional mass flow $F_f = u_f A_f$) is positive on the positive coordinate direction. Nevertheless, the value of the mass flow and the velocity on the face is unknown.

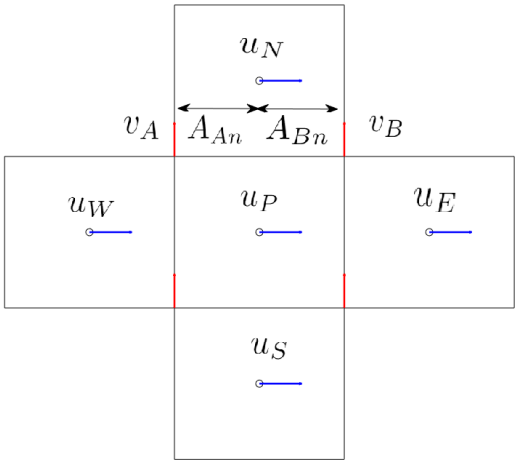

FIGURE 4.2: Representation of the Staggered-x mesh

In the figure 4.2 it can be appreciated the control volume of an internal node of the Staggered-x mesh, where it is also represented the velocities at the closest nodes (these nodes correspond to the Staggered-y mesh). From this figure, it can be obtained the vertical mass flow (northern and southern) as

$$F_n = v_A A_{An} + v_B A_{Bn} \tag{4.23}$$

and F_s can be computed in the same way; and the horizontal mass flow will be approximated to the mean of the two closest nodes' mass flow

$$F_e = \frac{u_E + u_P}{2} A_e \tag{4.24}$$

and the same for F_w.

The velocity at each control volume's face will be evaluated with the convective schemes discussed on section 3.3.1 and considering the mass flows that have been already computed.

4.3.2 Staggered-y mesh

In a similar way as in the previous subsection, this mesh will be used to calculate the vertical component of the velocity at each node, concretely v^p.

In this case, the expression for $R(v)$ is the following one

$$R(v) = \frac{1}{\Omega_{y_P}} \left(- \int_{\Omega_{y_P}} (\vec{v} \cdot \nabla) v dV + \int_{\Omega_{y_P}} \frac{1}{Re} \nabla^2 v dV \right) \tag{4.25}$$

where integrating (also applying the Gauss theorem) it can be obtained the following expression

$$R(v) = \frac{1}{\Omega_{y_P}}\Bigg(-\left[F_e v_e - F_w v_w + F_n v_n - F_s v_s\right] + \frac{1}{Re}\left[\frac{v_E - v_P}{d_{PE}}A_e - \frac{v_P - v_W}{d_{PW}}A_w + \frac{v_N - v_P}{d_{PN}}A_n - \frac{v_P - v_S}{d_{PS}}A_s\right]\Bigg) \tag{4.26}$$

In this case, the mass flows can be calculated as

$$F_e = u_A A_{Ae} + u_B A_{Be} \tag{4.27}$$

$$F_n = \frac{v_N + v_P}{2}A_n \tag{4.28}$$

and F_w and F_s can be evaluated analogously, respectively.

4.3.3 Main mesh

The objective of this mesh is to compute the pressure at each node and introduce the boundary conditions of the problem. After computing the pressure, the velocity at the new time instant will be computed.

In order to compute the pressure at each node, it will be departed from the equation 4.19, which integrating on the control volume and applying the Gauss theorem it is obtained the following equation

$$\int_{\partial\Omega_p} \nabla p^{n+1}\vec{dS} = \frac{1}{\Delta t}\int_{\partial\Omega_p} \vec{v}^{\,p}\vec{dS} \tag{4.29}$$

Operating, it results the following equation

$$\begin{aligned}&\frac{p_E^{n+1} - p_P^{n+1}}{d_{PE}}A_e - \frac{p_P^{n+1} - p_W^{n+1}}{d_{PW}}A_w + \frac{p_N^{n+1} - p_P^{n+1}}{d_{PN}}A_n - \frac{p_P^{n+1} - p_S^{n+1}}{d_{PS}}A_s \\ &= \frac{1}{\Delta t}\left[(u^p)_e A_e - (u^p)_w A_w + (v^p)_n A_n - (v^p)_s A_s\right]\end{aligned} \tag{4.30}$$

From this equation the only unknown parameters are the pressures, since the velocities at each face will have been calculated previously. So, as it has been done on the previous two chapters, it will be reorganized the equation to achieve the following discretization equation

$$a_P p_P^{n+1} = a_E p_E^{n+1} + a_W p_W^{n+1} + a_N p_N^{n+1} + a_S p_S^{n+1} + b_P \tag{4.31}$$

where the coefficient values are

$$a_E = \frac{A_e}{d_{PE}} \tag{4.32}$$

$$a_W = \frac{A_w}{d_{PW}} \tag{4.33}$$

$$a_N = \frac{A_n}{d_{PN}} \tag{4.34}$$

$$a_S = \frac{A_s}{d_{PS}} \tag{4.35}$$

$$a_P = a_E + a_W + a_N + a_S \tag{4.36}$$

$$b_P = -\frac{1}{\Delta t}[(u^p)_e A_e - (u^p)_w A_w + (v^p)_n A_n - (v^p)_s A_s] \tag{4.37}$$

The main difference with the previous chapters is that in this case all the coefficients will remain constant through out all the iterations for each time step (it only will vary b_P when it is changed the time instant). To solve this linear equations system it will be used Gauss-Seidel or line-by-line solvers developed on chapter 2.

Boundary conditions

It can be found two types of boundary conditions in a problem: the wall boundary condition and a prescribed velocity. For the wall boundary condition (see figure 4.3), it must be taken into account that the boundary layer is created on the wall, so

$$\frac{\partial p}{\partial n} = 0 \tag{4.38}$$

which means that

$$p_p = p_{nb} \tag{4.39}$$

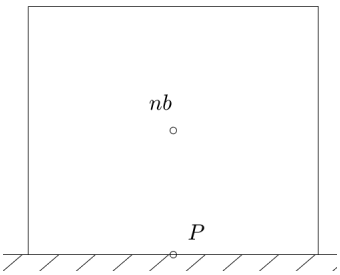

FIGURE 4.3: Representation of the wall boundary condition

For the prescribed velocity (see figure 4.4), taking into account equation 4.15 and imposing that

$$\vec{v}^p = \vec{v}^{n+1} \tag{4.40}$$

it will be obtained the same equation as 4.38, so the coefficients will be the same:

$$a_P = 1 \tag{4.41}$$

$$a_{nb} = 1 \tag{4.42}$$

and the rest of coefficients will be zero.

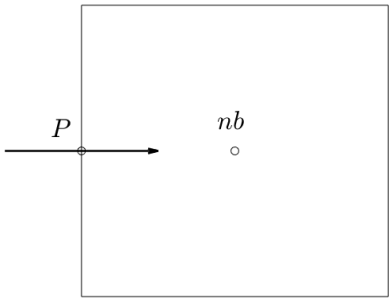

FIGURE 4.4: Representation of the prescribed velocity boundary condition

4.3.4 Coupling velocities and pressure

Once it has been solved the linear equations system, and p^{n+1} is known, the velocity on the nodes of the staggered mesh can be computed.

On the staggered-x mesh (figure 4.5), the horizontal velocity can be computed isolating u^{n+1} from the equation 4.15

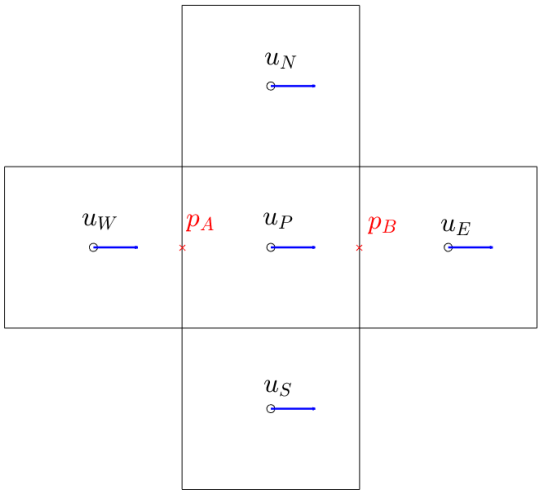

FIGURE 4.5: Representation of the pressure on the Staggered-x mesh

$$u_P^{n+1} = u_P^p - \Delta t \left(\frac{\partial p}{\partial x} \right)^{n+1} \Bigg|_p = u_P^p - \Delta t \frac{p_B^{n+1} - p_a^{n+1}}{d_{BA}} \tag{4.43}$$

For the staggered-y mesh it will be done the same process and it will be arrived to the following equation

$$v_P^{n+1} = v_P^p - \Delta t \frac{p_B^{n+1} - p_A^{n+1}}{d_{BA}} \tag{4.44}$$

4.3.5 Time step choice

Due to the fact it is going to use somehow an explicit numerical approximation (actually, it is a semi-explicit numerical approximation), there is a concrete time step needed to avoid instabilities. This time step should satisfy the Courant-Firedrich-Levy condition. This condition specifies that the maximum time step allowed to achieve the convergence in the case of the conduction phenomenon is

$$\Delta t_c = min \left[0.35 \frac{\Delta x}{|\vec{v}|} \right] \tag{4.45}$$

where Δx also includes Δy. Also, there is a maximum step in the case of the diffusion phenomenon

$$\Delta t_d = min \left[0.2 \cdot Re \cdot \Delta x^2 \right] \tag{4.46}$$

Finally, the maximum time step possible will be the minimum between these two time steps.

4.3.6 Algorithm of resolution

Although it has been talked briefly about the algorithm to solve the Navier-Stokes equations through out this section, in this subsection it will be presented the algorithm schematized

1. Input data
   - 1.1. Physical data: initial conditions, problem's height and width, fluid properties, boundary conditions.
   - 1.2. Numerical data: number of horizontal control volumes (N), number of vertical control volumes (M), relaxation factor (f_r), maximum error allowed (δ)
2. Previous calculations: mesh generation
3. Initial map: $\phi^n[i][j] = \phi(t=0)[i][j]$, $\phi^{n+1}[i][j] = \phi(t=0)[i][j]$ and $t = 0$, where $\phi = \vec{v}$
4. Discretization coefficients computation: a_P, a_E, a_W, a_S, a_N

5. Time step choice (section 4.3.5)
6. Time step: $t = t + \Delta t$, $\vec{v}^{n-1} = \vec{v}^{n}$ and $\phi^{n} = \phi^{n+1}$
7. Compute $\vec{R}(\vec{v})$
8. Compute $\vec{v}^{p}$, from equation 4.17
9. Estimate $p_P^{n+1^*} = p_P^n$
10. Computation of b_P
11. Computation of p_P^{n+1} with Gauss-Seidel or line-by-line, from equation 4.31
12. Is $max|\phi_P - \phi_P^*| < \delta$?
    a. Yes $\rightarrow$ go to 13
    b. No $\rightarrow$ $p_P^{n+1^*} = p_P^{n+1}$ $\rightarrow$ go to 11.
13. Computation of $\vec{v}^{n+1}$ from 4.43
14. New time step?
    a. Yes $\rightarrow$ go to 5
    b. No $\rightarrow$ go to 15.
15. Final calculations and print results
16. End

4.4 Verification

The verification carried out for the code elaborated in this chapter has consisted in the evaluation of the numerical error of each discretized equation and the comparison of the obtained results at different Reynolds number with the results available on the literature [10]. However, this last verification will be shown on the following section since it will be useful on the different cases analysis.

To begin with, the first verification done has been on the result obtained after the iterative process has converged. In this case, the equation that it has been verified is the following one:

$$0 = \int_{\partial\Omega_p} \nabla p^{n+1} \vec{dS} - \frac{1}{\Delta t} \int_{\partial\Omega_p} \vec{v}^{p} \vec{dS} \tag{4.47}$$

which has been discretized in the same way as in the section 4.3.3. The expected error should have the same magnitude order as δ. Thus, as it has been decided to work with

a δ of 10^{-9}, the error should be of around 10^{-9} and. As it has been expected, the maximum discretization error is about 10^{-9} independently of the mesh and the scheme used.

Another verification that it has been carried out is the verification of the mass conservation equation (or continuity equation). This verification has consisted in evaluating the following equation on all the nodes on the main, staggered-x and staggered-y meshes (on the staggered meshes the velocities have been calculated in the same way as it has been done on sections 4.3.1 and 4.3.2).

$$0 = F_e - F_w + F_n - F_s \tag{4.48}$$

Independently of the mesh and the convective scheme, the maximum error on each mesh has been around 10^{-10}.

Another numerical verification is the verification of the momentum equation (for both, x and y, directions). The equation that should be verified is the following one

$$0 = \frac{\vec{v}^{n+1} - \vec{v}^{n}}{\Delta t} - \frac{3}{2}\vec{R}(\vec{v}^{n}) + \frac{1}{2}\vec{R}(\vec{v}^{n-1}) + \nabla p^{n+1} \tag{4.49}$$

In this case the maximum numerical error has been of the order of 10^{-8}.

A part from the previous verifications, it has been carried out a manual verification, which has consisted in comparing the obtained results with the program of a case of a mesh of 4x4 (using the UDS scheme) for 3 different time steps to the ones calculated manually. And, as it has been expected, the results have been the same. This verification has made easier to find a code error which was hard to find due to its subtlety.

4.5 Results analysis

4.5.1 Lid-Driven Cavity

In this section it will be carried out numerical analysis on the results obtained for the *Lid-Driven Cavity* problem (figure 4.6) such as the influence of the mesh (considering only uniform mesh) on the solution, the influence of the scheme or the influence of the stretching factor γ (it will be described later) and also it will be made an analysis on the solution for different Reynolds numbers.

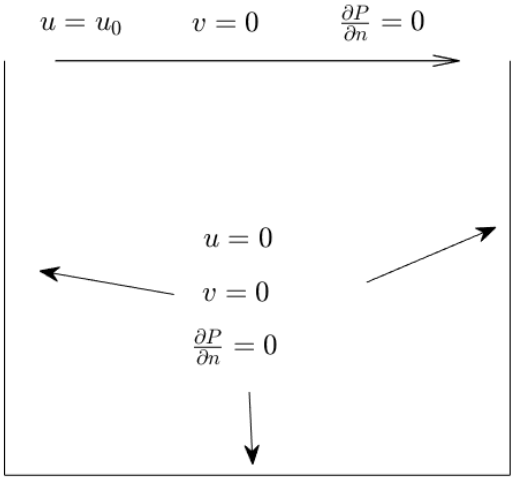

FIGURE 4.6: Representation of the Lid-Driven Cavity Problem

Influence of the mesh

In order to simplify the analysis, it has been decided to only work with the UDS scheme and test different uniform meshes at different Re. Concretely, it will be analyzed the influence of this meshes on the horizontal velocity at the vertical center line ($x = 0.5$ meters) and on the vertical velocity at the horizontal center line ($y = 0.5$ meters).

The first case analyzed has been the case for Re=100.

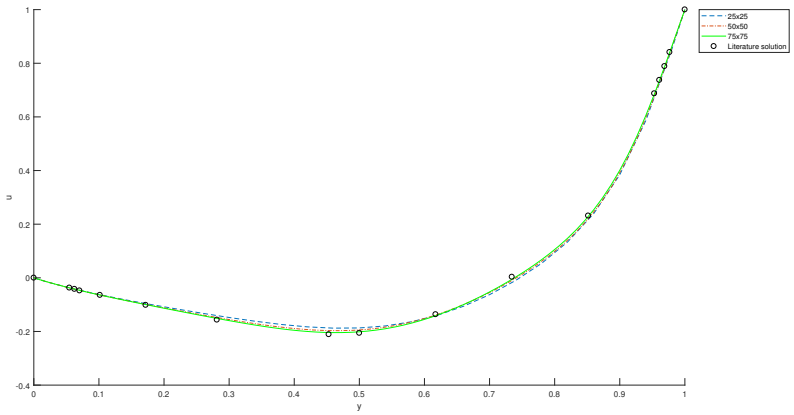

FIGURE 4.7: Horizontal velocity at x=0.5m for Re=100 and for different meshes

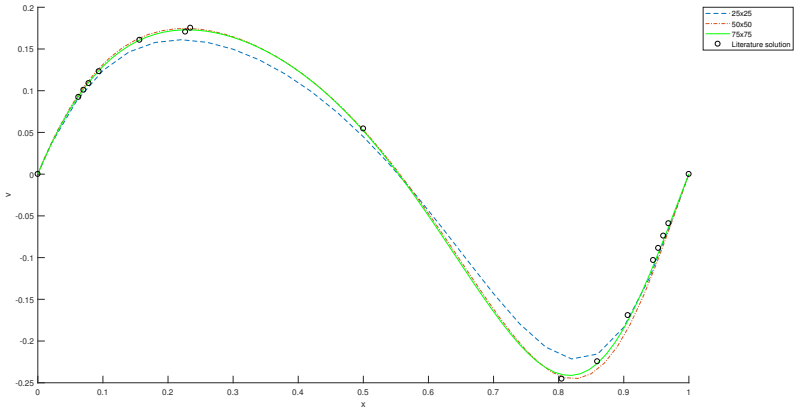

FIGURE 4.8: Vertical velocity at y=0.5m for Re=100 and for different meshes

As it can be seen from the previous figures, for a higher mesh the result gets closer to the solution proposed on the literature (concretely these solutions have been obtained from an article [10]). However, in this case there is not much difference between the 50x50 mesh and the 75x75 mesh [2].

The following case that it has been analyzed has been for a Reynolds of 1000.

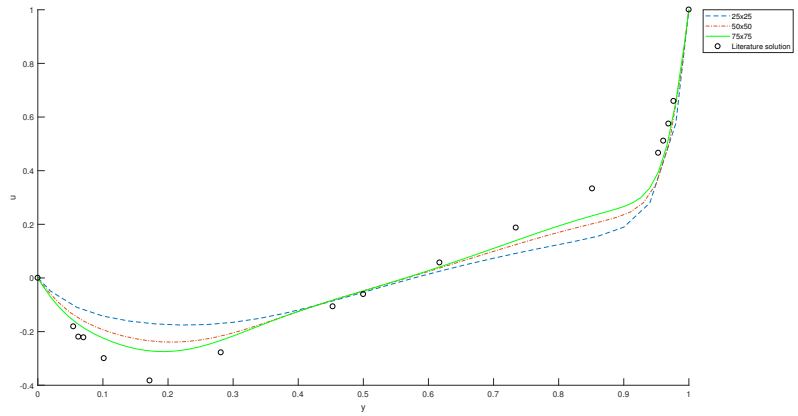

FIGURE 4.9: Horizontal velocity at x=0.5m for Re=1000 and for different meshes

[2]The number of this meshes corresponds to the number of control volumes of the main mesh, so the total number for nodes would be 52x52 or 77x77, respectively.

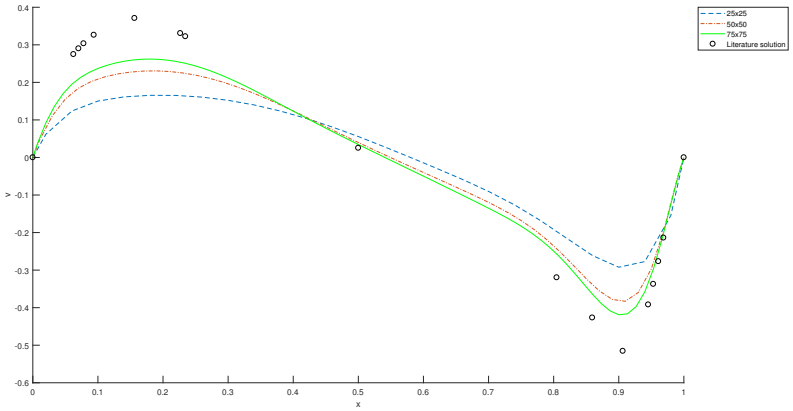

FIGURE 4.10: Vertical velocity at y=0.5m for Re=1000 and for different meshes

In this case, since the flux is more turbulent, the error has been increased considerably. First of all, the 25x25 mesh does not represent correctly the phenomenology since it has too much error. As the mesh increases, the solution obtained gets closer to the real one, but there is still too much error to correctly represent the actual solution. The main difference from the previous case is that in the previous case, since the Reynolds was low, the convective term did not play an important role, but in this case the convective term is more important and a first order convective scheme can be inaccurate. In this case, if it has been decided to work only with UDS, it would have been necessary to increase the mesh in order to get a more accurate solution.

Influence of the scheme

As it has been on the previous section, a first order scheme for high Reynolds number implies a huge error for little or medium meshes. In this section it will be evaluated the different type of schemes in order to analyse the influence of the convective term (and its approximation) on the solution. In order to simplify the analysis, it has been fixed an uniform mesh of 50x50.

In a same way as before, the analysis will start with Re=100.

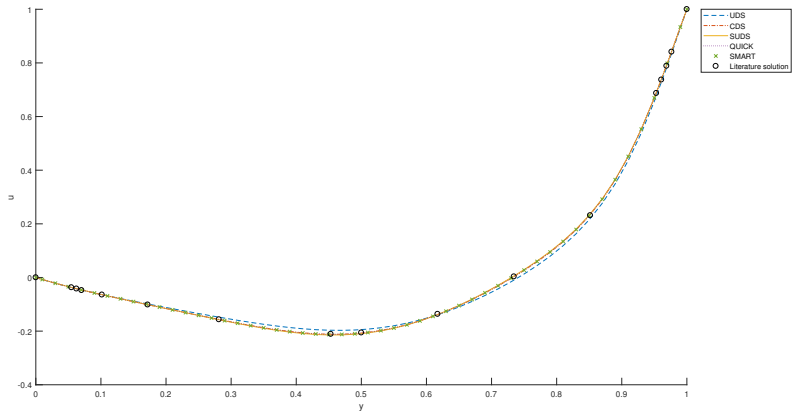

FIGURE 4.11: Horizontal velocity at x=0.5m for Re=100 and for different schemes

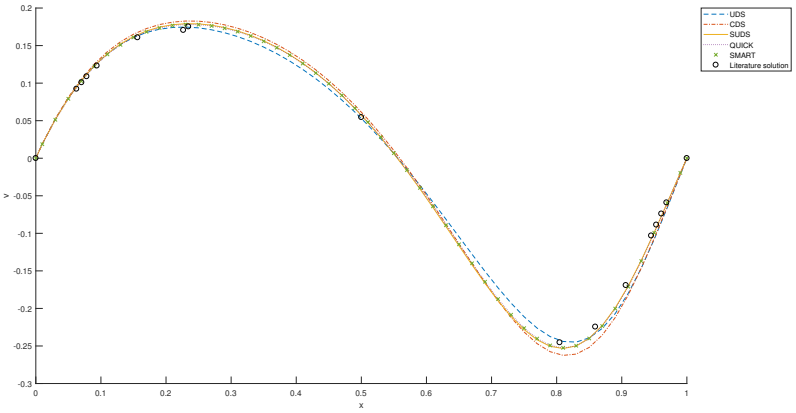

FIGURE 4.12: Vertical velocity at y=0.5m for Re=100 and for different schemes

As it can be seen from these figures, even for low Reynolds number there are some differences between schemes (mainly between the UDS and the others). It can be appreciated that the highest order schemes (SMART or QUICK) are the most accurate schemes, whereas the UDS is the most inaccurate (as it has been mentioned on the previous section). Also, for this Re, the obtained solution from the SUDS is the same or almost the same as the QUICK and SMART solutions, while the CDS slightly differs from the others (but it is still more accurate than the UDS scheme).

The following case that will be presented is the case for Re=1000.

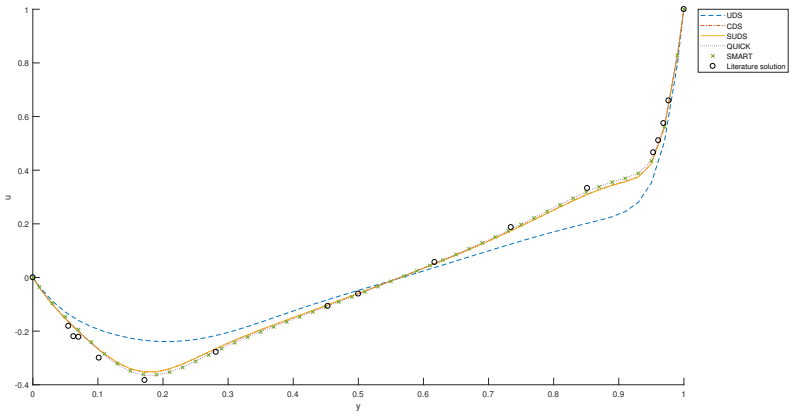

FIGURE 4.13: Horizontal velocity at x=0.5m for Re=1000 and for different schemes

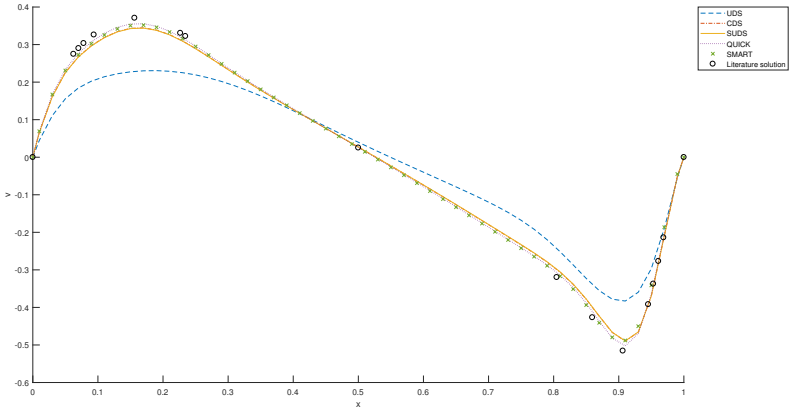

FIGURE 4.14: Vertical velocity at y=0.5m for Re=1000 and for different schemes

In this case it can be observed a higher difference between the UDS scheme and the other schemes due to the fact that the convective term has gain importance. Furthermore, it can be seen that the result for the higher order schemes is still accurate for a mesh of 50x50. However, it can be appreciated a little difference between second order schemes (CDS and SUDS) and higher order schemes (QUICK and SMART), which will be higher as the Reynolds number increases.

However, for higher Reynolds number, such as 5000 (figures 4.15 and 4.16) or 10000 (figures 4.17 and 4.18), even with a higher order scheme there is a noticeable error with a mesh of 50x50. This could be explained because for higher Reynolds number the flow is quite more turbulent and it is needed a higher mesh in order to get correctly this phenomenon.

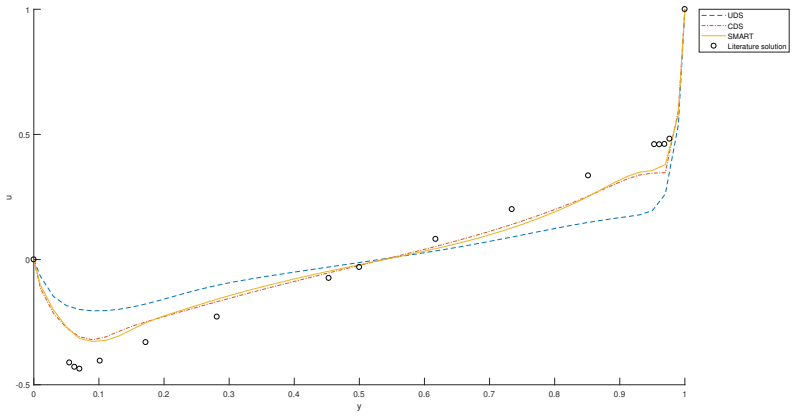

FIGURE 4.15: Horizontal velocity at x=0.5m for Re=5000 and for different schemes

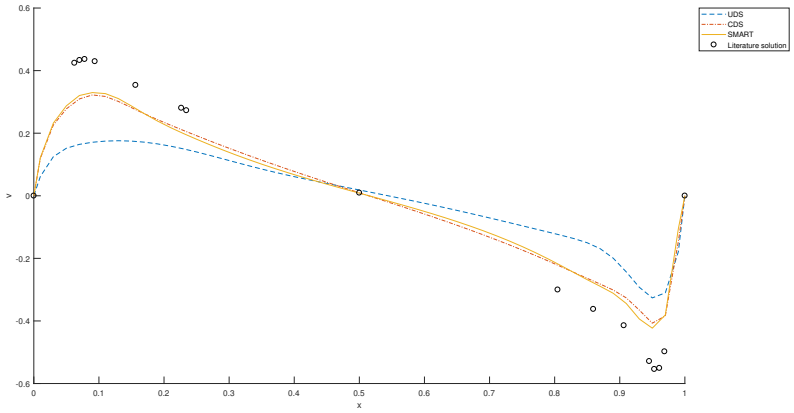

FIGURE 4.16: Vertical velocity at y=0.5m for Re=5000 and for different schemes

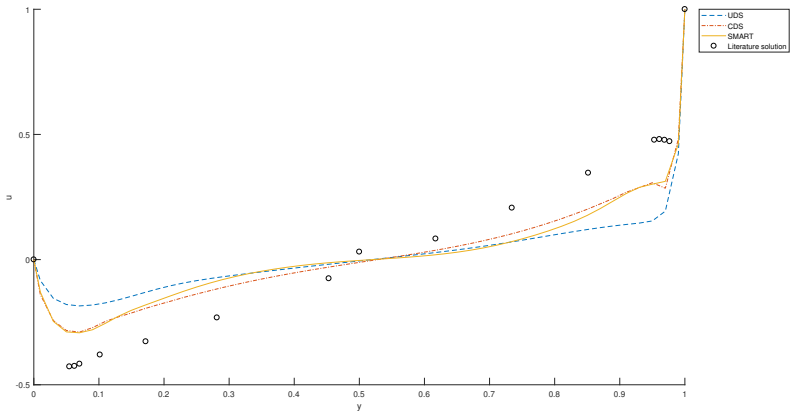

FIGURE 4.17: Horizontal velocity at x=0.5m for Re=10000 and for different schemes

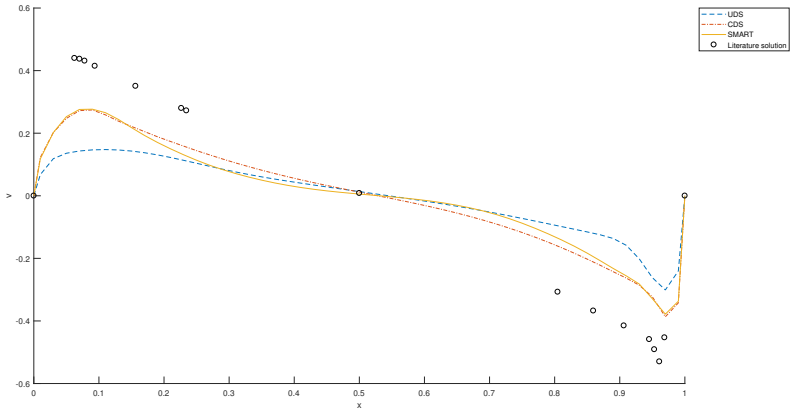

FIGURE 4.18: Vertical velocity at y=0.5m for Re=10000 and for different schemes

Even though there is not much accuracy on a 50x50 mesh for high Re, it could be remarked two different aspects. The first one is that the UDS scheme is more inaccurate than the second or higher order schemes, which is something that it has been seen too on the case of Re of 1000. The second aspect to remark is that on the previous figures (from 4.15 to 4.18), there are only represented the UDS, CDS and SMART scheme. This is due to the mesh size and the Re, where for QUICK and SUDS schemes appeared instabilities which made the program not to arrive to the steady case. These kind of instabilities could be solved increasing the mesh.

Influence of the stretching factor

In order to simplify the analysis, in this case it is only to be evaluated the scheme UDS and the mesh it will be fixed to 50x50, but it will not be an uniform mesh.

Mesh concentrations are a really good option when it is known that in a local zone it is needed a high number of nodes (because there is a high gradient of temperature, velocity, pressure, etc., in this case, the boundary layer) and on the same problem there is a wide zone there with a low number of nodes the phenomenon is represented correctly. There are different types of mesh concentrating. A mesh concentration can be full cosine which is commonly used on the *Discrete Vortex Method*, briefly explained on section 2.1, and defines the the control volume limits in the following way:

$$x_i = \frac{L}{2}\left(1 - cos\left(\frac{i}{N+1}\pi\right)\right) \tag{4.50}$$

where i goes from 0 to N, being N the number of control volumes desired. However, this mesh concentration has not been carried out due to the fact that it does not allow to increase or decrease the concentration without modifying the total number of nodes.

Another mesh concentration is the hyperbolic concentration. Considering a segment between two point $\vec{x}_1$ and $\vec{x}_2$, the intermediate points, which will be the control volume faces or limits [3], can be expressed as [4]

$$\vec{x}_i = \vec{x}_1 + s_i(\vec{x}_2 - \vec{x}_1) \tag{4.51}$$

where s_i it is the hyperbolic concentration:

$$s_i = 1 + \frac{tanh\left[\gamma\left(\frac{i}{N} - 1\right)\right]}{tanh(\gamma)} \tag{4.52}$$

where i will have the same values as in the full cosine and γ is the stretching factor, which is the parameter that will be analyzed in this section.

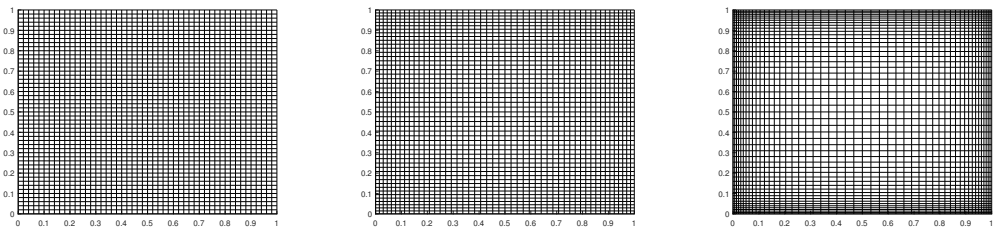

(A) $\gamma = 10^{-6}$ (B) $\gamma = 0.75$ (C) $\gamma = 1.5$

FIGURE 4.19: Main mesh representations for different stretching factors

[3] In order to calculate the i^{th} node's position, it is only necessary to carry out the arithmetic mean of the faces i and $i+1$.

On the following figures it will be represented the results of different Re numbers for a stretching factor of 10^{-6} (uniform mesh, figure 4.19a), 0.75 (figure 4.19b) and 1.5 (figure 4.19c). The idea of this mesh concentration on the walls has been to better simulate the boundary layer, where there is a high gradient of velocity and pressure and, with it, reduce the simulating error.

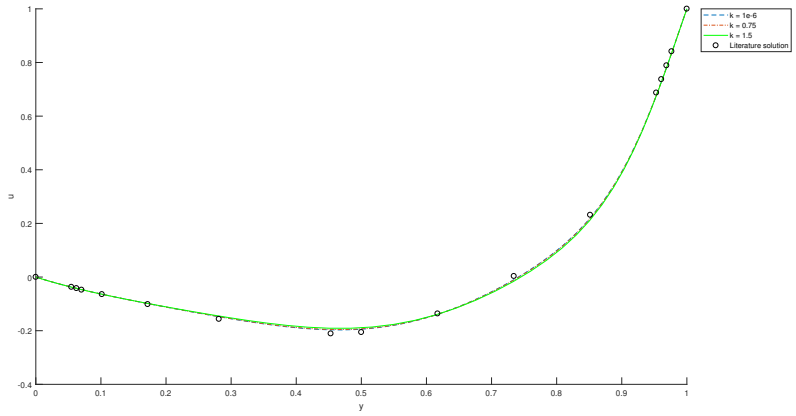

FIGURE 4.20: Horizontal velocity at x=0.5m for Re=100 and for different stretching factors

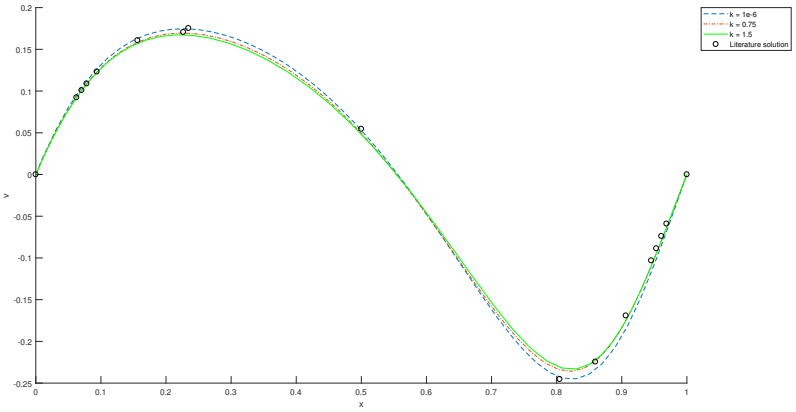

FIGURE 4.21: Vertical velocity at y=0.5m for Re=100 and for different stretching factors

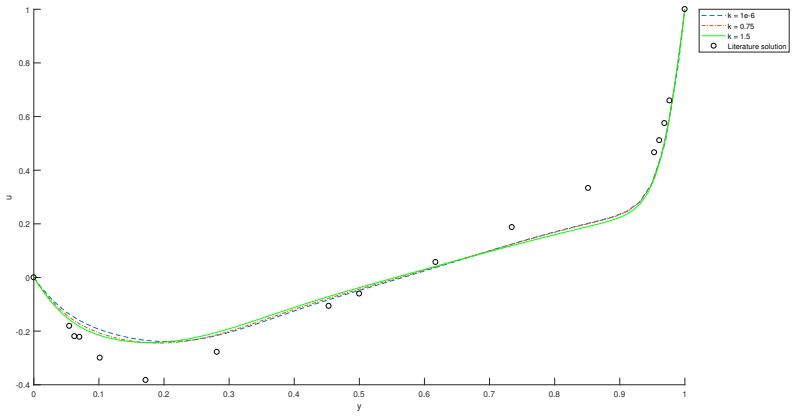

FIGURE 4.22: Horizontal velocity at x=0.5m for Re=1000 and for different stretching factors

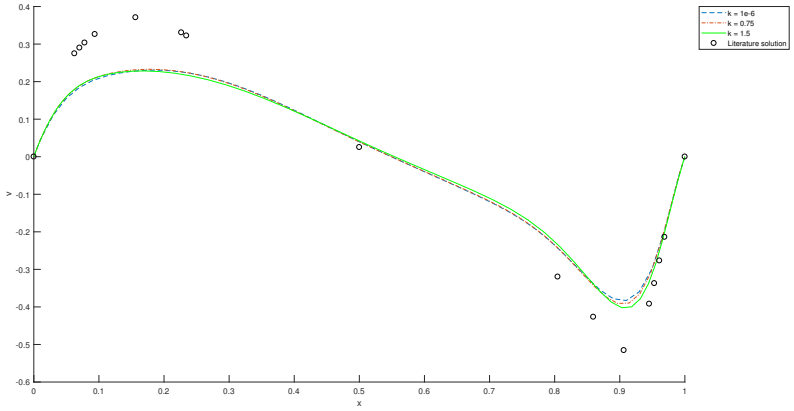

FIGURE 4.23: Vertical velocity at y=0.5m for Re=1000 and for different stretching factors

As it can be seen on the previous figures, the stretching factor practically does not influence on the solution since although the boundary layer can have a high resolution, if the rest of the flow has low resolution the boundary layer will not be simulated correctly due to the fact that both regions are connected and there is an exchange of information between them. For this reason, it should be increased the mesh in order to obtain a better solution, even if it has been used a stretching factor or not.

Physical analysis

Apart from analysing the numerical parameter such as the mesh or the stretching factor or the influence of the scheme, it is also interesting to analyze the obtained result for different Reynolds numbers. Concretely, the Reynolds number that have been tested are

100, 1000, 5000 and 1000, for a 50x50 mesh with the SMART scheme (which was the most accurate and the result had the lowest error).

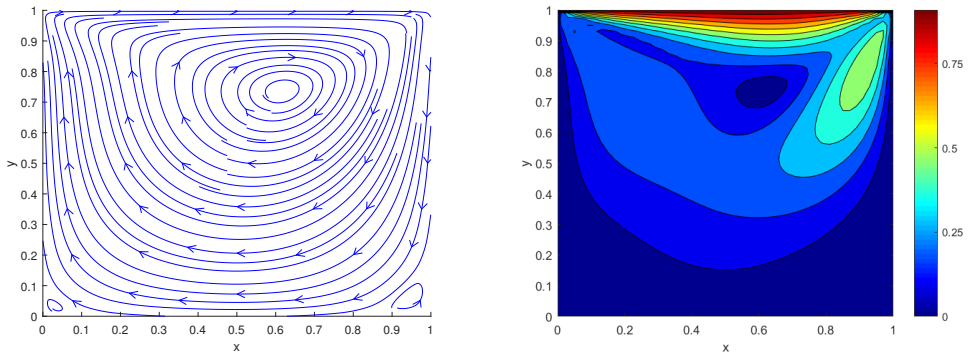

(A) Streamlines representation (B) Velocity modulus representation

FIGURE 4.24: Velocity representation for Re=100

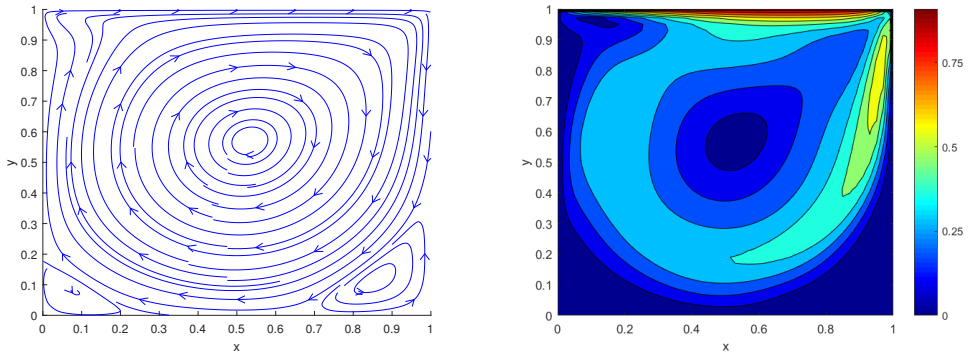

(A) Streamlines representation (B) Velocity modulus representation

FIGURE 4.25: Velocity representation for Re=1000

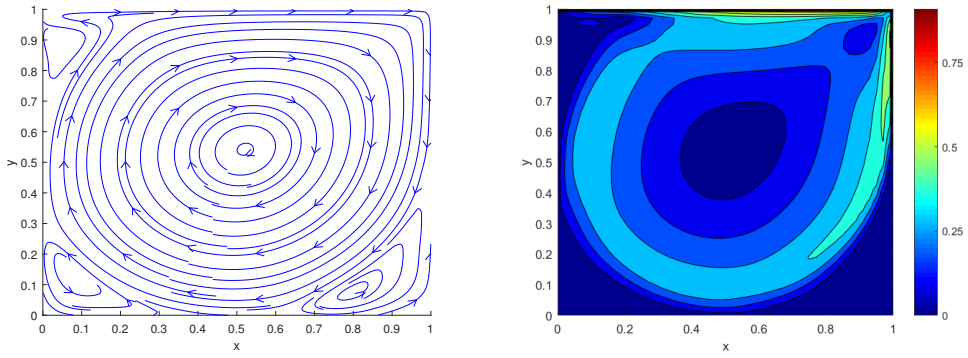

(A) Streamlines representation (B) Velocity modulus representation

FIGURE 4.26: Velocity representation for Re=5000

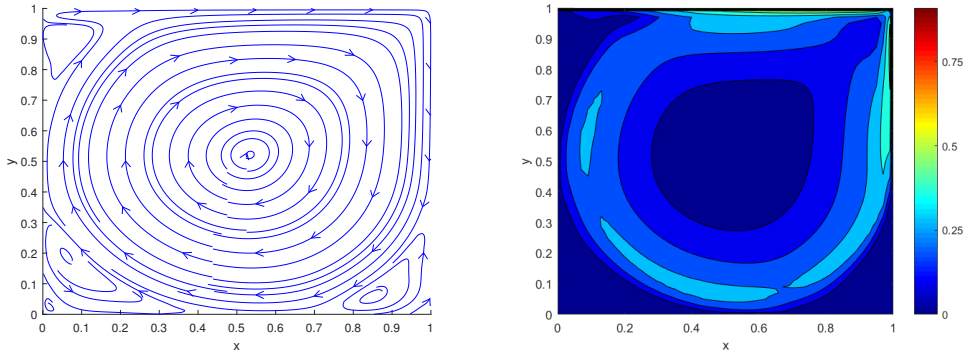

(A) Streamlines representation (B) Velocity modulus representation

FIGURE 4.27: Velocity representation for Re=10000

As it can be appreciated, with for the case of Re=100, there is a very little vortex on the bottom corners and it is also located another vortex on the top-right side of the corner. Also, it can be seen that the there is a high gradient of velocity on top of the cavity whereas on the rest of the cavity the velocity is practically zero.

When it is increased the Reynolds number, it can be seen that the "central" vortex gets closer to the center of the cavity and the corner vortex become bigger. Also, it can be seen that that the velocity gradient decrease and the velocity around the central vortex becomes lower (there is a higher zone around this vortex with velocity close to zero). Also, it appears an additional vortex with Re=5000 on the top left corner, which becomes bigger for Re=1000.

4.5.2 Differentially Heated Cavity

The differentially heated cavity is the case of a closed cavity where the top and bottom walls are adiabatic and the left and right wall are at different temperature. Inside this cavity it will occur a natural convection phenomenon, which means that the energy equation and the mass forces should not be decoupled or neglected, respectively. Because of this, the momentum equation should be slightly modified. So the equations that are the following:

$$\nabla \cdot \vec{v} = 0 \tag{4.53}$$

$$\frac{\partial \vec{v}}{\partial t} + (\vec{v} \cdot \nabla)\vec{v} = -\nabla p + \frac{1}{Re}\nabla^2 \vec{v} - \theta \vec{u}_g \tag{4.54}$$

$$\frac{\partial \theta}{\partial t} + \vec{v} \cdot \nabla \theta = \frac{1}{Re \cdot Pr}\nabla^2 \theta \tag{4.55}$$

where $\vec{u}_g$ is the unitary vector of the gravitational field and

$$\theta = \frac{T - T_0}{T_0} \tag{4.56}$$

$$Pr = \frac{c_P \mu}{\lambda} \tag{4.57}$$

and the reference velocity is defined as

$$u_0 = \sqrt{g \beta_0 T_0 L} \tag{4.58}$$

It should be noticed that as it is treated and incompressible flow it has been taken into account the Boussinesq approximation, which estimates the variation of density due to the temperature as

$$\rho = \rho_0 \beta_0 (T - T_0) \tag{4.59}$$

where β is the piezo-thermic coefficient. For ideal gases it is

$$\beta = \frac{1}{T} \tag{4.60}$$

With that, it should be made few modifications on the general procedure. First of all, the term $R(v)$ will the following expression:

$$R(v) = -(\vec{v} \cdot \nabla)v + \frac{1}{Re}\nabla^2 v + \theta \tag{4.61}$$

whereas $R(u)$ will not change. The integration of this term will be done in the same was as it has been explained on the current chapter except for the integration of the temperature term, which is presented on the following expression:

$$\int_{\Omega_P} \theta d\Omega = \Omega_a \theta_a + \Omega_b \theta_b \tag{4.62}$$

where a and b represent the same nodes of the main mesh as in the section 4.3.4, and the volumes are the half volumes of the main mesh node's control volumes that have been treated.

Apart from this, to compute the temperature it will be started from the following discretized energy equation

$$\frac{\theta^{n+1}-\theta^{n}}{\Delta t}=\frac{3}{2}R_t(\theta^{n})-\frac{1}{2}R_t(\theta^{n-1}) \tag{4.63}$$

where

$$R_t(\theta)=\frac{1}{Re\cdot Pr}\nabla^2\theta-\vec{v}\cdot\nabla\theta \tag{4.64}$$

Following the same procedure as it has been done in this chapter, it can be obtained the final expression of R_t

$$\begin{aligned}R_t(\theta)=\frac{1}{\Omega_P}\Bigg(&-\left[F_e\theta_e-F_w\theta_w+F_n\theta_n-F_s\theta_s\right]+\\&\frac{1}{Re\cdot Fr}\left[\frac{\theta_E-\theta_P}{d_{PE}}A_e-\frac{\theta_P-\theta_W}{d_{PW}}A_w+\frac{\theta_N-\theta_P}{d_{PN}}A_n-\frac{\theta_P-\theta_S}{d_{PS}}A_s\right]\Bigg)\end{aligned} \tag{4.65}$$

and then, the temperature at time instant $n+1$ can be obtained from the equation 4.63. This temperature could be obtained parallel to the velocity and pressure computation.

Also, for this case there is an additional maximum time step to take into account:

$$\Delta t_t=0.2\cdot Pr\cdot Re\cdot\Delta x^2 \tag{4.66}$$

With all this mathematical development, it has been developed a specific code for this case where it has been added the energy equation and the mass forces to the *Lid-Driven Cavity* code.

In this case, it will only analysed the influence of the two non-dimensional numbers (Pr and Re) on the solution.

Reference case

First of all, it has been carried out a reference case, which has had the following paramenters:

- Left wall's temperature (also reference temperature): 300K
- Right wall's temperature: 288 K (so, $\theta_R=-0.04$)
- Re=100
- Pr=1

So, with this parameters it has been obtained the following results.

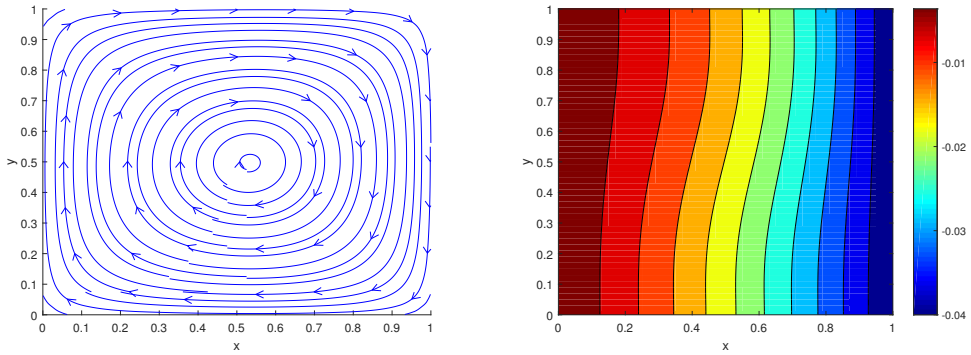

(A) Streamlines representation (B) Temperature representation

FIGURE 4.28: Solution for the reference case

It can be seen that on a natural convection it is formed a vortex located close to the center. Furthermore, it can be appreciated that on the hottest wall there is an ascending flow due to the fact that at higher temperature the density is lower and it tends get situated on top of the fluid. On the other hand, on the coldest wall there is an descending flow for the same reason as before, the density is inversely proportional to the temperature. It can also be appreciated that there are no vortex on the corners since it is treated a laminar flow with a very low velocity.

Influence of the Reynolds number

In this section it has been tested two different Reynolds number, maintaining the other parameters, in order to analyse its influence on the solution. Concretely, it has been tested the Reynolds of 10 and 1000.

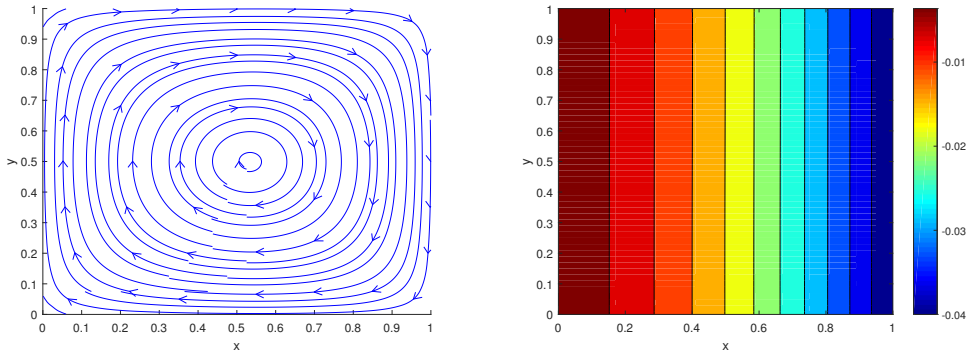

(A) Streamlines representation (B) Temperature representation

FIGURE 4.29: Solution for Re=10

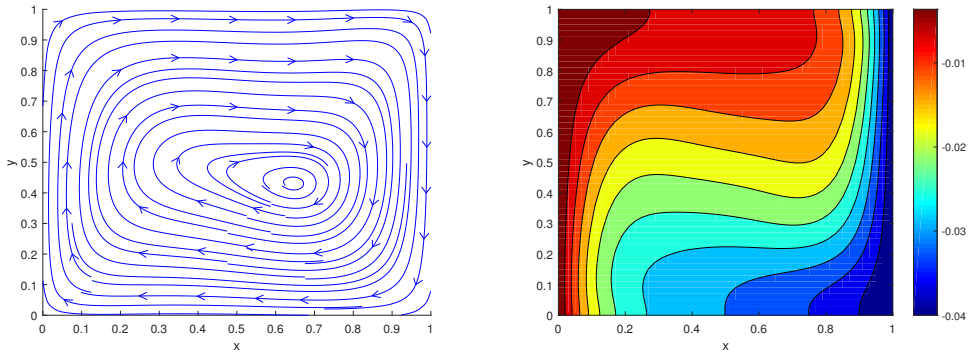

(A) Streamlines representation (B) Temperature representation

FIGURE 4.30: Solution for Re=1000

It can be appreciated that for a low Reynolds the phenomenon of diffusion is the most important, where the isotherms are parallel between them. However, for a higher Reynolds number it can be seen that the convective term gains force since in the middle of the cavity the isotherms are almost parallel to the flow direction (which means that practically there is no heat transfer on the horizontal direction, this phenomenon can be clearly seen on figure 3.6). Furthermore, it should be noticed that the central vortex has been slightly displaced on the direction to the left-bottom corner and there is a bit more turbulence around it.

Influence of the Prandtl number

In this case it has been maintained constant to 100 and it has been tested two different Prandtl numbers so as to be able to analyse the influence of this non-dimensional number on the solution. Concretely, it has been tested the Prandtl numbers of 0.1 and 10.

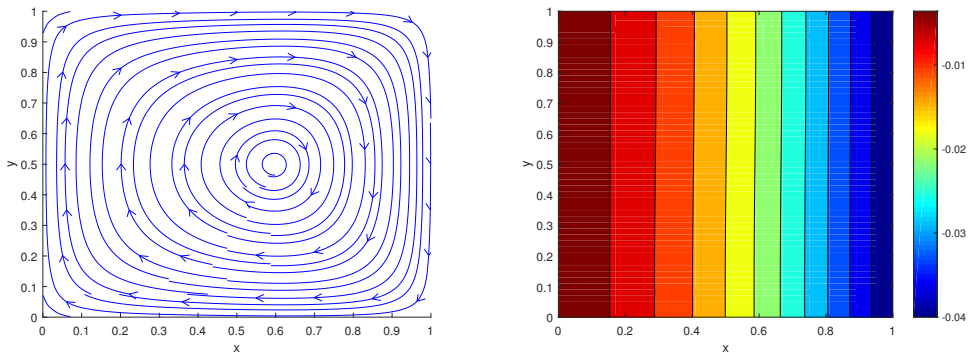

(A) Streamlines representation (B) Temperature representation

FIGURE 4.31: Solution for Pr=0.1

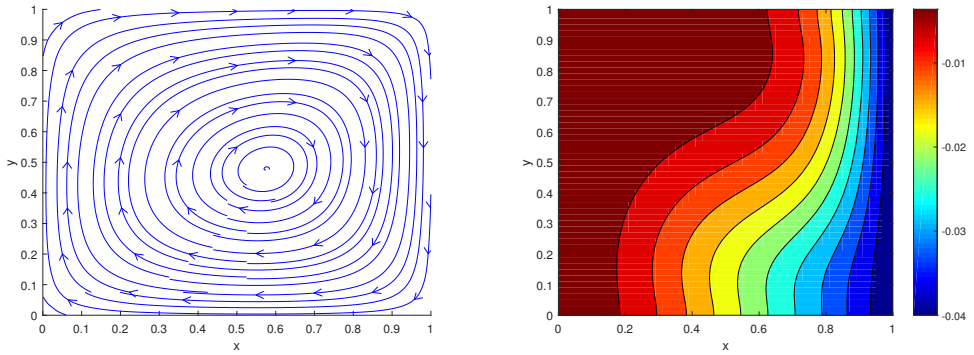

(A) Streamlines representation (B) Temperature representation

FIGURE 4.32: Solution for Pr=10

As it happened with a low Reynolds number, with a low Prandtl number there is also a dominant diffusion phenomena, since a low Prandtl number implies that the heat transfer is higher than the momentum transfer. However, for a high Prandtl number it can be seen that the convective term gains importance, as it happened too with high Reynolds number. The main difference between this analysis and the Reynolds' analysis is that in this case the location of the vortex does not significantly vary as a function of the Prandtl number.

4.6 Conclusions

In this chapter it has been developed the Fractional Step Method in order to solve the Navier-Stokes equations. In it, it has been treated two different cases. In the first case is has been decoupled the energy equation from the mass and momentum conservation equations since it has been neglected the influence of the temperature on the density and the mass forces, and with this code it has been able to solve the *Lid-Driven Cavity* problem. The other code has been an extension of the previous one, where it has been considered the energy conservation equation and it has been taken into account the Boussinesq approximation for the mass forces on the momentum equation, and with this code it has been able to solve the *Differentially Heated Cavity* problem.

On the other hand, it has been recollected the convective schemes functions from the previous code (the convection-diffusion code), since these functions have been verified and it was ensured that they would work correctly, instead of building new functions with the risk of making a mistake on them. Also, in this chapter it has been analysed the influence of the scheme on the solution and as it happened on the previous chapter it has been seen that the UDS scheme is the most stable but the less accurate.

Regarding the time step, it has been reduced the constants to them half value due to the fact that, otherwise, the time step would be enough big to generate some temporal

oscillations which would not make the system converge to a stationary status (so for the conduction phenomenon the constant has been 0.175 instead of 0.35 and for the diffusion phenomenon the constant has been 0.1 instead of 0.2).

A difference on the geometry from the previous chapters' codes is that in this case it has been developed a concentrated mesh towards the walls (with an hyperbolic concentration) and it has been analysed its influence on the solution. A part from this analysis, it has been carried out an analysis of the influence of the mesh on the solution only considering an uniform mesh.

Finally, it has been carried out a physical analysis on both cases (*Lid-Driven Cavity* and *Differentially Heated Cavity*) in which it has been analysed the solution for different Reynolds numbers and, for the *Differentially Heated Cavity* problem, for different Prandtl numbers.

As regards the code, it has been developed a general code for the case of decoupling the energy conservation equation, where it is easily adapted for a *Square Cylinder* problem (in which there is a square located inside a duct with a parabolic inlet flow), since there is already a connectivity matrix for the fluid and solid nodes and the mesh can be easily adapted to be concentrated near the object.

Chapter 5

Budget, Task Planning & Environmental Impact

5.1 Budget

As the aim of this project has been to program different numerical solvers, it would be reasonable that the direct cost would be much higher than the indirect cost due to the high amount of engineering behind this work and because the indirect cost are based on software, hardware and electricity consumption.

On the following table it is presented a summary of the budget, which has been widely presented on the *Budget* document. At the end, the total cost will be around 6,540€.

TABLE 5.1: Project costs

Direct Costs (€)	6,435
Indirect Costs (€)	100
Total Cost (€)	6,535

5.2 Task Planning

On this section it will be presented the starting project task planning and it will be commented and justified the deviations that it has been done during this study. On the following two figures it will be presented the GANTT diagram made for the project Charter. It must be remarked that the potential flow study started before the project GANTT elaboration so it has been only included the time expected to finish this study.

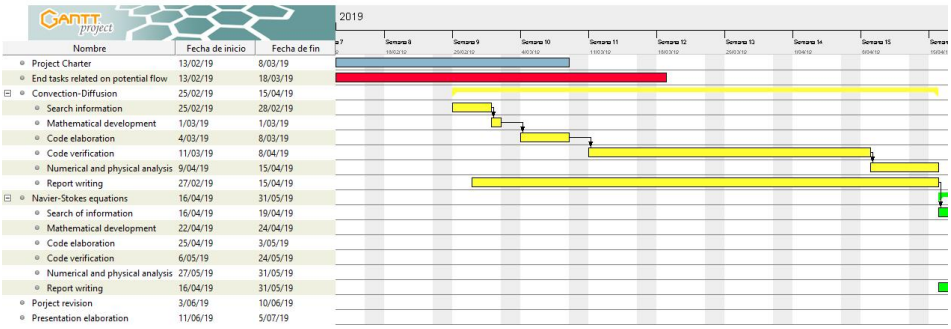

FIGURE 5.1: GANTT diagram (Part 1)

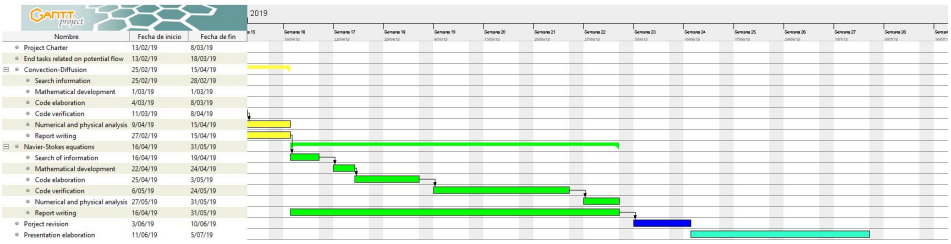

FIGURE 5.2: GANTT diagram (Part 2)

It must be said that the procedures for each study have been the same (theoretical study, mathematical approach, code elaboration, code verification, results analysis and report writing).

Although it has been let a high period of time to verify and correct the code since sometime it is quite hard to find a code mistake, it has not been able to carry out further physical analysis (for example, on the potential flow the analysis of an airfoil or on the Navier-Stokes the analysis of the *Square Cylinder*) for not having enough time for it since it has last too much to find code's issues (specially on the Navier-Stokes code). However, all the tasks has been completed on time and the last week project revision has been fully dedicated to correct format and content issues on the project documents.

5.3 Environmental Impact

In order to carry out this study, it has been used two main tools, for the mathematical development and all the calculations it has been used paper and a pen and for the documents writing, codes development and simulation it has been used a computer (and so, electricity).

As far as the paper is concerned, its impact is almost null because it has been used recycled paper and it has been used a little amount of it.

Regarding the electricity consumption, it has been estimated that the computer (concretely, the laptop) has been working 5 hours daily during 4 months, so considering the worst case of a consumption of 0.1 kW per hour [6], the total electricity consumption has been 60 kWh. Since this study has been carried out in Catalonia, it has been estimated that the generation of CO_2 is the average of the annual Peninsular production [7], which is 0.176 kg CO_2 per kWh. So, it has been produced an amount of 10.56 kg of CO_2.

It can be seen the the production of CO_2 is relatively low, and in a close future it could be lower since it is becoming more popular the use of renewable energy sources. The main advantage of carrying a simulation instead of a wind tunnel is that the cost of a simulation is lower in terms of energy (a wind tunnel can waste on the order of MWh [12] of electricity) and the requirements are not that expensive (it is only needed a computer wheres for the wind tunnel it is needed a structure to accelerate or recirculate the air).

Chapter 6

Conclusions

During this work it has been developed different types of numerical solvers. It has been started with a *case*, the potential flow, which it is a first approach to the Navier-Stokes equations. This approach is recommended for an early design study since it can provide quite accurate data with a low computational cost. The follow up of this case it has been the convection-diffusion equation, where it has been adapted the majority of the potential flow code and it has been added the convective term. The main intention of developing this code has been to develop and verify the convective term analysis in order to use it on the Navier-Stokes code. Finally, it has been developed a code for solving the incompressible form of the Navier-Stokes equations. In this part, it has been created a new code due to the fact that it has been worked with three different meshes, which has been something new. However, the convective term functions has been copied from the convection-diffusion code since they have been already verified.

At this point, it could be affirmed that the objectives of this project have been accomplished, since it has been developed the previously mentioned codes, it has been analysed the obtained solutions and they have been verified with other available solutions (analytical solutions or research groups' solutions).

Furthermore, it has been improved the knowledge of programming with *C++* language since it has not been learned previously working with vectors (which allow to work with bigger matrices since the static memory was limited and with a simple heat conduction case with a mesh 90x90 did not work for unavailable memory).

Also, it has been gained more experience on numerical methods, concretely on learning and thinking different ways to find the mistakes, due to the fact that the extension of the codes has been so big and it would be practically impossible to find a mistake with a sign if there is no a clear idea where the issue can be. However, although it has been learned this aspect, it has taken too much time to find the code issues and because of it, it has not been possible to go further with the physical analysis on the chapters of potential flow and Navier-Stokes.

6.1 Future work

Since the time available has been a crucial factor, there are many different fields that would be very interesting to work in but it has not been realized. However, as there has been the intention to keep on with this project it has been created the codes to be easily modified and be able to analyse different cases.

A very interesting field would be to work with NACA airfoils in potential flow, since there is a lot of data available and it could be made a comparison with the *Finite Vortex Method* solution (this code has been developed on another subject, *Aerodynamics*).

As regards the Navier-Stokes equations, it could be developed different codes to solve the different turbulent models (RANS and LES) and compare them solutions with the obtained with the Fractional Step Method. Moreover, it could be interesting to develop the compressible form of the Navier-Stokes equations and analyse the shock waves.

On the other hand, since the time of computation is quite high, it could be interesting to optimize the different codes. During this project it has been attempted to develop the *Additive Correction Multigrid Method* [3] but since it has not been obtained good results and it has not been a priority (it was not indispensable for the project development) it has not been introduced on this report, but it would be interesting make a second attempt in order to solve the different issues encountered. Apart from *Additive Correction Multigrid Method*, it would be also interesting to try other type of solvers in order to have quicker results.

As regards the mesh, it would be interesting to work with unstructured meshes, instead of working with blocking-off method, in order to get better the shape of the object which is going to be analysed its influence on the flow.

Bibliography

[1] John David Anderson et al. *Computational fluid dynamics: an introduction*. Springer Science & Business Media, 2013.

[2] M Darwish and F Moukalled. "The χ-schemes: a new consistent high-resolution formulation based on the normalized variable methodology". In: *Computer methods in applied mechanics and engineering* 192.13-14 (2003), pp. 1711–1730.

[3] M Darwish, T Saad, and Z Hamdan. "Parallelization of an additive multigrid solver". In: *Numerical Heat Transfer, Part B: Fundamentals* 54.2 (2008), pp. 157–184.

[4] CTTC department. "Fractional Step Method". UPC, Escola Superior d'Enginyeries Industrial, Aeroespacial i Audiovisual de Terrassa, course 2018-2019.

[5] CTTC department. "Numerical resolution of the generic convection-diffusion equation". UPC, Escola Superior d'Enginyeries Industrial, Aeroespacial i Audiovisual de Terrassa, course 2018-2019.

[6] Energuide.be. *How much power does a computer use? And how much CO2 does that represent?* [online]. 2019. URL: https://www.energuide.be/en/questions-answers/how-much-power-does-a-computer-use-and-how-much-co2-does-that-represent/54/ (visited on 06/02/2019).

[7] Red Eléctrica de España. *Series estadísticas nacionales*. [online]. 2019. URL: https://www.ree.es/es/estadisticas-del-sistema-electrico-espanol/series-estadisticas/series-estadisticas-nacionales (visited on 06/04/2019).

[8] Sebastián Fachini and Óscar López García. *Introducción a la ingeniería aeroespacial*. Ibergarceta, 2012.

[9] Joel H Ferziger and Milovan Peric. *Computational methods for fluid dynamics*. Springer Science & Business Media, 2012.

[10] UKNG Ghia, Kirti N Ghia, and CT Shin. “High-Re solutions for incompressible flow using the Navier-Stokes equations and a multigrid method”. In: *Journal of computational physics* 48.3 (1982), pp. 387–411.

[11] Boris Marcial Ortega. “Development of Computational Fluid dynamic codes for the numerical resolution of the Navier-Stokes equations applied to benchmark problems using finite volume method”. MA thesis. UPC, Escola Superior d’Enginyeries Industrial, Aeroespacial i Audiovisual, 2018.

[12] NASA. *Flying on the Ground*. [online]. 2009. URL: `https://www.nasa.gov/centers/glenn/about/fs05grc.html` (visited on 06/04/2019).

[13] Enrique Ortega. “The Discrete Vortex Method”. UPC, Escola Superior d’Enginyeries Industrial, Aeroespacial i Audiovisual de Terrassa, course 2017-2018.

[14] Suhas Patankar. *Numerical heat transfer and fluid flow*. CRC press, 1980.

[15] Engineering ToolBox. *Helium - Thermophysical Properties*. [online]. 2008. URL: `https://www.engineeringtoolbox.com/helium-d_1418.html` (visited on 06/01/2019).